NOTICE

The quality of this microform is heavily dependent upon the quality of the original thesis submitted for microfilming. Every effort has been made to ensure the highest quality of reproduction possible.

If pages are missing, contact the university which granted the degree.

Some pages may have indistinct print especially if the original pages were typed with a poor typewriter ribbon or if the university sent us an inferior photocopy.

Previously copyrighted materials (journal articles, published tests, etc.) are not filmed.

Reproduction in full or in part of this microform is governed by the Canadian Copyright Act, R.S.C. 1970, c. C-30.

AVIS

La qualité de cette microforme dépend grandement de la qualité de la thèse soumise au microfilmage. Nous avons tout fait pour assurer une qualité supérieure de reproduction.

S'il manque des pages, veuillez communiquer avec l'université qui a conféré le grade.

La qualité d'impression de certaines pages peut laisser à désirer, surtout si les pages originales ont été dactylographiées à l'aide d'un ruban usé ou si l'université nous a fait parvenir une photocopie de qualité inférieure.

Les documents qui font déjà l'objet d'un droit d'auteur (articles de revue, tests publiés, etc.) ne sont pas microfilmés.

La reproduction, même partielle, de cette microforme est soumise à la Loi canadienne sur le droit d'auteur, SRC 1970, c. C-30.

Canada

Picosecond Flash Photolysis of TiO_2 Colloids And Time-Resolved Photoacoustics

Claude Arbour

A Thesis

in

The Department

of

Chemistry

Presented in Partial Fulfillment of the Requirements
for the Degree of Doctor of Philosophy at
Concordia University
Montréal, Québec, Canada

September 1987

ISBN 0-315-41661-0

ABSTRACT

Picosecond Flash Photolysis of TiO_2 Colloids
and Time-Resolved Photoacoustics

Claude Arbour, PH.D.
Concordia University, 1987.

The first part of this thesis consists of the study of the semiconductor TiO_2 under the form of colloidal particles. Colloidal particles of TiO_2 show a red shift in the absorption band edge for particles going from 20 Å to 200 Å. This red shift is interpreted as a quantification effect in the particles. The flash photolysis of colloidal TiO_2 particles shows a transient which is formed within the pulse. The transient decays with a second order rate constant of $2,4 \times 10^{-10}$ n_e^{-1} s^{-1} and is attributed to absorption of electrons in the conduction band. The rate constant is a direct measurement of the recombination in the particles.

Upon addition of a dye to the TiO_2 suspension, a new transient starts to grow after 500 ps with a rate constant of 5×10^8 s^{-1}. This new transient with an absorption maximum at 630 nm is attributed to a hole trapped in a p-type site. The mechanism proposed involved a two photon process where both the TiO_2 and the dye are excited. An

electron is transfered from the CB of the TiO_2 to the excited dye leaving the hole in the VB which is trapped later.

The second part of this thesis presents the results of the construction of a microsecond time-resolved photoacoustic apparatus. The detection system consists of a piezoelectric tube which is also used as the cell and a boxcar for time resolution. A sensitivity of $6{,}1 \times 10^{-3}$ is achieved with a pulse energy of 20 µJ.

The system has shown to be able to measure the energy of states which have a lifetime longer than 100 µs. The energy of the triplet state of the $ZnTPPS^{4-}$ was measured to be 1,4 eV compared to the literature value of 1,61 eV. We have measured the energy of the n-type trap sites in TiO_2 and we have obtained a value of 2,0 eV below the CB which corresponds to the blue color of the n-doped TiO_2.

Acknowledgement

The first person I would like to thank is my supervisor, Dr. Cooper H. Langford, who never dispair of this project even when the results were discouraging. I owe a great respect to this man who always has great scientific ideas and who is willing to share them. I want to thank Dr. D.K. Sharma who helped me in the picosecond experiments and with whom I had fruitful discussions.

The production of this thesis would not have been easy without the great help of Stella Bulzan for the editing and Donald Gutzman for the figures. I would also like to thank the members of my group who helped me at different stages of this research: Dr. Andrew Crouch ($ZnTPPS^{4-}$, Ishmael Ordonez ($CuPcTS^{4-}$) and David Biro.

I am grateful to NSERC and FCAR for their support during my graduate studies.

A ma mère.

TABLE OF CONTENTS

I. Introduction: Essential semiconductor concepts 1
I.1 Introduction 1
I.2 The semiconductor 4
I.2.1 TiO_2 as a semiconductor 4
I.2.2 The electronic properties of a TiO_2 semiconductor 5
I.3 Colloidal semiconductor particles 9
I.3.1 Size quantization 9
I.3.2 Size effects 16
I.4 Trapped states 20

II. Introduction: Photoacoustics 24
II.1 History of photoacoustics 24
II.2 The photoacoustic effect 25
II.2.1 The theory of photoacoustic in a gas 25
II.2.2 The theory of photoacoustic in condensed matter 26
II.3 The piezoelectric detector 29
II.4 Relation between absorption and photoacoustic signal 30
II.5 Sensitivity of the photoacoustic method 33
II.6 Excited state measurements by photoacoustics 34
a) Excited state lifetime 34
b) Energy of excited states 36

III. Experimental 39
III.1 Samples 39
III.2 Absorption 42
III.3 Picosecond apparatus 42
III.4 Photoacoustic apparatus 49

IV. Results 53
IV.1 Absorption 53
IV.2 Picosecond flash photolysis 59
a) TiO_2 alone 59
b) TiO_2-$CuPcTS^{4-}$ system 61
c) TiO_2-$RuPPS^{4-}$ system 64
d) TiO_2-erythrosin system 69
e) pH effect 69
f) Concentration effect 71

g) Temperature effect 71
h) Energy effect 72

V. Discussion 74
V.1 The colloidal particles of TiO_2 74
V.2 The TiO_2-dye systems 79
V.2.1 Absorbance and excited species 79
V.2.2 Fate of the carriers 80
a) Proposed mechanism 80
b) TiO_2-$CuPcTS^{4-}$ system 81
c) TiO_2-$RuPPS^{4-}$ system 88
d) TiO_2-erythrosin system 92
e) Overall reaction scheme 93
f) Nature of the trapped states 96
g) Effects on the transient absorption 97
V.2.3 Kinetic consideration 102

VI. Results and discussion on photoacoustic 106
VI.1 The signal 106
VI.2 Relation between signal and absorption 108
VI.3 Sensitivity 113
VI.4 Time resolution 114
VI.5 Energy level measurement 116
VI.6 Energy of trapped states of TiO_2 118
VI.7 Comparison with picosecond experiments 121

VII Conclusion 123
VII.1 TiO_2 particles 123
VII.2 Picosecond experiments 123
VII.3 Photoacoustic experiments 125

References 128

Appendix A 130

Appendix B 137

Appendix C 142

Appendix D 159

LIST OF FIGURES

Figure I.1	Energy bands of solids	2
Figure I.2	Energy bands of semiconductors	3
Figure I.3	Energy levels of TiO_2	6
Figure I.4	Energy bands of a single crystal of TiO_2	8
Figure I.5	Formation of the bands in a semiconductor	11
Figure I.6	Formation of energy gaps in crystals	13
Figure I.7	Representation of the band bending in semiconductor particles	18
Figure I.8	Trap sites in TiO_2	22
Figure II.1	Energy levels and decay pathways of a simple molecule	27
Figure II.2	Energy levels and decay pathways of a molecule with two excited states	35
Figure II.3	Jablowski diagram of a non-luminescent molecule having a triplet state	37
Figure III.1	Representation of the three different dyes used	40
Figure III.2	Schematical representation of the picosecond flash photolysis experimental set-up	43
Figure III.3	Schematical representation of the photoacoustic detection system	50
Figure IV.1	Absorption spectra of TiO_2 colloidal particles at different concentrations	54

Figure IV.2 Absorption spectrum of TiO_2 colloidal particles at pH=1.5 and pH=3.0 ____ 56

Figure IV.3 Absorption spectrum of the $CuPcTS^{4-}$ ____ 57

Figure IV.4 Absorption spectrum of the $RuPPS^{4-}$ ____ 58

Figure IV.5 Picosecond flash photolysis of a TiO_2 suspension ____ 60

Figure IV.6 Kinetic analysis of the picosecond flash photolysis of a TiO_2 suspension ____ 62

Figure IV.7 Picosecond flash photolysis of a solution of TiO_2 and $CuPcTS^{4-}$ ____ 63

Figure IV.8 Kinetic analysis of the picosecond flash photolysis of a solution of TiO_2 and $CuPcTS^{4-}$ ____ 65

Figure IV.9 Picosecond flash photolysis of a solution of TiO_2 and $RuPPS^{4-}$ ____ 66

Figure IV.10 Kinetic analysis of the picosecond flash photolysis of a solution of TiO_2 and $RuPPS^{4-}$ ____ 68

Figure IV.11 Picosecond flash photolysis of a solution of TiO_2 and erythrosin ____ 70

Figure IV.12 Picosecond flash photolysis of a solution of TiO_2 and $CuPcTS^{4-}$ at different temperatures ____ 73

Figure V.1 Proposed mechanism for the interpretation of the picosecond flash photolysis results ____ 82

Figure V.2 Picosecond flash photolysis of a solution of TiO_2-$CuPcTS^{4-}$ and a solution containing only $CuPcTS^{4-}$ ____ 84

Figure V.3 Subtraction of the transient observed at 500 ps from the transient at 10 ns for a solution of TiO_2-$CuPcTS^{4-}$ ____ 86

Figure V.4	Energy levels for the reduction of the $^*CuPcTS^{4-}$ by the conduction band of the TiO_2	89
Figure V.5	Molecular diagram of the CuPc	90
Figure V.6	Schematical representation of the overall process	94
Figure V.7	Schematical representation of the transient signal as a function of the energy squared	100
Figure VI.1	Photoacoustic signal of a solution of $K_2Cr_2O_7$ as a function of time	107
Figure VI.2	First photoacoustic pulse of a solution of $K_2Cr_2O_7$	109
Figure VI.3	Photoacoustic signal as a function of the absorbance of solutions of $K_2Cr_2O_7$.	111
Figure VI.4	Photoacoustic signal of a solution of $ZnTPPS^{4-}$ and a solution of $Fe(phen)_3^{2+}$	117
Figure VI.5	Photoacoustic signal of a solution of TiO_2-$RuPPS^{4-}$ and a solution of $Fe(phen)_{32}^{+}$	119
Figure A.1	Schematical representation of the electronic circuit used in photoacoustic experiments	131
Figure B.1	Time process of the signal in photacoustic experiments	139
Figure B.2	Photoacoustic signal acquisition with the boxcar	141

LIST OF TABLES

Table IV.1	Absorption coefficient of TiO_2 at different concentrations	53
Table V.1	Absorbance of the TiO_2 and the dyes at 355 nm before and after mixing	79
Table V.2	Absorption maxima of reduced porphyrines and phthalocyanines and the transient observed for the TiO_2-$CuPcTS^{4-}$ system	83
Table A.1	Typical photoacoustic experimental conditions	136

I. INTRODUCTION: ESSENTIAL SEMICONDUCTOR CONCEPTS

I.1 Introduction

In 1833, Faraday found that the resistance of silver sulfide decreases with an increase of temperature. This phenomenon contradicted with the usual behaviour of metals. This gave rise to a new classification of solids based on their resistivity as a function of temperature. Three different classes of solid are obtained based on the occupation of their energy bands (Fig. I.1).

The insulator has all its energy bands filled or empty, whereas the metal has an energy band partially filled. The semiconductor has one band slightly filled or one band slightly empty along with a nearby band or nearby carrier states which can influence the filling on the slightly perturbed band. The semiconductor with one energy band slightly filled will have more electrons than holes and will be an n-type semiconductor. The semiconductor with one partially empty band will have more holes than electrons and be a p-type semiconductor. The semiconductor has decreasing resistivity with an increase of temperature due to the increase of charge carriers with temperature.

The semiconductor is usually seen as having two major energy bands (Fig. I.2). The valence band (VB), which consists in the assembly of mainly the bonding orbitals of

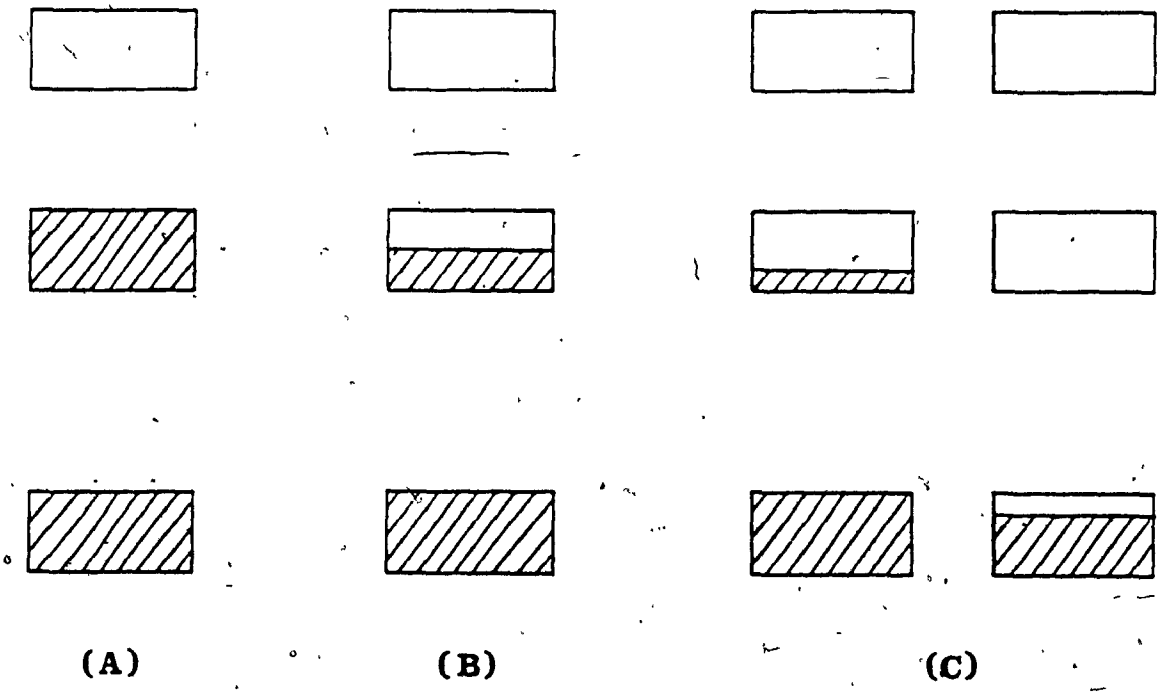

Figure I.1 The energy bands of solids.
A) insulator, B) metal, and C) semiconductor.

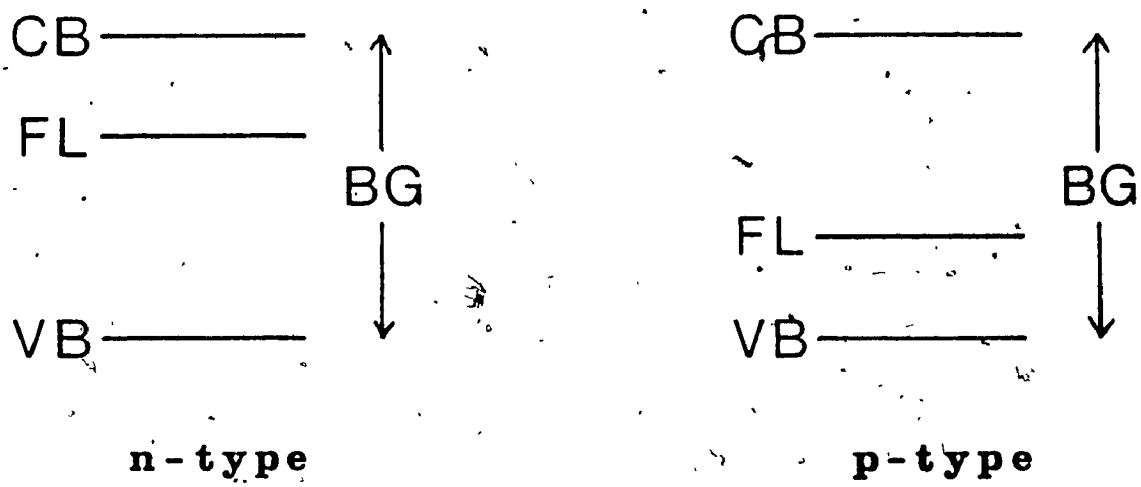

Figure I.2 Energy bands of semiconductors. The Fermi level (FL) is closer to the conduction band (CB) for the n-type whereas it is closer to the valence band (VB) for the p-type. The band gap (BG) is the energy between the CB and the VB.

the atoms which constitute the solid, whereas the conduction band (CB) consists mainly of the assembly of the antibonding orbitals of the atoms of the solid. The two bands are separated by a gap of forbidden electron energy which is called the band gap.

The band gap must be smaller than 2,0 eV for an intrinsic semiconductor. This value permits electrons from the valence band to be promoted to the conduction band upon heating of the solid. Extrinsic semiconductors may have a band gap larger than 2,0 eV and they are made semiconducting by the addition in the lattice of a foreign species which has a different electron configuration (doping). A p-type semiconductor will have a dopant which has one less electron (one more hole) than the core material, whereas the n-type semiconductor will have a dopant with an extra electron.

I.2 The semiconductor

In this thesis we deal with the photochemical electron transfer characteristics of colloidal TiO_2. In the next few sections, the background concepts needed for the experiments described are given.

I.2.1 TiO_2 as a semiconductor

Before choosing a specific reactant for the industrial application of a reaction, one must first consider the theoretical aspects of the reaction in addition to the

economic factors of this reactant. The choice of TiO_2 as a catalysis in solar energy conversion has been motivated first by its properties as a semiconductor, and second by its low cost and high availability. We will not consider this last point since in this thesis we are dealing only with fundamental aspects and the work remains far from industrial application.

The energy levels of TiO_2 are the aspects that have drawn most attention of researchers. Figure I.3 represents the energy levels of TiO_2 compared with the energy level for the reaction of water cleavage vs the normal hydrogen electrode scale. As one can see in the figure, the conduction band of TiO_2 at -0,1 V is just above the energy for the reduction of water into hydrogen and also the valence band of TiO_2 at +3,0 V permits the oxidation of water to oxygen. It is then obvious that TiO_2 will meet the theoretical conditions to be a catalyst for water cleavage. Nevertheless, the band gap of TiO_2 at 3,1 eV gives absorption at 350 nm for band gap edge excitation. It is thus outside the range of the visible spectrum and into a low intensity domain of the spectrum emitted by the sun. Potentially, this problem might be overcome by the use of a sensitizer.

I.2.2 The electronic properties of a TiO_2 semiconductor.

As we have mentioned previously, TiO_2 is commonly prepared as an n-type semiconductor so that it will have

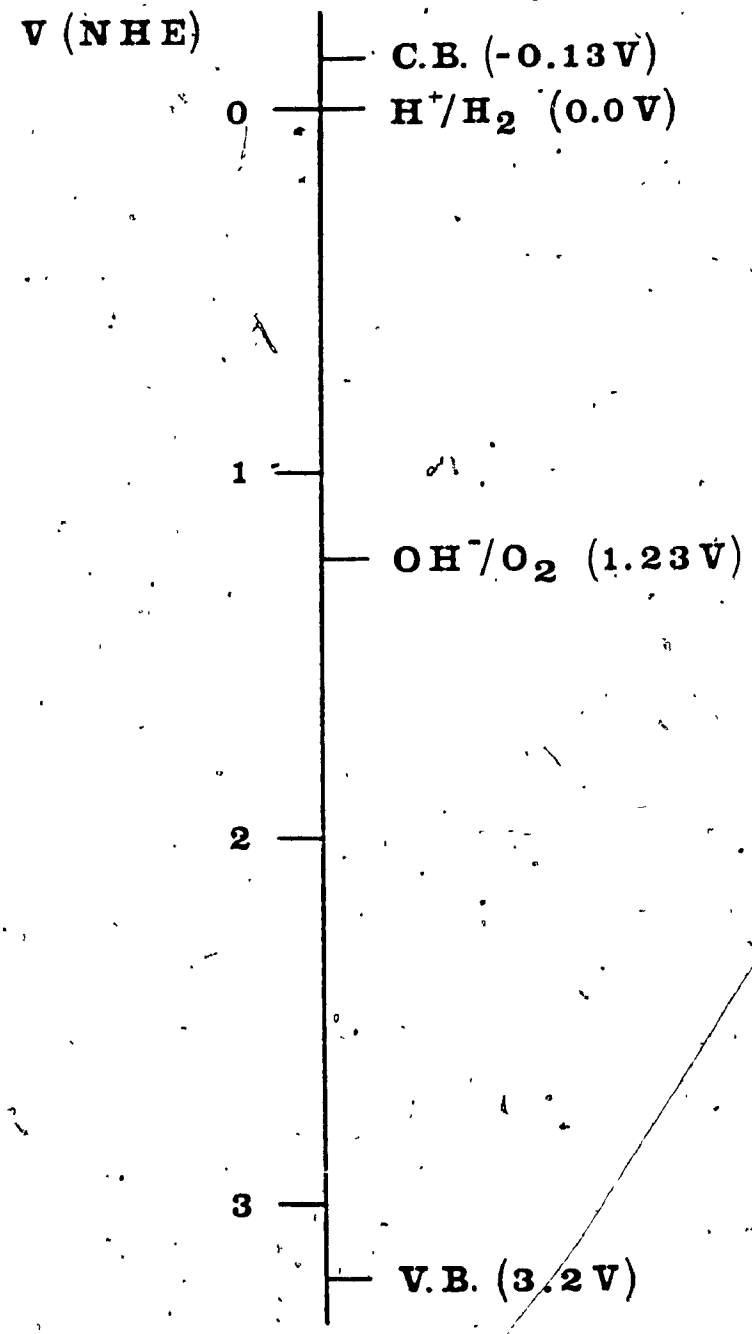

Figure I.3 Energy levels of TiO_2. Respective energy level (NHE) of the C.B. and V.B. of the TiO_2 with the energy levels of the water cleavage.

its Fermi level closer to the conduction band than to the valence band (Fig. I.4a). The exact position of the Fermi level depends on the number of charge carriers in the TiO_2 or the number of dopant molecules in the crystal. Typical values for doping concentrations vary between 10^{15} cm^{-3} to 10^{19} cm^{-3} depending on the treatment applied to the crystal.

Upon contact of the semiconductor with an electrolyte solution, the equilibrium Fermi level of the semiconductor will become equal to the Fermi level of the solution and charges will accumulate at the surface of the semiconductor (Fig. I.4b). This will give rise to a bending of the CB and the VB and is called band bending. The width of the region of band bending depends on the difference of potential between the two Fermi levels (semiconductor and solution) and also the density of doping molecules. Upon illumination of the semiconductor (Fig. I.4c), electrons will be transferred from the VB to the CB leading to an increase in the Fermi level of the semiconductor. Electrons will move to the interior of the semiconductor, whereas the holes created in the valence band will move to the surface.

A steady state will be reached when the rate of generation of electrons and holes equals the rate of recombination plus the rate of transfer of holes and electrons across the surface of the semiconductor. There

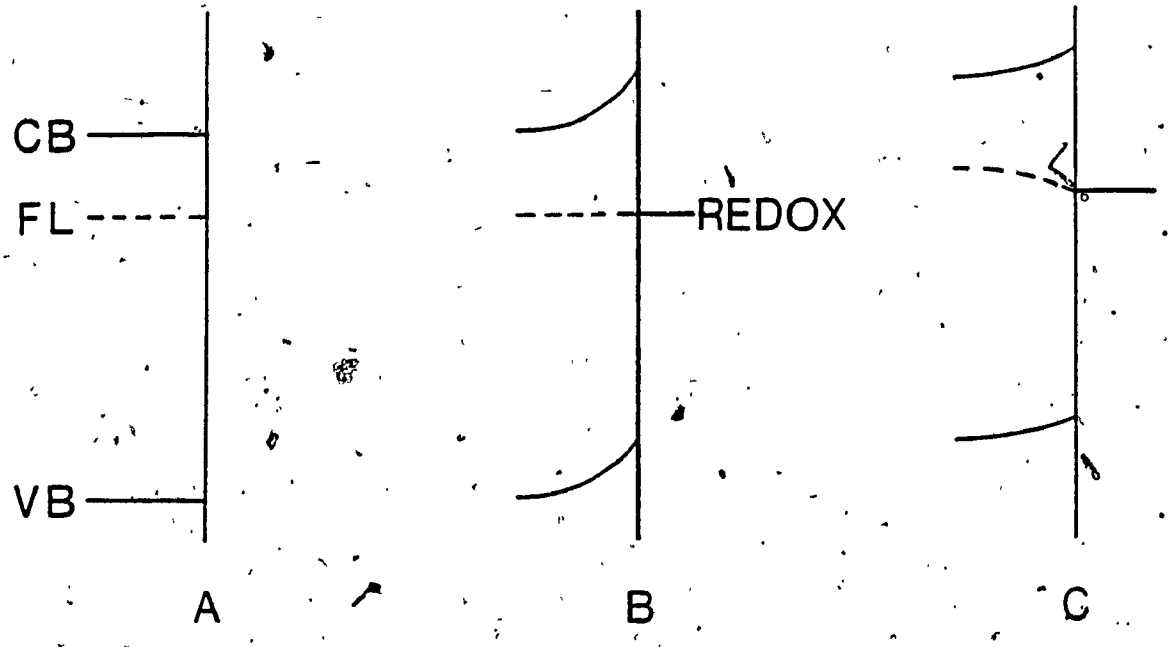

Figure I.4 Energy of a single-crystal of TiO_2: A) as a solid, B) in contact with an electrolyte, and C) upon illumination.

are many factors reducing the quantum efficiency of semiconductor photochemistry, specifically the recombination reaction mentioned previously and also the back reaction where the reduced (oxidized) species gives back the electron (hole) to the semiconductor providing only heat to the system.

I.3 Colloidal semiconductor particles.

Duonghong et al. (1982) were the first to develop a technique to work with colloidal particles of TiO_2. Their work was motivated by the fact that colloidal particles do not exhibit large light scattering. The low intensity of light scattering permits the analysis of elementary events using spectroscopic methods. Another advantage of the absence of scattering is the increase of quantum efficiency due to the increase of light absorption.

I.3.1 Size Quantization.

The advantages of colloidal particles make it very interesting to use these particles for the study of semiconductor chemistry. However, two questions must be answered: 1) is a colloidal particle a semiconductor and to what size limit; 2) what is the relation between the colloidal "semiconductor" and the semiconductor as bulk material? Let's go back to the previous section and build the bands we have defined there.

If we take an isolated atom or molecule in space, the

electrons of this atom will have energy levels called orbitals separated by a certain amount of energy and following the Pauli principle. If we now take two of these atoms and we bring them together in space, each of the atoms having the same energy levels, the energy levels will be doubled, one bonding and one antibonding (Fig. I.5a). If we continue to bring other identical atoms up to these two, we will form a lattice of identical atoms having identical energy levels (Fig. I.5b). The combination of these identical energy levels is at the origin of the band structure of the crystals.

For the semiconductors, we take into account only the highest occupied band (HOB) and the lowest unoccupied band (LUB) since the other ones will not have any effect on the semiconductivity. The HOB is formed from the valence orbitals of each atom and is called the valence band (VB). It corresponds to bonding orbitals of molecules. The LUB is responsible for the conduction of the electron and is called the conduction band (CB); it is formed from the antibonding orbitals.

The origin of the bands in semiconductors can also be visualized by solid state physics using the nearly-free-electron model for which the band electrons are weakly perturbed by the periodic potential of the ion cores (Kittel, 1976). Starting with the free-particle Schrodinger equation in three dimensions and confining the elec-

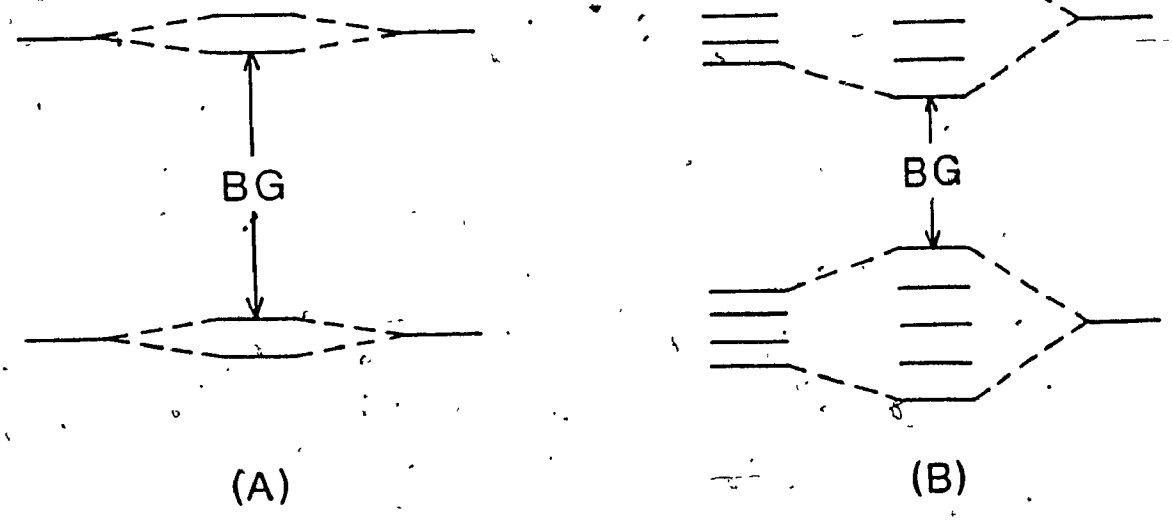

Figure I.5 Formation of the bands in semiconductors. Upon interaction of two atoms (A) and n atoms (B).

trons to a cube of edge L, the energy E_k of the orbital with wavevector k is defined as:

$$E_k = \frac{\hbar}{2m}(k_x^2 + k_y^2 + k_z^2) \qquad (I.1)$$

where, for periodic boundary conditions,

$$k_x, k_y, k_z = 0; \pm \frac{2\pi}{L}; \pm \frac{4\pi}{L}. \qquad (I.2)$$

m is the free electron mass and $\hbar$ is the Plank constant over 2π.

As is seen in X-ray crystallography, the Bragg reflection is a characteristic feature of wave propagation in crystals. Unlike the entirely free electrons where there are values of energy for any value of the k vector, the nearly free electrons in a crystal will have certain regions of energy where solutions of the Schrodinger equation do not exist. Those energy gaps are the results of Bragg reflection of electron waves in crystals and can be visualised for a system in one dimension as shown in Figure I.6.

Both molecular chemistry and solid state physics show how atomic interactions give rise to bands in the crystal and forbidden energy levels called band gaps. Both cases are valid for large assemblies of molecules forming crystals, but will not necessarily be acceptable for very small semiconductor particles. In the case of the nearly free-electron model, we have assumed that the electron had

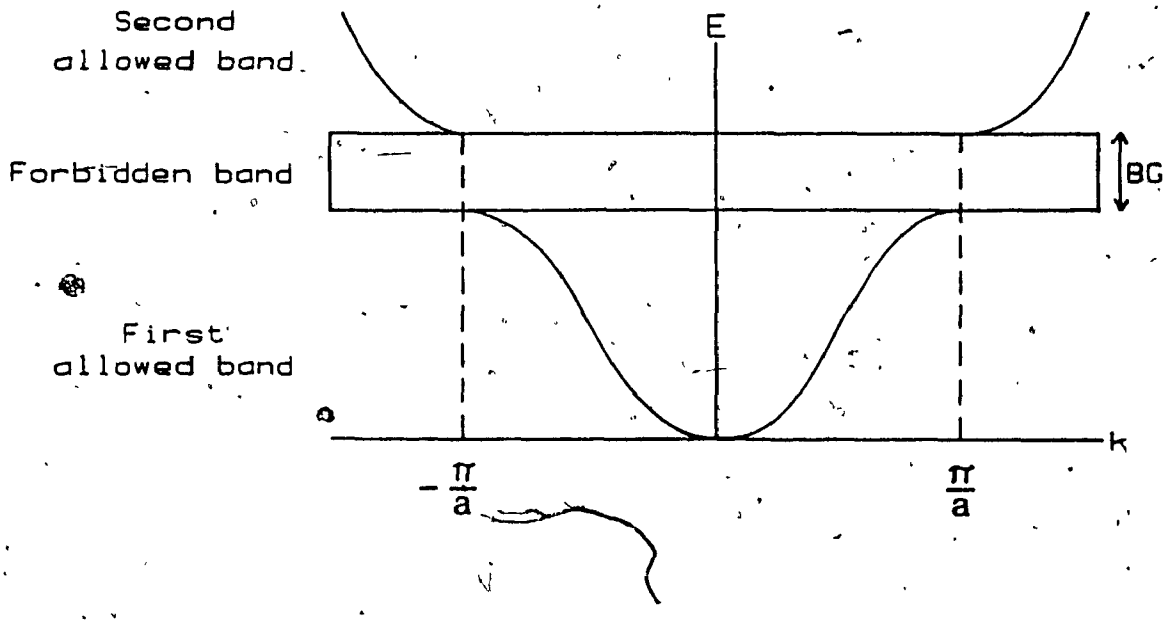

Figure I.6 Formation of energy gaps in crystals. At $\pm\pi/a$, there is no solution of the Shrödinger equation giving rise to a band gap (B.G.). (Redrawn after Kittle, 1976).

little interaction with the ion core which will not be the case in small semiconductor particles. The electrons in the semiconductors are in potential wells defined by the conduction and valence bands (Nozik et al., 1985). This confinement leads to the creation of discrete levels in the conduction and valence bands if the semiconductor is small due to the interaction between the electron and the ion core. Also, we have assumed an infinite periodicity of the lattice which is not at all the case for small semiconductors.

In the case of molecular chemistry, we have previously seen that the formation of the bands is started by the contact of two identical atoms (molecules) followed by the addition of other atoms (molecules) to form a lattice. If we stop the addition of atoms (molecules) before having a large crystal, the spacing between the valence band and the conduction band will be larger. This can be seen in Figure I.5b where the spacing between the HOB and the LUB is decreasing with the addition of new atoms (molecules) and a limit is reached when a lattice large enough is formed. The size of the lattice necessary to reach this limit depends on the electronic properties of the material, but is often found to be between 50 and 200 Å, or an assembly of about 1×10^4 atoms (molecules) (Rossetti et al., 1985). Then, for semiconductor colloidal particles, the band gap should decrease with the increase of particle size approa-

ching a limit, which is the band gap of the bulk material. Below this limit, one speaks of quantization effects. At the limit, an addition of orbitals to the valence band or conduction band will not increase the stability of the electrons in the bands.

Brus (1984) has developed a model for the determination of the size of semiconductor particles that can display quantization effects. Starting with the fact that the band gap of a semiconductor is, by definition, the energy necessary to create an electron and a hole far enough apart so that their Coulomb attraction is negligible, he defined the energy of the band gap as the energy slightly above the first exciton. An exciton is an electron and a hole created upon excitation and having Coulombic interactions with each other sufficient to create a bound state. The exciton radius can be defined as the Bohr radius of the hole and is given by:

$$r_{exc.} = \frac{\varepsilon \hbar^2}{m_e e^2} \quad \text{(CGS)} \qquad \text{(I.3)}$$

where ε is the dielectric constant of the material, $\hbar$ is the Plank constant over 2π; m_e the effective mass of the electron and e the charge of an electron.

Bruss suggests that the size of the 1S exciton provides a natural, intrinsic measure of linear dimension at which quantization size effects will occur. At sizes lower than this exciton radius, the particle is essentially

not large enough for the intrinsic band gap to form, i.e., to sustain noninteraction of holes and electrons. The combination of small effective masses and weak Coulombic attraction in semiconductor material causes the exciton radius to extend over a large region. For example, the lowest 1S exciton of CdS has a diameter of ~60 Å.

I.3.2 Size effects.

a) Optical absorption:

Since absorption spectra give a direct representation of the energy levels in a compound, the size quantization effect described will be first observed in absorption spectra of small semiconductor particles. The absorption spectra of colloidal particles can be predicted from the bulk properties of materials via Mie Scattering theory (Born and Wolf, 1965) if the colloids have the same wavelength dependent dielectric constant as the bulk material. The absorption cross section contains only the electric dipole term and can be expressed as:

$$\sigma = 8\pi^2 r^3 \left[\mathrm{Im} \frac{\varepsilon' - 1}{\varepsilon' + 2}\right] \qquad (I.4)$$

where r is the sphere radius and ε' is the ratio of the complex dielectric coefficient of the bulk material $\varepsilon(\lambda)$ over the real dielectric coefficient of the solvent.

This implies that the optical absorbance of a colloi-

dal solution is simply proportional to the total amount of colloidal mass. Equation I.4 should be valid only if the lattice structure of the colloidal particle is the same as the bulk material and also if there are no size effects in the electronic structure. This latter condition can not be true for very small particles as discussed previously giving rise to a deviation of the Mie theory. This is observed by a blue shift in the absorption edge of small semiconductor particles as compared to the bulk material. This blue shift can reach values as large as 2 eV (~200 nm) (Rosetti et al., 1984).

b) Band bending:

Even if it is unlikely that there will be quantization effects on band bending, there will still be size effects due to the lack of average separation between holes and electrons. For a TiO_2 semiconductor particle, assuming a voltage drop of 1 V and a density of donors (N_d) equal to 1 x 10^{15} cm^{-3}, the band bending width will only be 0,87 µm. The colloidal particles which have dimensions lower than the band bending width will not be able to sustain the required voltage. This can be seen in Figure I.7 where the colloidal particle with $r_0 >> W$ shows a band bending of 1 V whereas the particle with $r_0 << W$ shows a very small band bending (10,9 µV) for the same material and the same N_d.

The band bending acts as a field in particles to produce the migration of the electrons at the surface and

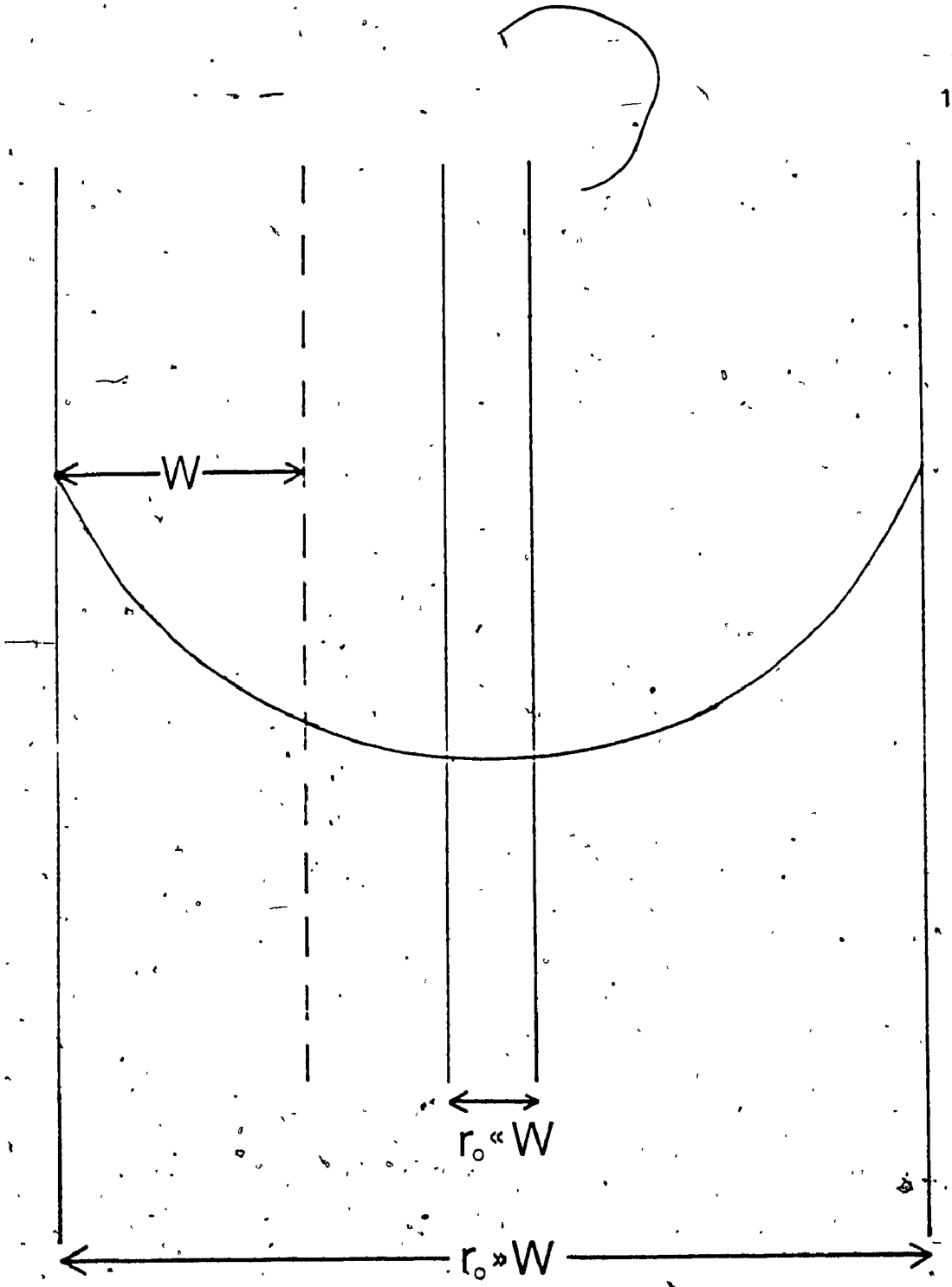

Figure I.7 Representation of the band bending in semiconductor particles. Semiconductor particle with the radius larger than the band bending ($r_0 >> W$) and the radius smaller than the band bending width ($r_0 << W$).

the holes in the interior of the particle. Since in the case where $r_0 << W$ the band bending is too small to create a field, the hole and the electron will not be forced to migrate. This is another proof that the hole and the electron will always have interaction between them.

c) Charge separation:

As we have seen in the previous section, charge separation between the hole and the electron cannot be achieved due to the absence of band bending. The only mechanism that can prevent the charges recombination will be the diffusion of the charges at the surface of the colloidal particles where one of the charges can be removed by the presence of a scavenger (or by trapping in an impurity deep site). Since the particles are very small, the time of diffusion will be very short. As an example, the time of diffusion of an electron in a colloidal particle of TiO_2 may be approximated by the Ficks diffusion law (Gratzel and Frank, 1982):

$$\tau_D = r_0^2 / (\pi^2 D_{e-}) \qquad (I.5)$$

where D_{e-} is the diffusion coefficient of the electron which has been determined to be $2,0 \times 10^{-2}$ cm^2/s (Yana, 1963). The time for an electron to diffuse from the center of a 50 Å radius particle to the surface is 1,3 picoseconds (ps). This implies that if the rate of electron transfer or hole transfer through the surface of the particle is

large, the recombination of the hole and electron should not be important. In spite of the absence of band bending, charge separation will be efficiently obtained through the diffusion mechanism which gives another reason to suppose that colloidal particles will be very efficient for photoreactions.

I.4 Trapped states

The TiO_2 colloids have physical properties depending on the defects and impurities in the crystal lattice. Contrary to a single crystal, the defects in colloids will be very important due to the size of the particle. Most of the colloids which are smaller than 50 Å are amorphous to X-ray (Dimitrijevic et al., 1984). Particles bigger than 50 Å, but smaller than 200 Å show single crystal diffraction patterns of low intensity. The amorphous characteristic of these colloids is a signal of the large number of defects in the lattice structure of TiO_2 colloids.

The impurity density in colloids depends mostly on the preparation procedure. It is not easy to characterize and it is very difficult to reproduce. The impurities can vary from cationic species trapped during the formation of the colloids to reduced titanium species (Ti^{3+}). They can also be anionic species replacing the oxygen atoms in the lattice or variations of the oxo to hydroxo ratio.

The defects and impurities in the lattice of TiO_2 colloids are at the origin of the trap sites. The trap

sites are responsible for the capture of a hole or an electron inside or at the surface of the colloids. Bulk semiconductor studies suggest that trap sites can be classified in two groups: The "shallow traps" having ionization energies lower than 1 eV and the "deep traps" with ionization energies greater than 1,5 eV. The shallow traps are mainly caused by defects in the lattice whereas the deep traps come mostly from impurities.

Figure I.8 shows the main trap sites of a TiO_2 single crystal observed by Ghosh et al. (1969) with their assignments of ionization energies. These levels were measured using thermal ionization, photothermal ionization and photoconductivity. In this work, we will not pay attention to the shallow traps since they absorb in the far infrared, which is not in the domain accessible in our experimental set-up. The five important trap sites which have been discussed by Ghosh et al. are the ones absorbing between 420 and 630 nm and they are represented in Figure I.8.

There is not yet any general agreement on the nature of these trap sites, but some trends can be observed. The majority of researchers have observed a large band in the region of 650 nm, which is responsible for the blue color of n-doped TiO_2, and this has been attributed to an n-trap site defined as Ti^{3+} in the lattice or at the surface (Kolle et al., 1985). There are no major differences of

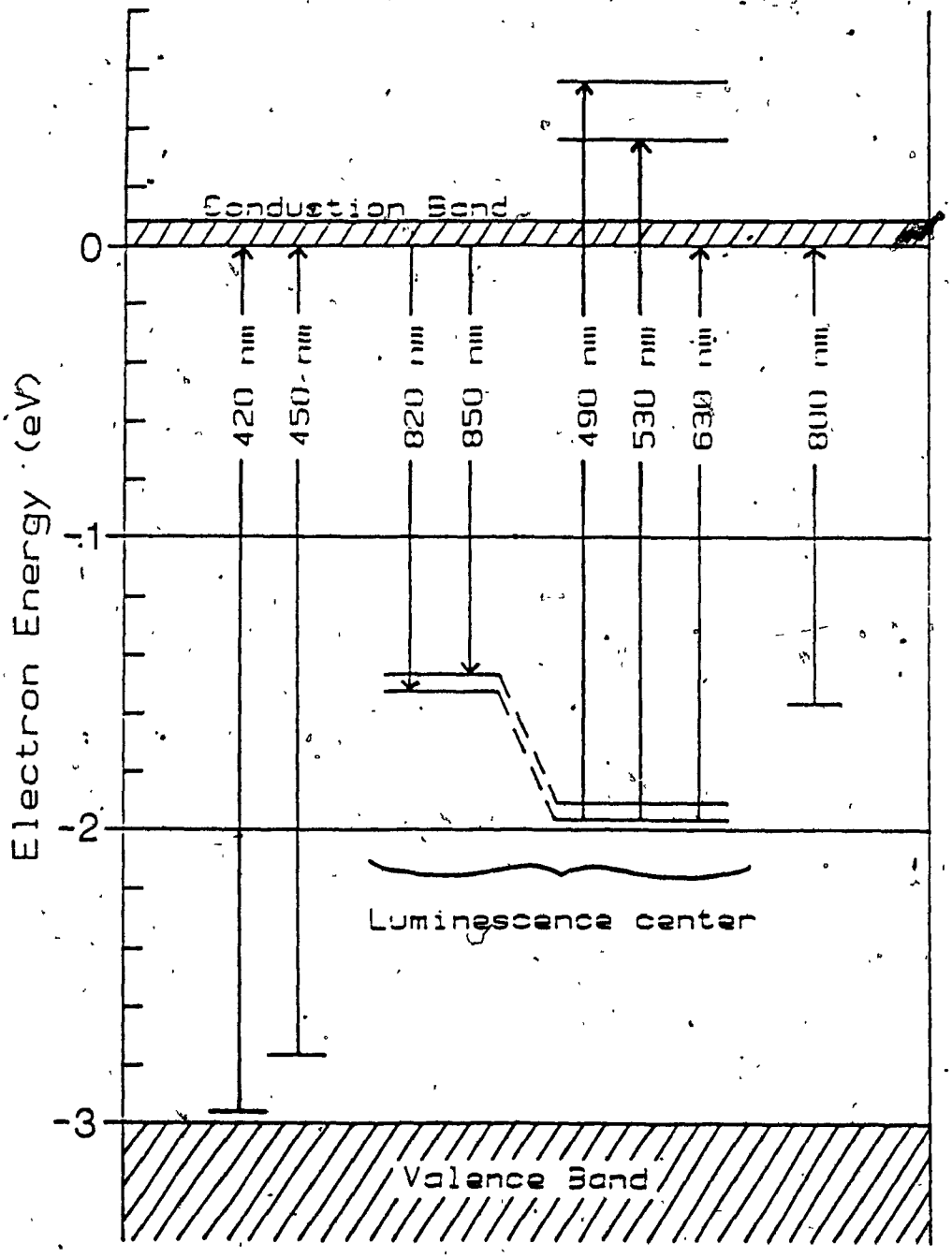

Figure I.8 Trap sites in TiO_2. Representation of the deep trap sites in n-doped TiO_2 measured by ionization energy. (Redrawn from Ghosh et al., 1969).

opinion on the attribution of this band, except for the question of spatial position of the Ti^{3+} atom in the lattice (Howe and Gratzel, 1985).

Assignment is not so easy for the band appearing on the blue side of the absorption spectra. n-type sites near the conduction band (Figure I.8) or p-type sites near the valence band can be responsible for the blue absorption. The n-type trap site is attributed to a Ti^{3+} species since the absorption maximum corresponds with the absorption maximum of $Ti(OH_2)_6^{3+}$ observed in solution (Henglein, 1982). The p-type site is attributed to an oxygen defect giving an electron vacancy at that position. The species will then be O^- inside the semiconductor or an hydroxyl radical ($OH^\cdot$) at the surface of the semiconductor (Anpo et al., 1985).

One point which seems to be common to all the bands observed is that they are very broad which is an indication that the transition involves a broad band level as origin or destination (Royce and Kay, 1984). Both the valence band and the conduction band have levels broad enough to account for this type of transition.

II. INTRODUCTION: PHOTOACOUSTICS

II.1 History of Photoacoustics:

In 1880, Bell briefly reported the accidental discovery of the photoacoustic effect during his work on the photophone (Bell, 1880). His photophone[1] consisted of a voice-activated mirror, a selenium cell, and an electrical telephone receiver. The modulated sunlight beam was focused onto the selenium cell giving electrically reproduced telephone speech. While experimenting with his photophone, Bell discovered that an audible signal could be obtained in non-electrical systems when the beam was modulated at 1000 Hz.

After minor changes in his photophone system to study this specific effect, Bell (1881) discovered the optical absorption dependance of the photoacoustic effect in solids, liquids, and gases. In the 1880s, the gas laws were already well known so that the photoacoustic effect in gases was fairly well understood. The case was not the same for solids and liquids and only recently has a complete theory been accepted even though many authors of the nineteenth century came close to the modern theory.

[1] Bell's photophone is kept in a museum in Nova Scotia, Canada.

No further improvements were reported before the development of the modern microphone. In 1938, Viengerov (1938) reported the use of a microphone in a photoacoustic apparatus to measure the concentration of gaseous species in gas mixtures. All the experiments following this one dealt with gaseous samples. Limited work continued up to 1950 when the photoacoustic effect fell again into oblivion. In the early 1970s, with the entrance of lasers, the photoacoustic effect started to regain popularity and it was in 1973 that Parker (1973) gave the first theory of nongaseous photoacoustics to account for the absorption of light at the window of his gaseous chamber. This theory is still used for a simple description of the photoacoustic effect in condensed media. In 1975, Rosencwaig and Gersho (1975) gave a general theory of the photoacoustic effect in condensed media which continues to be improved year after year.

II.2 The Photoacoustic Effect

II.2.1 The theory of photoacoustics in a gas.

By definition, the photoacoustic effect is composed of two different processes: the absorption of light by molecules, and the release of the energy absorbed to produce an acoustic wave.

Suppose that we have a gas in a closed container with a window to let the light penetrate the container. The

absorption of a part of the spectrum by the molecules of gas in the chamber will bring these molecules from the ground state (E_0) to an excited state (E_1) (Figure II.1). From this excited state, the molecules can follow different processes to release the energy absorbed: radiative deexcitation (k_r), photochemistry (k_p), radiationless decay (k_h), etc. The radiationless deexcitation involving the collision of an excited molecule with any gas molecule in the container by means of which both molecules increase their kinetic energy, is at the origin of the photoacoustic signal.

This increase in kinetic energy will be seen as an increase of the heat energy monitored by a change of temperature in the chamber. Since the container is closed, the local heating of the gas will cause a small fluctuation of the pressure which can be modulated if the light entering the chamber is modulated at a frequency much lower than the energy releasing process. This periodical change in pressure is an acoustic wave or a sound wave that can be detected by a microphone.

II.2.2 The theory of photoacoustics in condensed matter

Two different approaches can be used to monitor the photoacoustic signal in condensed matter. The first one consists of using a gas-microphone system similar to the one described above for detection. The heat produced during the radiationless decay of excited molecules is

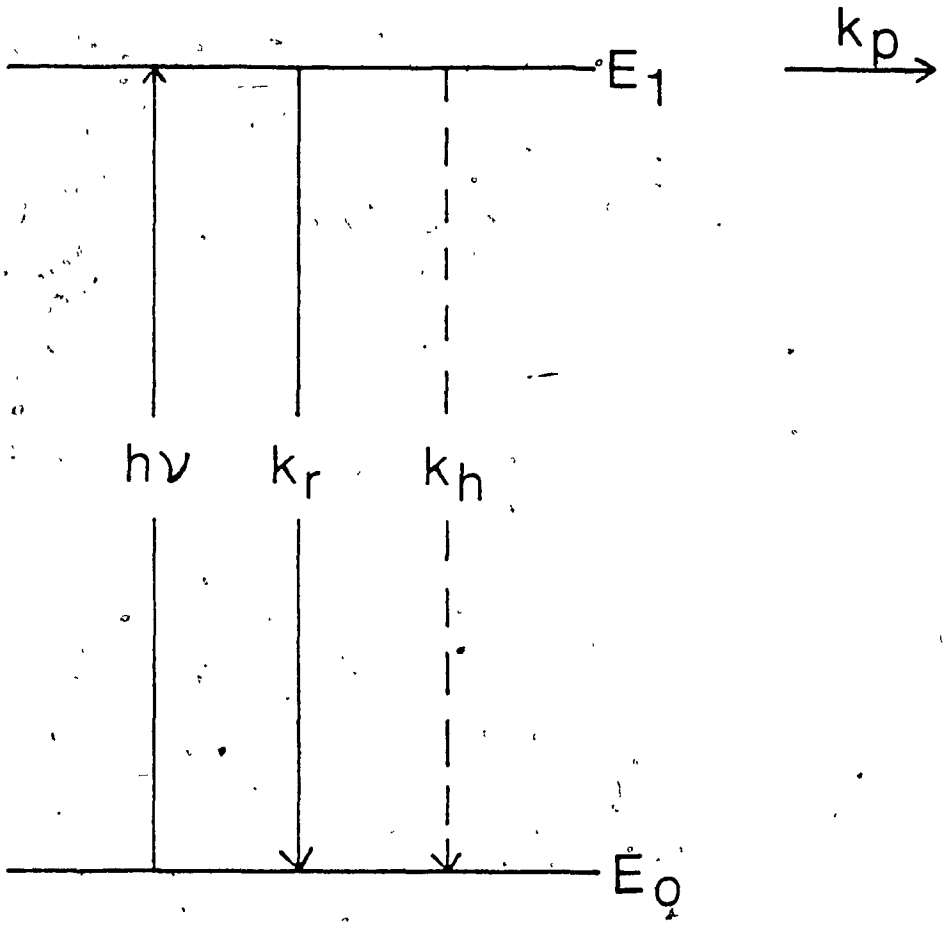

Figure II.1 Energy levels and decay pathways of a simple molecule. Major deactivation pathways following the absorption of light ($h\nu$) by a molecule that goes from the ground state (E_0) to an excited state (E_1). K_p is the photochemical deactivation, K_r is the radiative decay, and K_h is the radiationless decay.

transferred at the surface of the condensed matter to an inert gas in a closed chamber. The same periodical pressure fluctuations as described previously will be detected via a microphone.

The acoustic wave is detected directly in the condensed matter in the second approach. When molecules of condensed matter have absorbed modulated light, the deexcitation of these molecules produces a periodic heating of a local area in the medium. This periodic heating can be dissipated through two mechanisms. The first one consists of the conduction and diffusion of the heat to the surroundings. The distance over which heat is transferred will depend upon the thermal diffusivity of the material and the modulation frequency of the light. This energy transfer mechanism is called the thermoacoustic mode and is measured with a gas-microphone detection system.

The second mode of dissipation of energy involves the thermoelasticity of the material. The heat is coupled with the acoustic phonons of the lattice to produce acoustic waves in the material. The propagation distance is limited only by the walls of the container and the propagation rate will be equal to the speed of sound in the medium. In the coupling of the heat with the phonons, all the molecules of the lattice vibrate in the same mode, whereas in the thermoacoustic mode, the molecules vibrate randomly.

The gas-microphone system cannot be used for the

detection in the thermoelastic mode since the transfer of the acoustic waves from the condensed matter to the gas at the surface is very inefficient. A piezoelectric detection system is used to detect the acoustic waves in a condensed medium.

II.3 The piezoelectric detector:

Piezoelectric materials have ferroelectric properties such that below the ferroelectric Curie point, the electric dipoles inside the materials are all aligned in the same direction. In addition to the ferroelectric properties, the absence of a center of symmetry is another condition for the material to be piezoelectric.

Piezoelectricity involves the interaction between the electrical and mechanical properties of the material. Upon applying a voltage through the piezoelectric material, it responds with a mechanical strain. The reverse is also true which means that in response to a stress, the piezoelectric material will give a voltage. This coupling between the mechanical and electrical function of the material shows that both the elastic and dielectric constants are involved in the piezoelectric properties of the material.

At the beginning, piezoelectric materials were made of crystals such as quartz and Rochelle salt and even if these are still widely used, they have been replaced by polycrystalline ceramics in most of the applications. The ceramics

are usually made of a solution of lead zirconate titanate (PZT) that can be modified with other additives. The polycrystalline ceramic is an assembly of small crystals, each one having several ferroelectric domains. The ceramic as a whole is isotropic when it is first produced, but it is made piezoelectric by polarization. The poling treatment consists of applying a high electric field to the ceramic plunged in a heated oil bath at a temperature just below its Curie point. The piezoelectric ceramics are usually coated with silver or nickel for the attachment of the electrical wires.

The amplitude of the voltage measured across a piezoelectric is proportional to the stress applied to the material through its elastic and dielectric constants. It is then possible to have a measure of the acoustic wave produced in a condensed matter by measuring the stress caused by this acoustic wave on a piezoelectric. The detection with a piezoelectric is less sensitive than with a gas-microphone system, but it is very useful for large samples of condensed matter.

II.4 Relation between absorption and photoacoustic signal.

We can derive the relation between the absorbance of a solution and the corresponding photoacoustic signal without going into complicated mathematical arguments. Suppose we have molecules in solution which absorb at a certain

wavelength. The heat produced in the solution due to radiationless decay after the absorption of one pulse of light is:

$$H = E_a - E_r - E_p \qquad \text{(II.1)}$$

where E_a is the energy absorbed, E_r is the energy lost by radiation decay, and E_p is the energy lost through photochemical reactions. For a more general situation, we will have:

$$H \cong E_a - \Sigma\, \phi_i\, E_i \qquad \text{(II.2)}$$

where E_i is the energy of a process which is not producing heat in the solution and ϕ_i is the quantum yield of that process. As we have seen before, the heat deposited in a solution can be dissipated in two modes so that by detecting the signal with a piezoelectric, only a part will be detected. The heat dissipated through the thermoelastic mode will be:

$$Q = H - E_t \qquad \text{(II.3)}$$

where E_t is the energy lost in the thermoacoustic mode. By including the energy lost through the thermoacoustic mode in all the processes not giving heat (eq. II.2), the energy input that goes into the thermoelastic mode is:

$$Q = E_a - \Sigma\, \phi_i\, E_i \qquad \text{(II.4)}$$

The photoacoustic stress seen by the piezoelectric will depend mostly on the thermal and mechanical properties of the solution.

$$P = \frac{B\, \alpha_t\, Q}{\rho C - 1} \qquad \text{(II.5)}$$

where B is the bulk modulus, α_t is the coefficient of linear thermal expansion, ρ is the density, C is the specific heat, and l is the thickness of the sample. The stress applied to the piezoelectric is coupled to the electric field created by the coupling constant k and the piezoelectric constant g in the direction of the stress so that the voltage read across the piezoelectric will be equal to

$$V = k\ g\ P \qquad \text{(II.6)}$$

By replacing the equation II.5 in the equation II.6, we get:

$$V = \frac{A}{l}\ Q \qquad \text{(II.7)}$$

where A is a constant depending on the mechanical and electrical properties of the piezoelectric as well as the thermal properties of the solution. By substituting the equation (II.4) in this equation, we obtain:

$$V = \frac{A}{l}\ (E_a - \Sigma_i\ \phi_i\ E_i) \qquad \text{(II.8)}$$

In photoacoustics, we usually study molecules having a very large quantum yield for radiationless decay so that we can assume that the quantum yield for the other processes is zero. We can make a further approximation by assuming that all the heat generated by radiationless decay is dissipated through the thermoelastic mode. This is not an extreme approximation since if we keep the same medium, the

fraction of the heat that will go through thermoacoustic modes will be the same and this factor will be included in the constant A. We can then simplify the equation (II.8) so that for a specific medium:

$$V = A\ E_a \qquad (II.9)$$

where the energy absorbed per pulse will be:

$$E_a = E_i\ (1 - e^{-\beta l}) \qquad (II.10)$$

E_i is the incident energy, β is the molar absorptivity coefficient, and l the optical path length.

We then have a direct relation between the absorption of a sample and the photoacoustic signal detected with a piezoelectric. By using a known absorber, one can standardize the conditions and obtain the value of A for a certain medium. The photoacoustic signal can be used to measure the concentration of a compound if we know the quantum yield for the radiationless decay.

II.5 Sensitivity of the photoacoustic method.

One of the important advantages of the photoacoustic method is the possibility to measure the absorption of samples which exhibit some light scattering. The other important advantage is sensitivity. The photoacoustic detection of gaseous molecules can easily reach absorption coefficients in the order of 10^{-6} cm^{-1}. Leugers and Atkinson (1984) have detected acetaldehyde by pulsed-laser photoacoustic spectroscopy down to an absorption coefficient of 9×10^{-9} cm^{-1}.

The sensitivity to condensed matter is lower by four orders of magnitude with the utilization of a gas-microphone system. This decrease in sensitivity is due to the difference in acoustic impedance between the condensed matter and the gas in the gas-microphone system. The use of a piezoelectric detector can avoid this problem so that it is a suitable detector for liquid and solid samples. The piezoelectric has a sensitivity two orders of magnitude less than a microphone so that an absorption coefficient in the order of 10^{-7} cm^{-1} should be measurable. Absorption coefficients of 4 x 10^{-6} cm^{-1} have been obtained by Voigtman et al. (1981) in the detection of tris(2,4-pentadiono) chromium (III) in hexane.

The major limiting factor in sensitivity is the background absorption from the solvent and the walls of the sample cell. The electrical noise can also be a major limiting factor since typical voltages of nV are measured.

II.6 Excited state measurements by photoacoustics.

a) Excited state lifetime:

Heritier (1983) has developed a very powerful system in which he is able to measure the absorptivity of excited states as a function of time. The system consists of two pulses of a Nd:YAG laser focused in a cell with a delay between the two pulses. This system is similar to the one that we will describe later for picosecond absorption

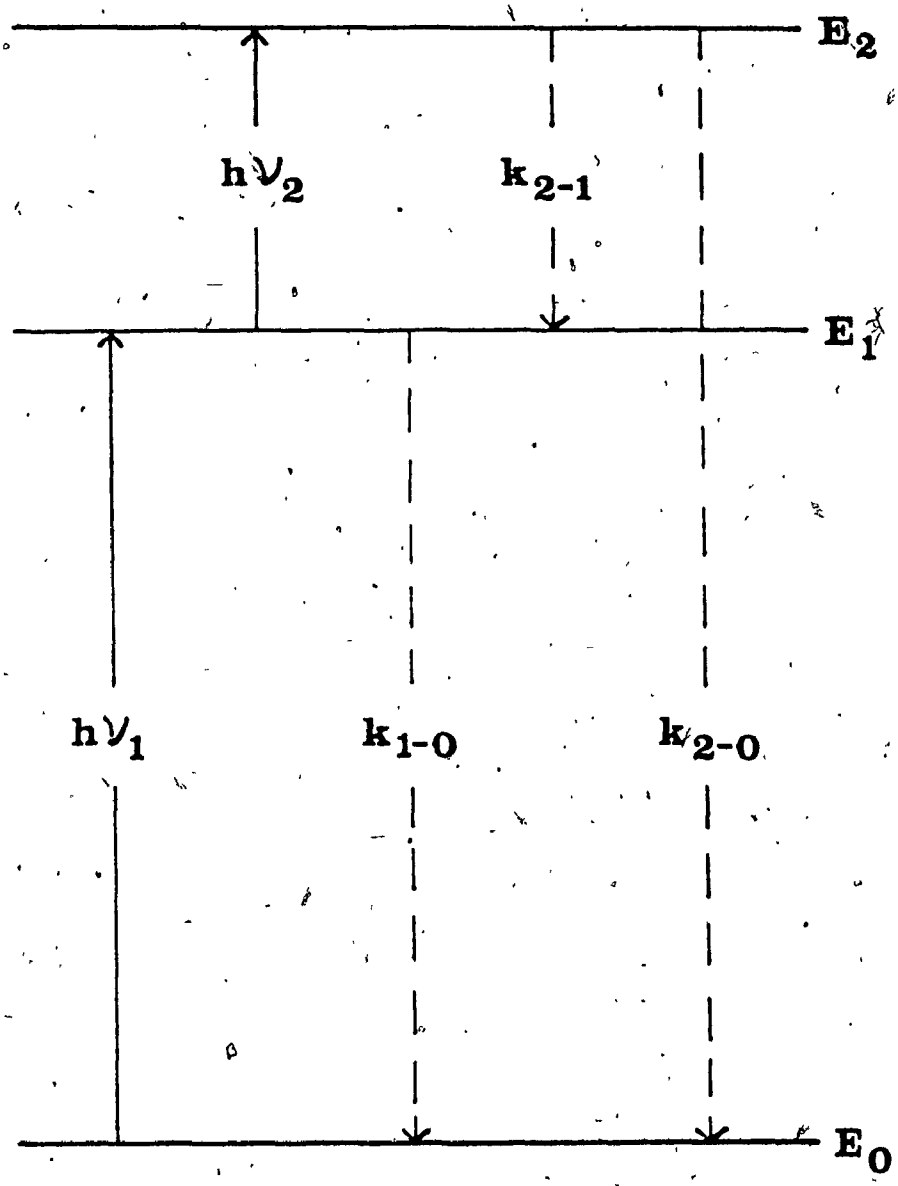

Figure II.2 Energy levels and decay pathway of a molecule with two excited states. Absorption and decay processes for photoacoustic measurements of an excited state molecule.
See description in text.

measurements.

Figure II.2 shows a typical energy level diagram of a molecule. If we excite the ground state (E_0) molecules with light ($h\nu_1$), the radiationless decay will produce a photoacoustic signal proportional to the number of molecules excited. Now, if we excited the molecules which are in the first excited state (E_1) before they have time to relax to the ground state, the energy input ($h\nu_2$) will bring the molecule from the first excited state (E_1) to a more energetic excited state (E_2). The photoacoustic signal obtained for the radiationless decay of the molecules in the E_2 state to the E_0 (k_{2-0}) will be the sum from the decay of the E_2 to E_1 (k_{2-1}) and the decay of E_1 to E_0 (k_{1-0}). By subtracting the signal obtained previously by exciting the molecules to the first excited state (E_1) from this signal, one gets the absorption of the first excited state (E_1). If we do this for different delays between the two pulses, the lifetime of the first excited state can be obtained.

Heritier (1983) has measured the excited state lifetime of dyes such as rhodamine 6G and he has obtained values in excellent agreement with values measured by time-resolved absorption.

b) Energy of excited states.

The photoacoustic method can be used to measure the energy of excited states of molecules which do not lumines-

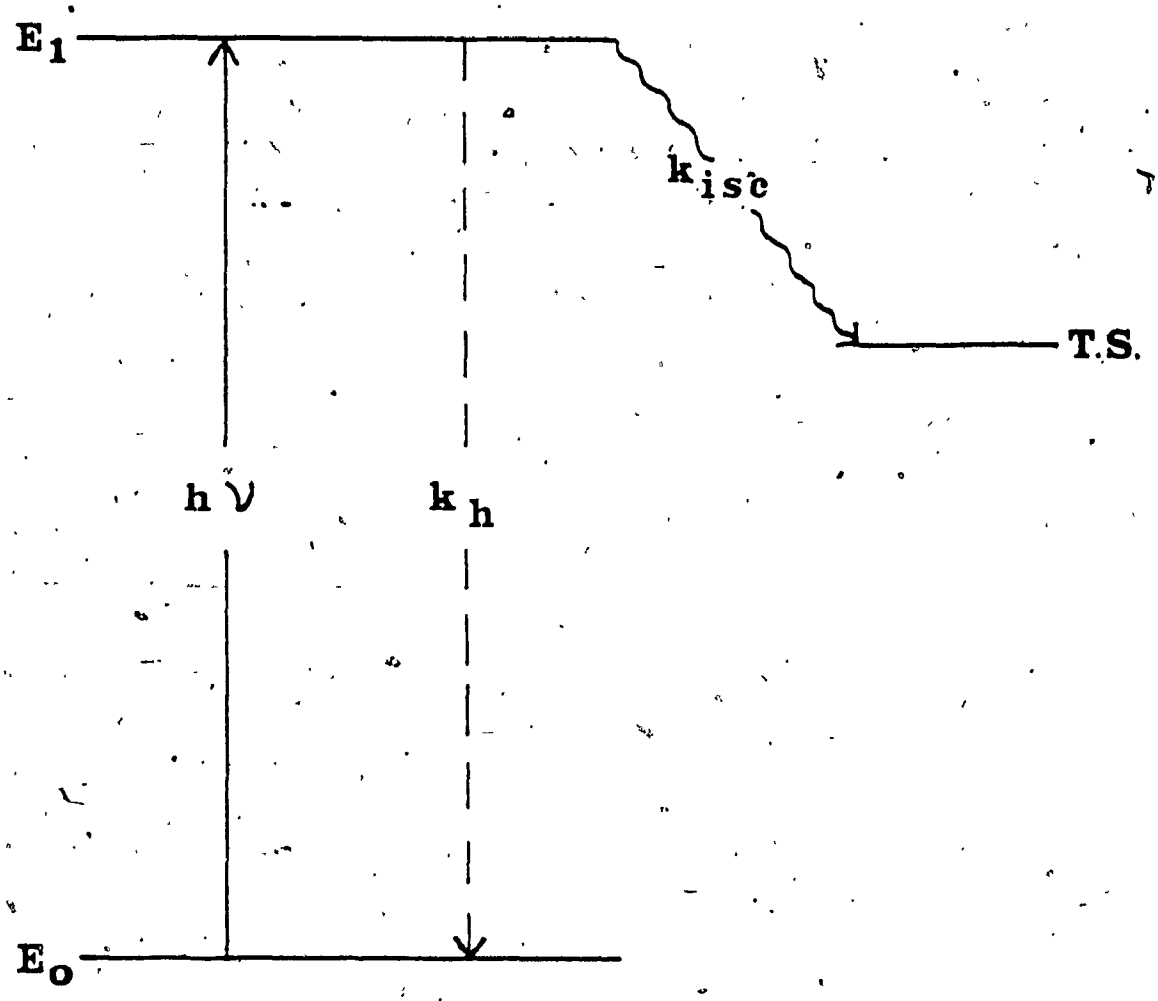

Figure II.3 Jablowski diagram for a molecule having a triplet excited state (T.S.). The molecule can decay from the singlet through radiationless decay (K_h) or intersystem crossing (K_{isc}).

ce. Figure II.3 shows the Jablowski diagram of a non-luminescent molecule having a triplet state (T.S.) in addition to its first excited state (E_1). If we pump the molecules to the excited state (E_1), these molecules can undergo radiationless decay to the E_0 (k_h) or intersystem crossing to the T.S. (k_{ISC}).

If the lifetime of the T.S. is longer than the formation time and dissipation time of the photoacoustic pulse, the first photoacoustic pulse will result only from the radiationless decay from E_1 to E_0 and the heat produced during the intersystem crossing (E_1 to T.S.). By knowing the quantum yield of the intersystem crossing, we can measure the relative energy of the T.S. if the system has been calibrated.

This method will be used to measure the energy of the trap sites in TiO_2. After band gap excitation, a free hole and a free electron are created in the TiO_2 semiconductor. If we scavenge the hole or the electron fast enough that there is no recombination, the electron (or hole) can be trapped in a trap state. By measuring the energy lost during the trapping process, we can obtain the energy of the trap states. Knowledge of this energy level is required if one wants to use this electron (hole) in a reduction (oxidation) process.

III. EXPERIMENTAL

III.1 Samples

The samples of TiO_2 were prepared following a procedure described by Moser and Gratzel (1982). Titanium tetrachloride ($TiCl_4$, Fisher) was slowly added (drop by drop) to doubly-deionized water at temperatures close to 0 C. The suspensions were prepared according to the concentration needed. The necessary amount of $TiCl_4$ was always added to the same amount of water which was 100 ml. No protective agents were added and the suspensions were kept for a maximum of three days. When needed, the pH was changed using the dialysis method. The pH was read using a pH indicator paper since the TiO_2 particles block the pores of the glass electrode.

Three different anionic dyes were added to TiO_2 solutions. The first one was a 4, 4', 4", 4''' tetrasulfonato (29H, 31H, phthalocyaninato (2-)-N^{29}, N^{30}, N^{31}, N^{32}) copper (II) (tetrasulfonated copper phthalocyanine, later called $CuPcTs^{4-}$) and supplied by Dr. A.B.P. Lever, York University (Fig. III.1a). This dye has a four minus charge which makes it very soluble in water. The second dye used is tris[4, 7-di(phenyl-4'-sulfonate)-1, 10-phenanthroline] ruthenium (II) (later called $RuPPS^{4-}$) (Fig. III.1b). The $RuPPS^{4-}$ is a gift from Dr. Ann English (Concordia Universi-

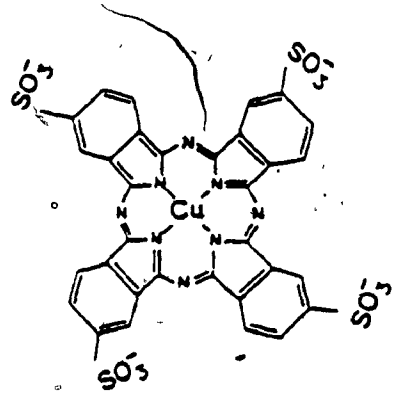

A

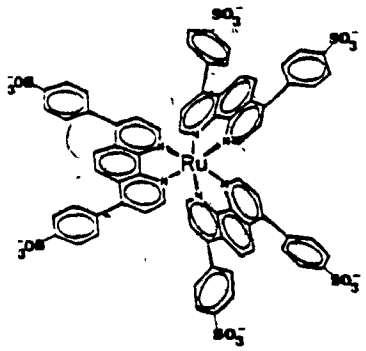

B

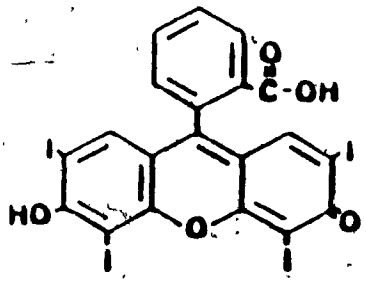

C

Figure III.1 Representation of the three different dyes used. (A) $CuPcTS^{4-}$, (B) $RuPPS^{4-}$, and (C) erythrosine.

ty). We have also used the 3', 6'-dihydroxy-2', 4', 5', 7' tetraiodospiro (isobenzofuran-1(3H), 9'-(9H) xanthen)-3-one (erythrosin) (Sigma Chemicals) which is an organic dye having a charge of minus two (Fig. III.1c).

All the dyes were used as provided without any further purification except for the $CuPcTS^{4-}$ which had been extensively purified by recrystalization. Addition of the different dyes to TiO_2 suspensions followed the same procedure. The desired concentration of the dye was poured into a 10 ml volumetric flask. 1 ml of water was added to partially dilute the dye. The solution of TiO_2 was added rapidly into the volumetric flask up to the mark and the mixture was thoroughly shaken. All the suspensions were kept in the refrigerator until used. The pre-dilution of the dye with water was done to prevent coagulation when the TiO_2 solution was mixed with the concentrated dye.

Three different standards were used in the photoacoustic experiments. Potassium dichromate ($K_2Cr_2O_7$) (Fisher) was used to measure the sensitivity of the apparatus. The tris (5-methyl-1-10-phenanthroline) ferrous perchlorate ($Fe(phen)_3^{2+}$) (Frederick-Smith Chem. Co.) was used also as a standard to calibrate the energy-photoacoustic signal relation. The tetrasulfonato-5, 10, 15, 10-tetraphenyl, 21H, 23H-porphine zinc ($ZnTPPS^{4-}$) (Stem Chem. Inc) was used for the measurement of its triplet state in order to test the time resolution of the apparatus and to evaluate the

precision of excited state energy measurements.

III.2 Absorption

The absorption spectra of solutions were obtained using an HP-8452 spectrophotometer (Hewlett-Packard) connected to an IBM PC computer. The resolution of this apparatus is 2 nm so that the absorbance values that will be given later in this thesis at 355 nm is an average between the absorbance measured from 354 to 356 nm. The absorbance at 337 nm is the average of the absorbance from 336 to 338 nm. The blank used was always water.

III.3 Picosecond apparatus:

The picosecond absorption and luminescence experiments were completed at the Canadian Centre for Picosecond Laser Flash Photolysis (CCPLFP) at Concordia University using the system built by Dr. D.K. Sharma and Prof. N. Serpone. The system is schematically represented in Figure III.2.

The light source is a mode-locked Nd:YAG laser (Quantel YG 402G) having a cavity length (l) of 1.1 m. The passive mode-locking is done with the dye Q-switch-I (Kodak, 9470) contained in a specially designed cell (Quantel). The output of the oscillator is a train of 12 pulses at 1064 nm (pulsewidth of 30 ps) separated by 6.5 ns (2l/c). The energy of the middle pulse is approximately 80 μJ. The beams are expanded before entering the pulse selector to avoid damage to the polarizer.

Figure. III.2 Schematical representation of the picosecond flash photolysis experimental set-up.

1 - Laser: a) Head
b) Mode-locking cell
c) Mirror
2 - Beam expander
3 - Glann-Air polarizers
4 - Pulse selector
5 - Amplifiers
6 - Second harmonic crystal
7 - Third harmonic crystal
8 - Delay ramp
9 - Continuum cell
10 - Energy detector
11 - Energy meter
12 - Sample cell
13 - Double monochromator
14 - Photodiode array detector
15 - Multichannel analyzer
16 - Computer
DM - Dichroic Mirror

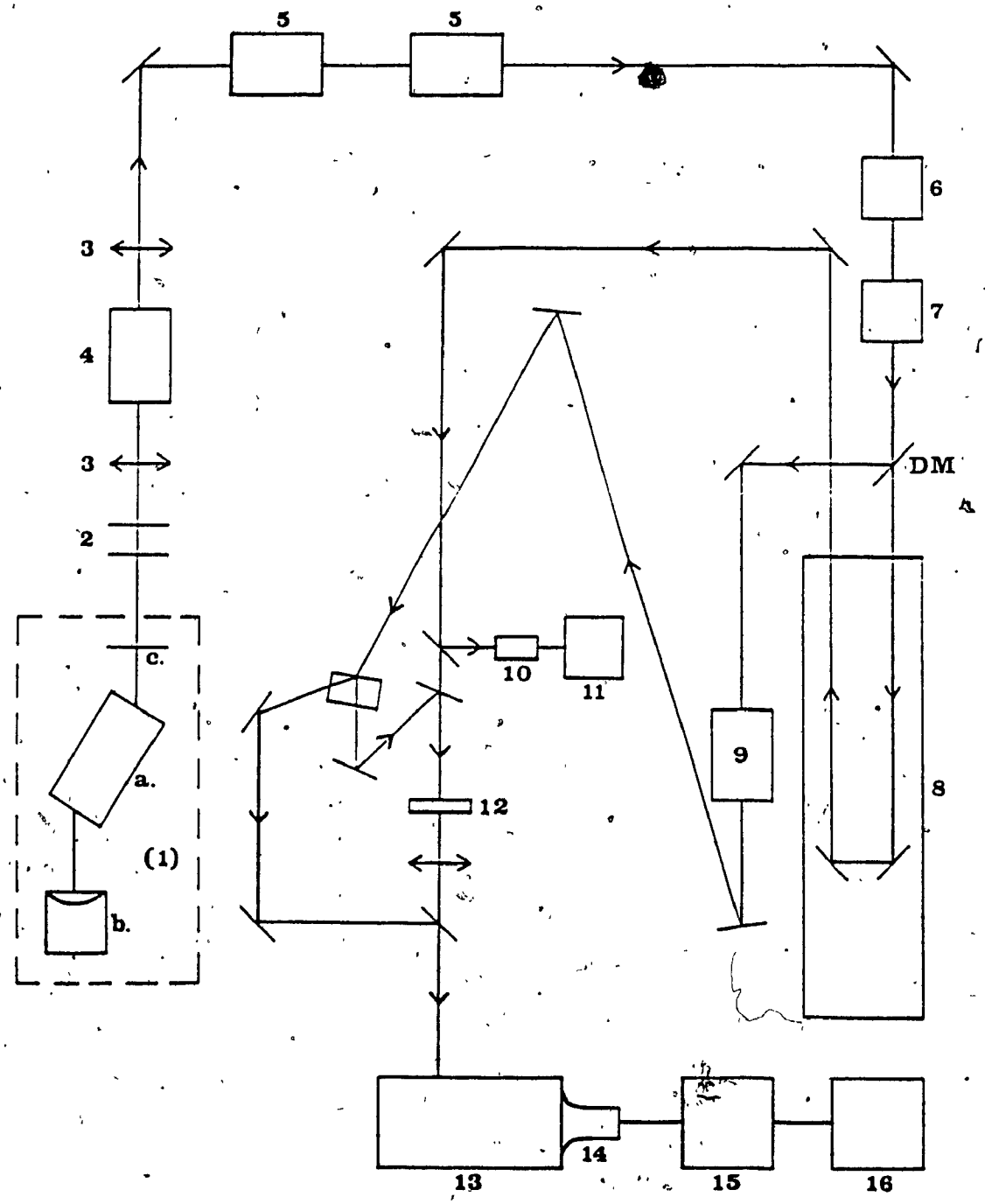
5
5
6
7
DM
3
4
3
2
c.
a.
(1)
b.
10
11
9
8
12
13
14
15
16

The pulse selector (Quantel, PF 302) consists of two cross-polarizers and a birefringent crystal with an electronic circuit to drive the crystal. The train of pulses coming from the oscillator are passed through a Glan-air cross-polarizer to remove the minor vertical component of the light. The train of pulses then go into the birefringent crystal (KD^*P) which changes the polarization of one pulse. This change of polarization is due to a short voltage pulse of 3,6 KV applied to the crystal following the trigger signal from the earlier pulses. At the exit of the pulse selector, there is another Glan-air cross-polarizer vertically polarized which lets through only the pulse that had its polarization changed in the crystal.

This lone pulse is sent through two amplifiers giving an average output of 80 mJ. The next step is the second and third harmonic generation. The frequency doubler crystal and the third harmonic crystal are both made of KD^*P (potassium dihydrogen phosphate deuterated). The difference is in the cut of the crystal. The frequency doubler crystal is a Class II crystal so it takes the circularly polarized light and gives horizontally polarized light. There is approximately 20% of the 1064 nm light which is converted into 532 nm (20 mJ). When needed, the 1064 nm and the 532 nm light are combined in the third harmonic crystal (Class I) to give vertically polarized

light at 355 nm with a yield between 10 and 15% (2 to 3 mJ).

After the second and third harmonic crystals, dichroic mirrors are used to separate the different wavelengths. The 1064 nm pulse is sent through a D_3PO_4 solution to generate a continuum pulse. The probe continuum pulse is split into two parts where one part of the pulse is focused into the sample cell (reading pulse) and the other part is passed beside the cell and it is used as the reference pulse. The second or third harmonic (the fourth harmonic can also be generated) can be used as the pump pulse. It is passed along a ramp delay and focused into the sample cell. The ramp delay can vary the time of arrival of the pump pulse compared to the probe pulse between 0 ps and 11 ns.

The reading and the reference probe pulses are passed through a double monochromator (SPEX) and sent to a silicon enhanced photodiode array detector (EG and G). A multichannel analyzer (PAR) reads two arrays of 250 photodiodes (each photodiode corresponding to a specific wavelength) and sends the results to a microcomputer (PAR). The two arrays (I_0 and I) are stored on a diskette and used later by a minicomputer (PDP 11, DIGITAL) to calculate the absorbance at each wavelength.

During the first shot, the pump beam is blocked so that the I_0 and I values correspond to the ground state

absorption. The next shot (s) consists on the measurement of the absorption of the sample following the pump pulse. We then have I_0 and I for the excited states. Between 6 to 15 shots are taken for the ground state absorption and the same number for the excited state absorption at every time delay.

Rejection of a shot may arise for one of two reasons. The first one is experimenter choice before storing the data onto the disk because of: 1) a double train of pulses created in the oscillator; 2) a too high or low energy of the pump pulse; 3) a saturation of the photodiodes by one of the probe beams; or 4) a bad continuum pulse generated in the D_3PO_4 cell. The second uses the noise calculation for each shot described next.

The PDP minicomputer calculates the absorbance of the sample for each shot ($a = \log I_0/I$) and does an average for the sum of the shots done for the ground state and each time delay excited state. The noise on each shot is calculated by the relation:

$$N_i = \Sigma_k \frac{(a_{ik} - a_k)^2}{a_k} \qquad \text{(III.1)}$$

where N_i is the noise for the curve i, a_{ik} is the value of absorbance of that shot at the wavelength k, and a_k is the average absorbance value at the same wavelength for all the shots on a specific state. For normal solutions (clear), when the noise value for a curve was higher than 3, the

curve was rejected and a new average was calculated. For solutions containing colloidal particles, the noise of each curve was higher due to the scattering by the particles. Noise values between 3 and 7 were often obtained and were considered as acceptable. Except for experiments involving very large particles, curves with noise value lower than 7 were accepted and the others were rejected. Nevertheless, a minimum of six shots was always used for calculations. The PDP computer subtracts the absorbance of the ground state from the absorbance of the excited state. The result is a Δa (absorbance change) value for every wavelength.

Two sources of error can lead to a misinterpretation of the results. First of all, since the continuum has a bell shape, the numbers of counts in the blue and red extremities are very low. This increases the noise ratio at these wavelengths and can cause spurious features at these wavelengths. We must take into account this possible error in the interpretation of the spectra for wavelengths lower than 440 nm and higher than 635 nm.

Another source that can lead to one being misled is the appearance of an absorbance at all the wavelengths after long time delay. This "DC shift" can reach values as high as 0,1 absorbance unit at 10 ns. We think that this "DC shift" is due to scattering of the probe beam passing through the cell by ultrasonic waves ("shock waves"). These "shock waves" are created when the energy of the pump

pulse is concentrated in a small volume. We usually used a 2-mm-waist pulse (2,5 mJ) to avoid this "DC shift".

A last point that has to be mentioned is the fact that the arrival of the light at the sample cell is not the same for all wavelengths. The difference is so small that it is not seen in the results except at very short delays (20 ps).

III.4 · Photoacoustic Apparatus

The photoacoustic data were obtained using a newly fabricated home-made time resolved photoacoustic detection system (Fig. III.3). The system consists first in a nitrogen pulse laser (PRA-LN103). The wavelength output is a pulse of 10-60 μJ at 337.1 nm. The pulsewidth is approximately 300 ps. The laser can be run at frequencies up to 100 Hz. The laser pulse is focused into the sample cell.

The cell consisted of a piezoelectric detector tube (PZ5-A, Modern Piezoelectric). The tube has a radius of 1,25 cm and a length of 1,25 cm. A quartz window is glued to the bottom of the tube and the solution is directly poured inside the piezoelectric. The piezoelectric cell is mounted over a photodiode positioned at the center of the cell. The signal of the photodiode is read by the computer (IBM PC) which controls the movement of two positioning motors to ensure that the laser pulse is centered in the piezoelectric cell.

Figure III.3 Schematical representation of the photoacoustic detection system. The laser pulse coming from the nitrogen laser is sent inside the piezoelectric (PZ) by the top (M=mirror, L=lens). A photodiode (PD) ensures that the pulse is coming at the center of the cell. The photoacoustic signal is passed by a pre-amplifier before being sent to the boxcar. The computer is controlling the movement of the positioning motors as well as collecting data.

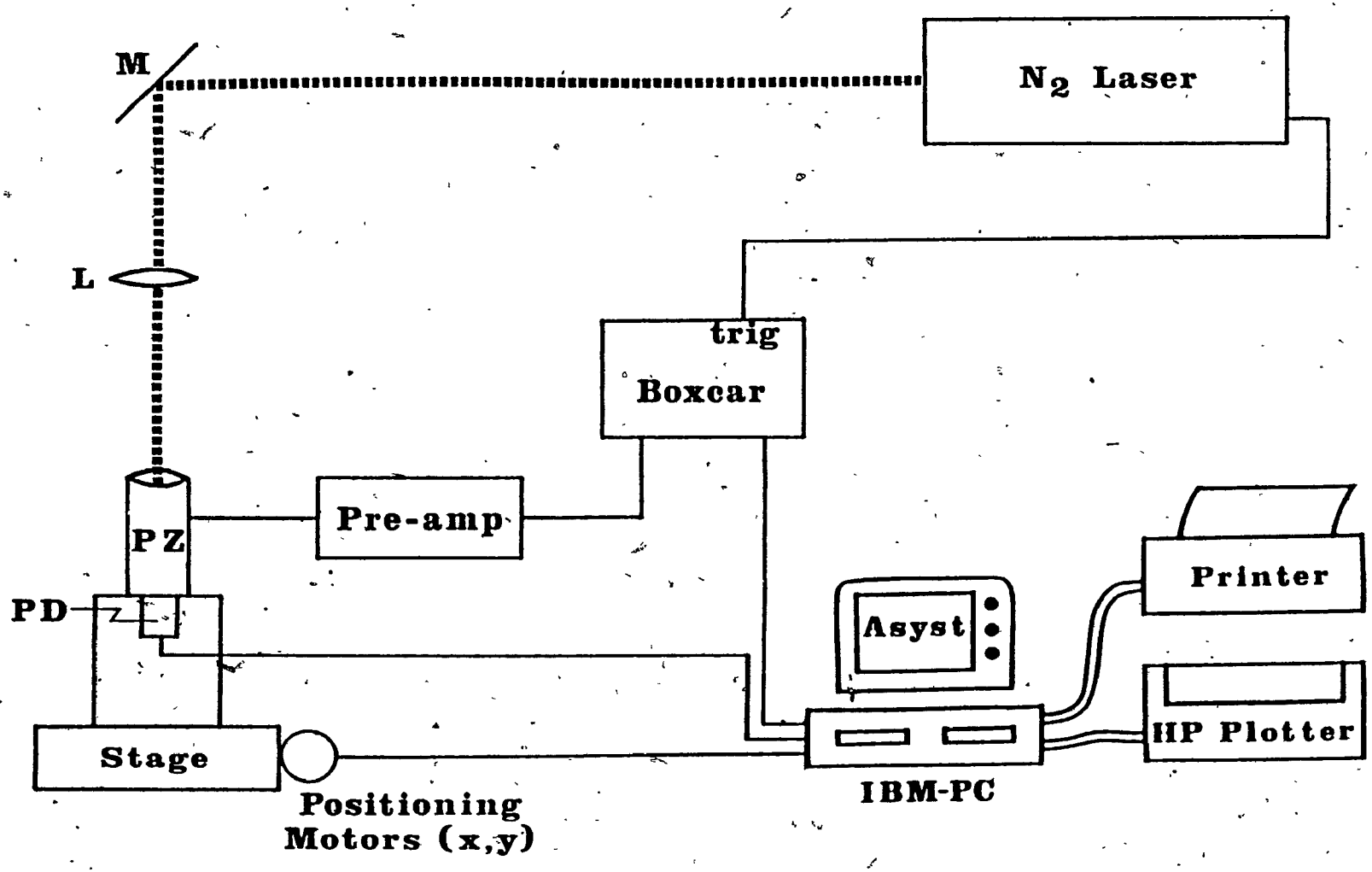

PHOTOACOUSTIC SYSTEM

The photoacoustic signal is amplified by a pre-amplifier (Model 1201, Ithaco) and sent to a boxcar (Model 162-164, PAR). In the amplifier, the signal is filtered to remove all the frequencies lower than 3KHz and higher than 100 KHz. The signal is processed in the boxcar before being sent to the computer. Appendix B gives the detail of the time processing of the signal in the boxcar. Following the trigger of the laser, a reading window of 50 ns is moved along the signal according to a delay ramp generated in the boxcar by the computer. Each reading of the window at a certain delay is an average of 100 shots.

The signal obtained at the end of the experiment is a wave of frequency equal to the traveling time of the sound in the solution. The first maximum in the wave is the result of the formation of the first acoustic wave in the solution and the other maxima are the result of the echoes if there are no other acoustic waves produced in the solution.

All the steps of the experiment are controlled by the computer through an A/D interface (DT-2801, Data Translation). Full details of the experimental set-up as well as the electronic circuit used are given the Appendix A. The data acquisition and analysis program (Appendix C) was implemented using the software package ASYST (Macmillan Software).

IV. Results:

IV.1 Absorption:

When looking through the suspensions of TiO_2, one cannot "see" particles for suspensions containing 10 g/l or less of TiO_2. The suspensions look completely transparent to the eye and no precipitation is observed. Fig. IV.1 shows the absorption spectra of TiO_2 for different concentrations. All these suspensions come from the same batch, which means all are aliquots from the mother solution taken during the addition of $TiCl_4$. We can see in Figure IV.1 that an increase in concentration of TiO_2 shifts the band edge to the red side of the spectrum. The increase of mass of TiO_2 cannot account for all the red shift. Table IV.1 shows the absorption coefficient of the four different suspensions at 350 nm and 360 nm.

Table IV.1 Absorption coefficient of TiO_2 at different concentrations.

C(g/l)	$\varepsilon_{350}(lg^{-1}cm^{-1})$	$\varepsilon_{360}(lg^{-1}cm^{-1})$
4	.0669	.0176
8	.0968	.0290
12	.1291	.0393
16	.3094	.1197

The increase of the absorption coefficient with the

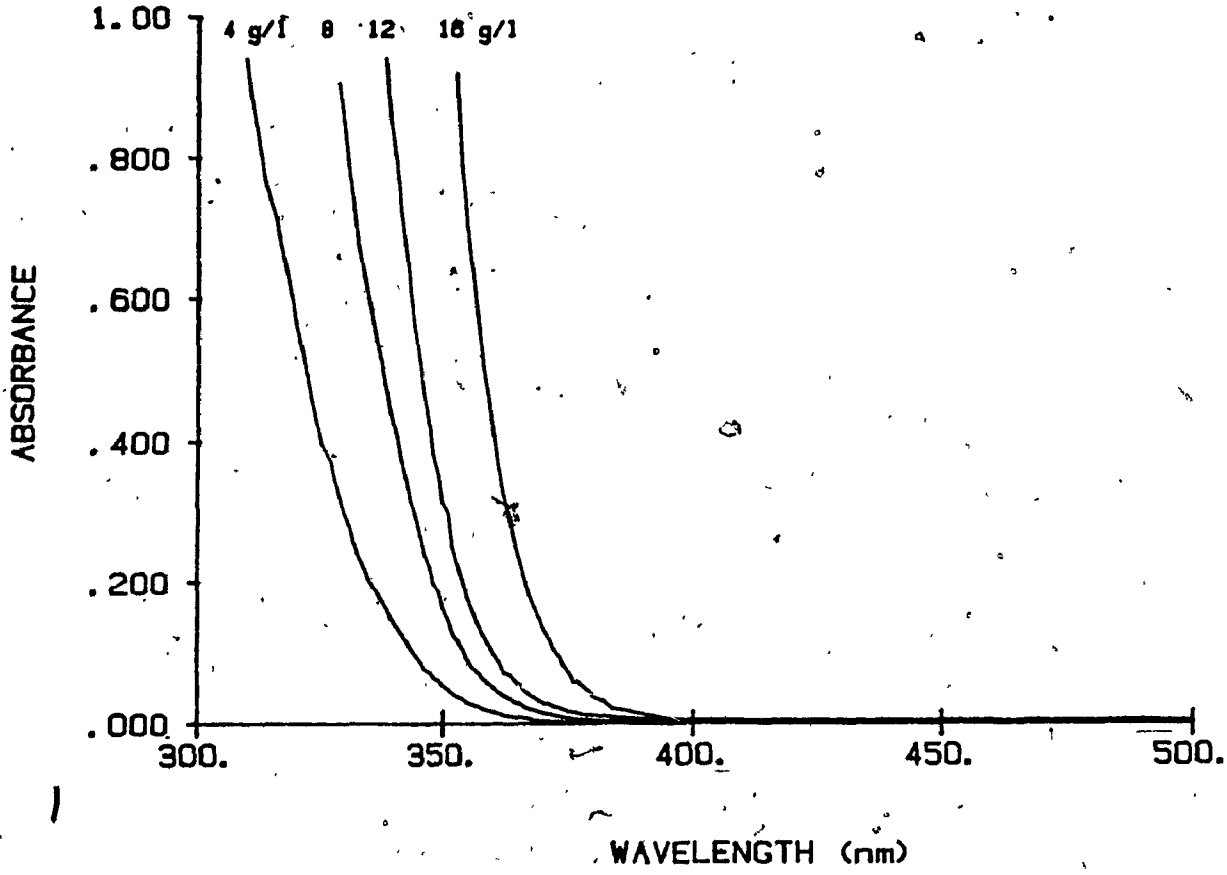

Figure IV.1 Absorption spectrum of TiO_2 colloidal particles at different concentrations. The different concentrations are aliquots taken during the same preparation.

concentration of TiO_2 can only be accounted for by the increase in the size of the particles.

Size measurements of TiO_2 colloids have been done using the technique of dynamic light scattering[1]. The radius of the particles measured were 300 Å and 500 Å for two different suspensions showing no more red shift in their absorption spectra. The size of the particles in other suspensions was estimated following these results by comparison of the absorption spectra. The same absorption spectra of TiO_2 suspensions at a specific concentration is very difficult to reproduce since the size of TiO_2 varies with the details of the preparation procedures. Temperature, rate of addition of $TiCl_4$, amount of water, and many other factors will affect the size of the TiO_2 particles.

By dialyzing the suspensions to give a pH of 3, the particles grow and we can observe a red shift in the band edge of the absorption spectra of the solution (Fig. IV.2). The reverse is true when we add a few drops of concentrated HCl to the starting solution.

The absorption spectra of the tetraanionic dye $CuPcTS^{4-}$ is shown in Fig. IV.3. $CuPcTS^{4-}$ has an absorption maximum at 620 nm for the concentrations used in these experiments. The dye has an absorption coefficient of 2,9 x 10^4 $M^{-1}cm^{-1}$ at 355 nm. Fig. IV.4 shows the absorption

---

[1] We thank Professor Janos Fendler for his assistance with these measurements and access to his equipment.

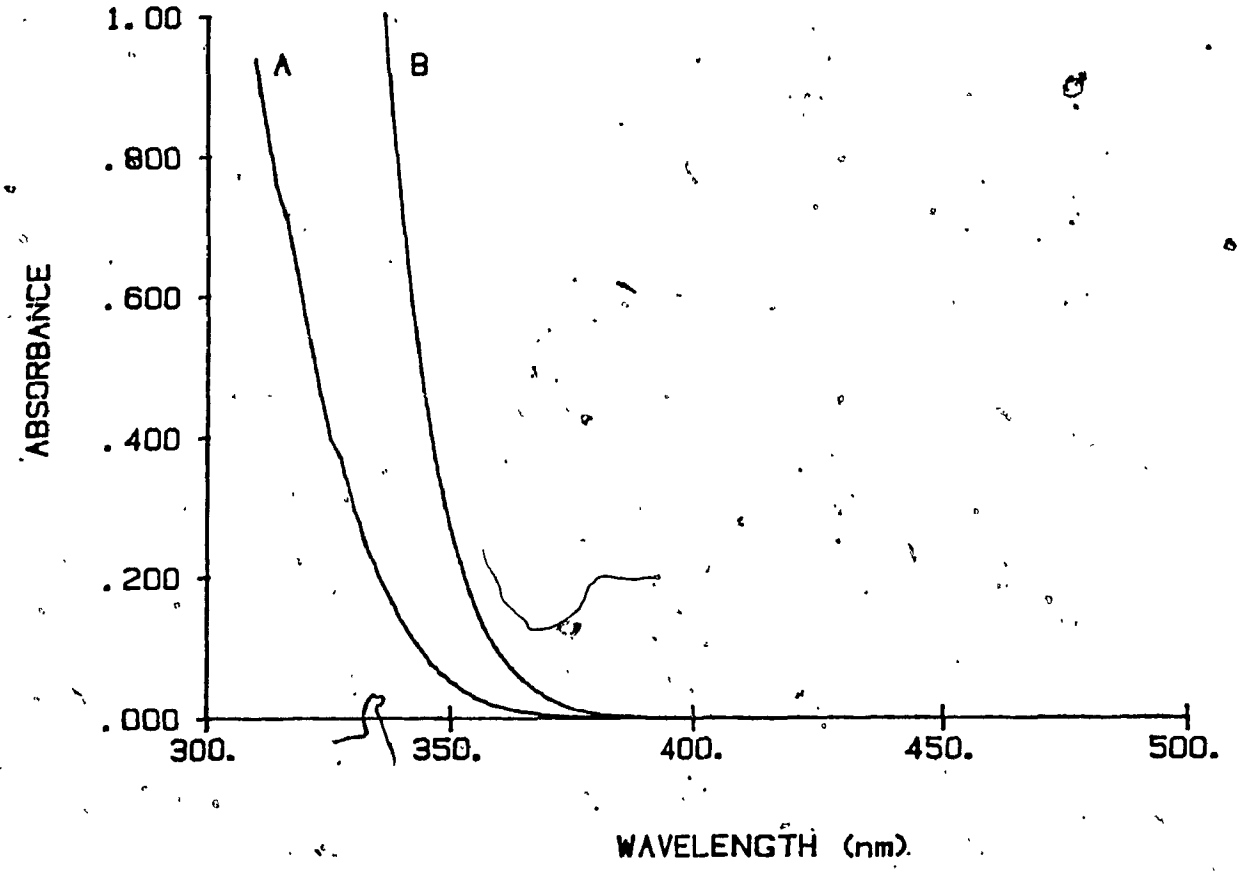

Figure IV.2 Absorption spectrum of TiO_2 colloidal particles at pH=1,5 (A) and pH=3 (B). The pH has been increased by dialysis. The concentration of TiO_2 is 4 g/l.

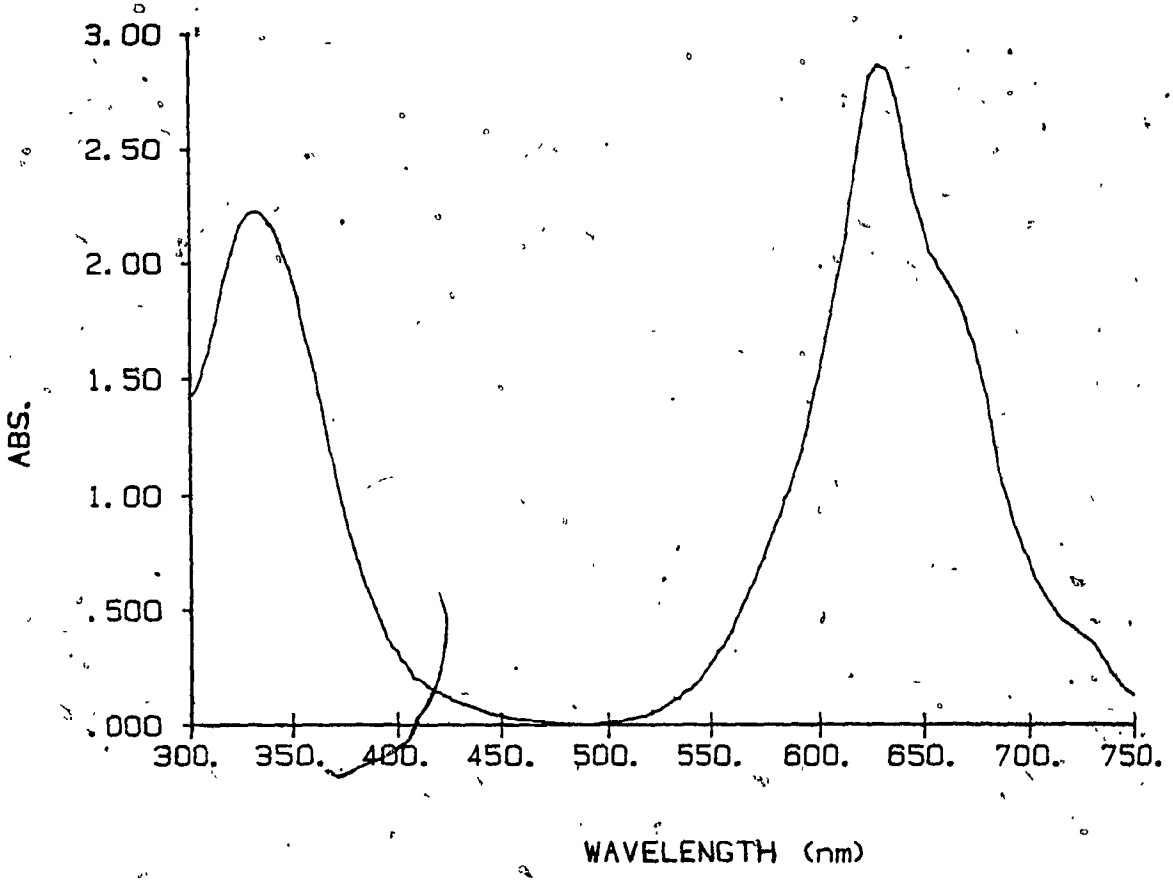

Figure IV.3 Absorption spectra of the $CuPcTS^{4-}$. The concentration of the $CuPcTS^{4-}$ is 6,65 x 10^{-5} M.

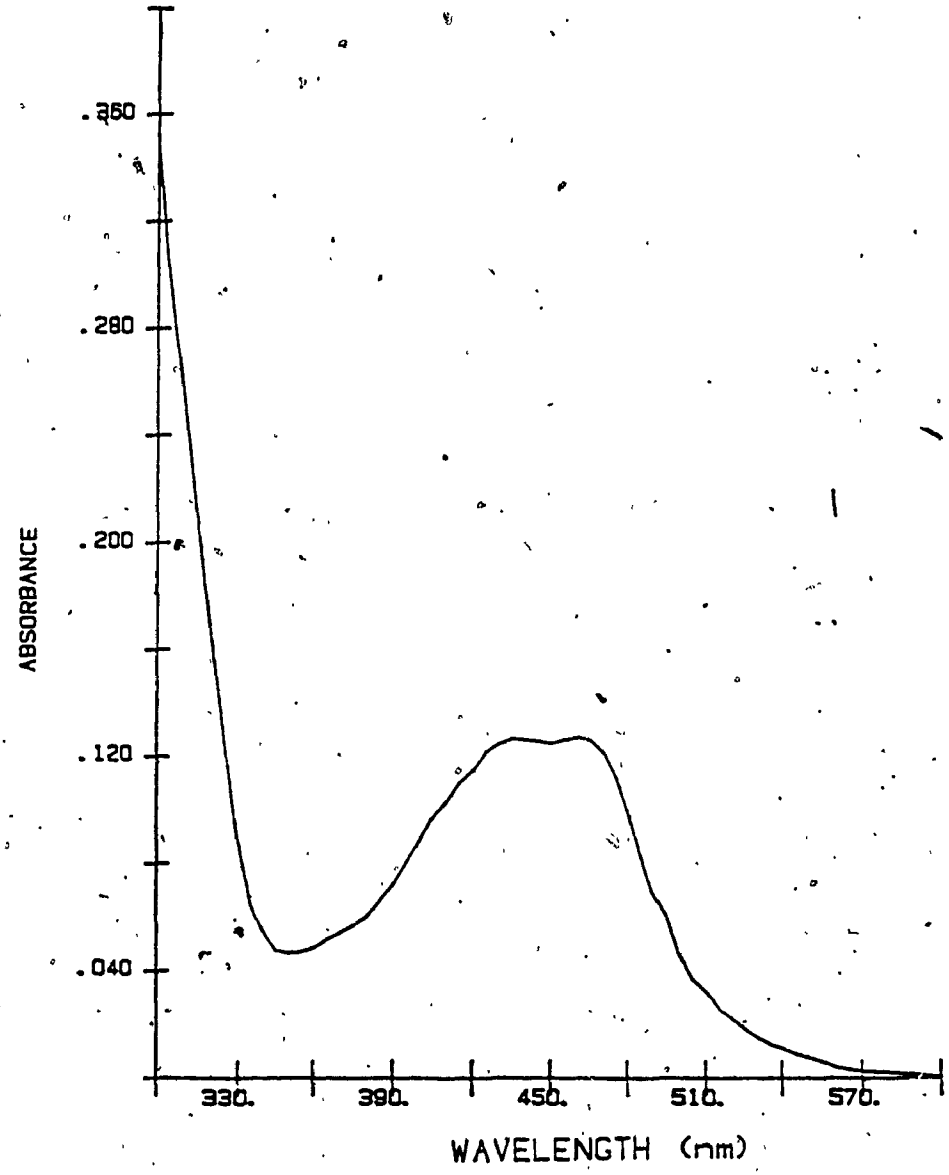

Figure IV.4 Absorption spectra of the $RuPPS^{4-}$. The concentration of the $RuPPS^{4-}$ is $2,25 \times 10^{-5}$ M.

spectra of the $RuPPS^{4-}$. It has a maximum at 464 nm and the absorption coefficient at 355 nm is $6,5 \times 10^3$ $M^{-1}cm^{-1}$. On mixing a dye into a suspension of TiO_2, there is no change in the absorption of the dye, but there is a small red shift in the band edge of the TiO_2 spectra. It is obvious by looking at the suspensions that there is a coagulation process that occurs during mixing, but the red shift is not dramatic; the TiO_2 particle size has not increased much. It is possible that part of the coagulation is due to bridging of more than one particle by one molecule of the dye since the $CuPcTS^{4-}$ has four negative charge positions and the $RuPPS^{4-}$ has six negative charge positions so that they can bridge as many as 4 and 6 particles respectively.

IV.2 Picosecond Flash Photolysis:

a) TiO_2 alone:

Upon flashing a suspension containing only TiO_2 with 2,5 mJ of the third harmonic of the Nd:YAG laser (355 nm), we observe a transient absorption at 20 ps formed within the pulse (Fig. IV.5). This transient decays with time and it has mostly vanished after 1 ns. The transient does not show any maximum in the visible region accessible with this instrument. The signal rises from the blue side of the spectrum toward the red side. This signal was obtained with a suspension containing 18 g/l of TiO_2.

The same signal can also be seen with suspensions less

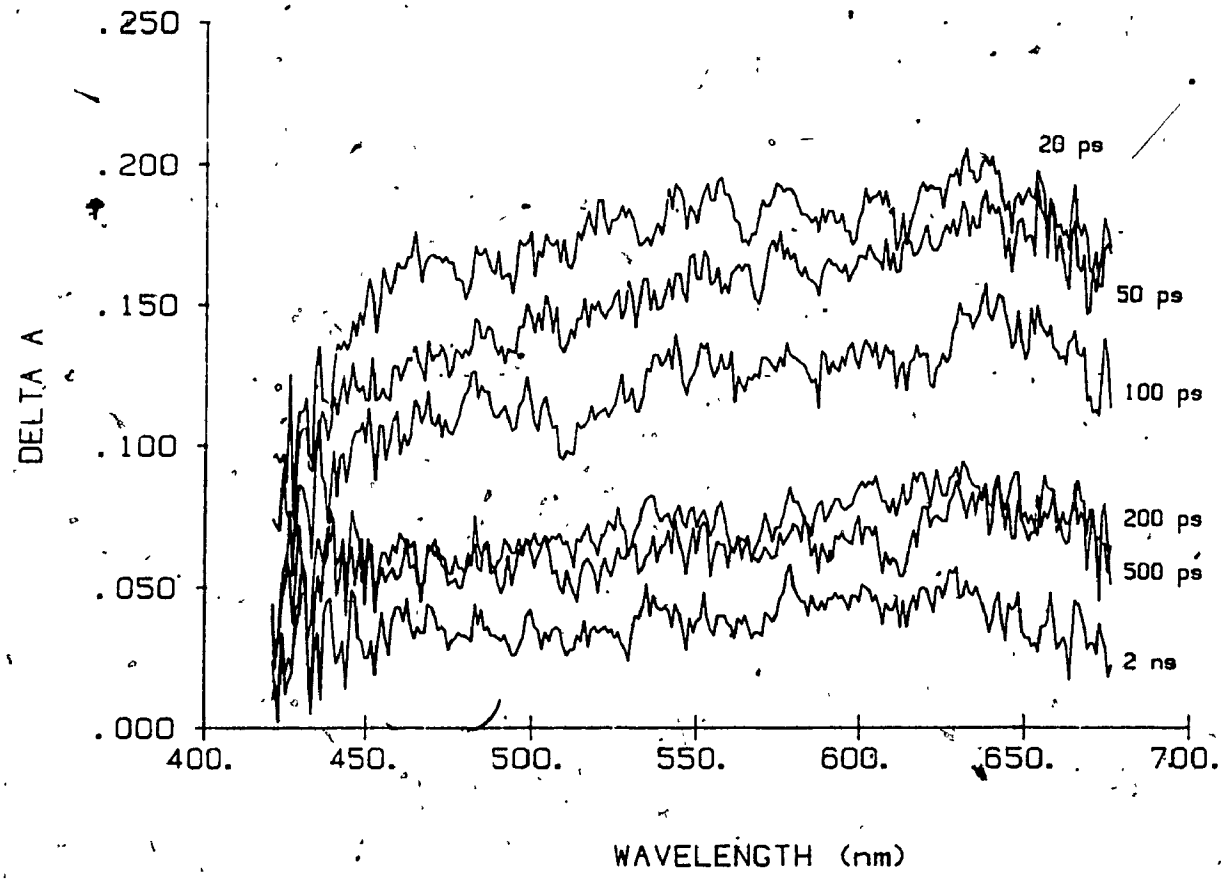

Figure IV.5 Picosecond flash photolysis of a TiO_2 suspension. The pH was 1,5 and the concentration was 18 g/l. The excitation wavelength is 355 nm.

concentrated, but for concentrations lower than 4 g/l, the signal is too small to be observed. By decreasing the concentration of TiO_2, the intensity and the lifetime of the transient decreases. The same effects were also observed upon addition of HCl to a suspension of 18 g/l of TiO_2. The signal was completely removed by the addition of HCl at a concentration of $3,3 \times 10^{-2}$ M. The same kind of transient was also observed for other TiO_2 preparations, but the shape and the lifetime varies slightly from one preparation to another.

The transient absorption from the TiO_2 band gap excitation shows a linear dependance on the energy of the pump pulse. The intensity of the transient is proportional to the energy up to a value of 2,5 mJ. The kinetic analysis (Fig. IV.6) gives a second order rate constant for the decay of the transient if analysis is limited to $t \leq 500$ ps. The rate constant is proportional to the energy.

b) TiO_2 - $CuPcTS^{4-}$ system:

A suspension containing 1,3 g/l of TiO_2 and $6,7 \times 10^{-5}$ M of the $CuPcTS^{4-}$ dye where the absorbance of the TiO_2 and the dye were 0,26 and 0,34 respectively gives a completely different behavior when pumped with the 355 nm pulse (Fig. IV.7). At 20 ps, we can observe partial bleaching of the dye at 620 nm and the presence of an excited state with an absorption rising from the blue side to the red side. This excited state absorption decreases with time and at 100 ps,

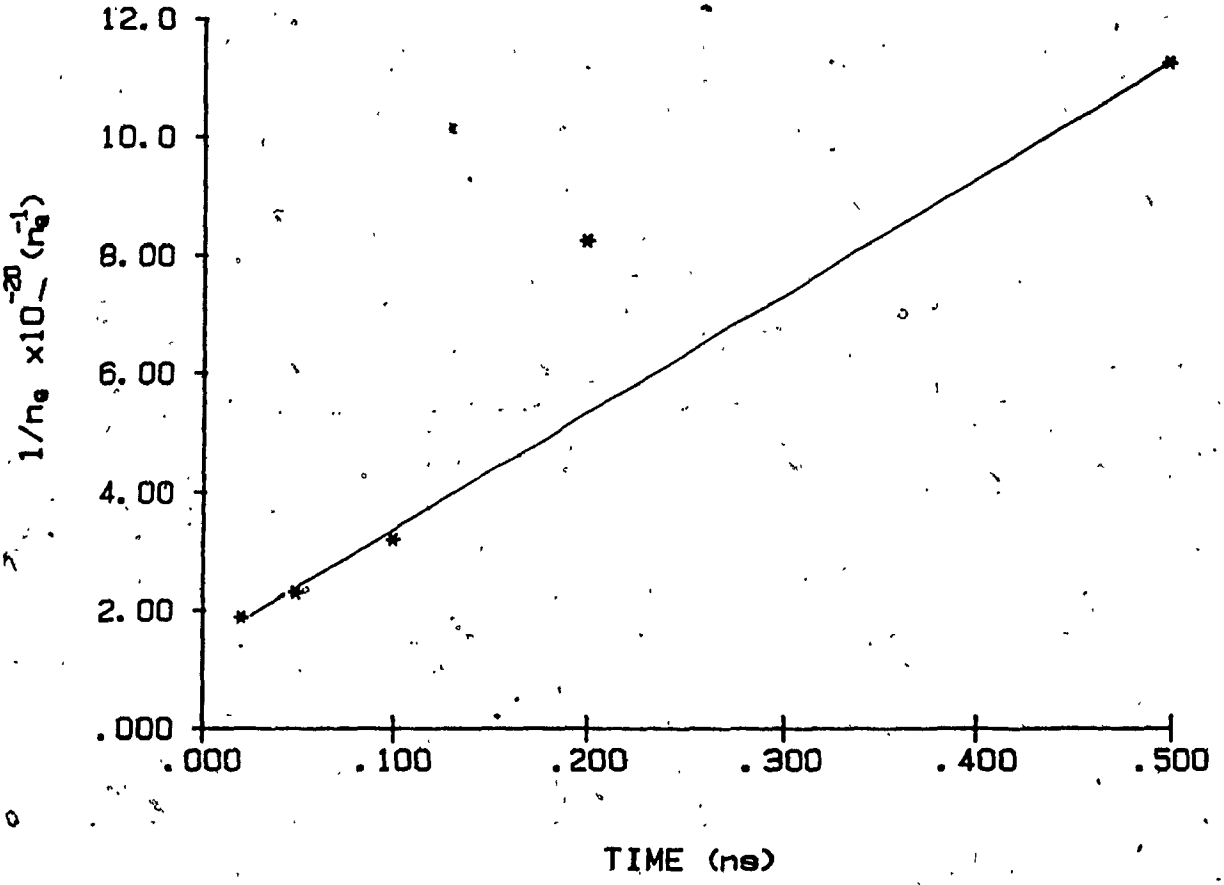

Figure IV.6 Kinetic analysis of the picosecond flash photolysis of a TiO_2 suspension. The values used are coming from Figure IV.5. n_e corresponds to the total number of electrons calculated by using an absorption coefficient of 2200 M^{-1} cm^{-1} at 525 nm.

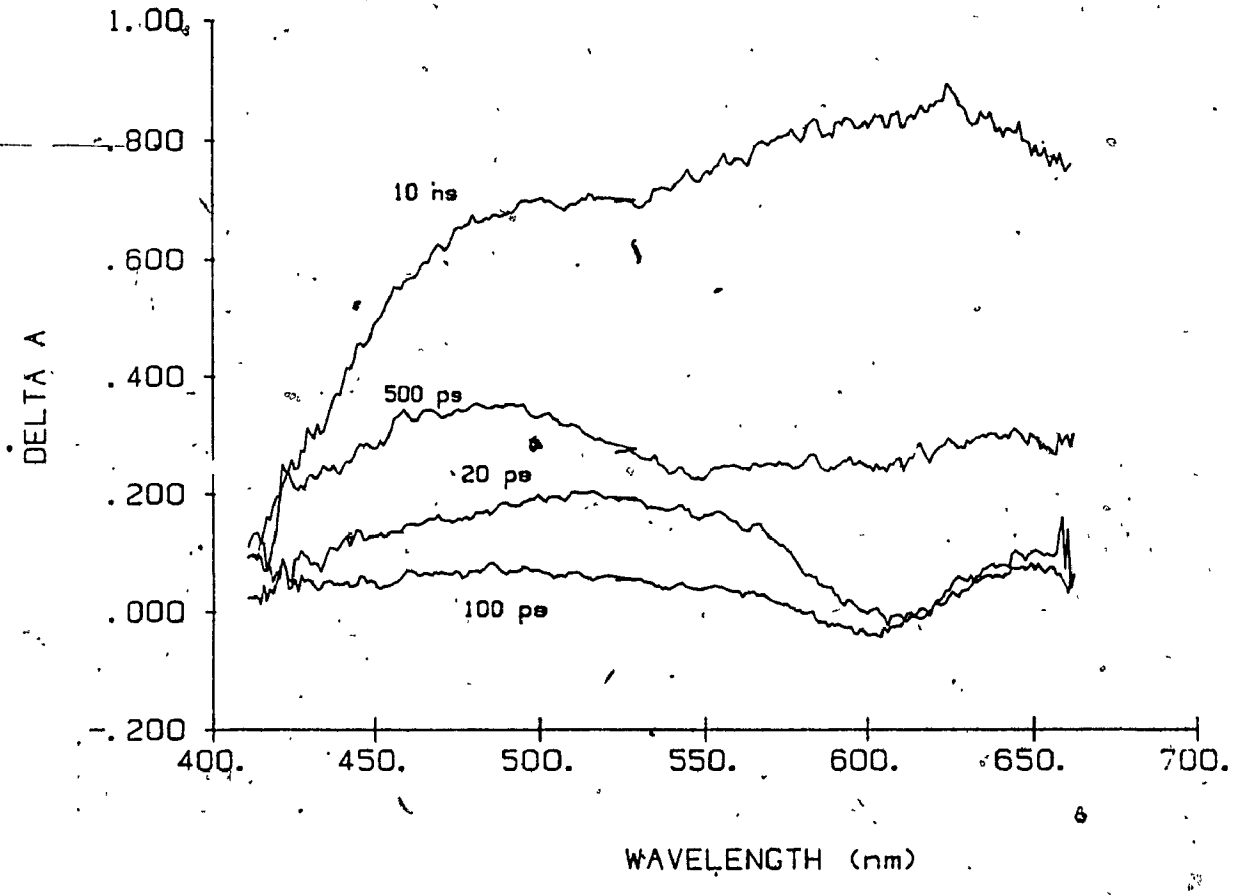

Figure IV.7 Picosecond flash photolysis of a solution of TiO_2 and $CuPcTS^{4-}$. The concentration of the TiO_2 is 1,3 g/l and the concentration of the $CuPcTS^{4-}$ is $6,65 \times 10^{-5}$ M. The excitation wavelength is 355 nm.

we can observe at most very little bleaching of the $CuPcTS^{4-}$.

Subsequently, there is a transient at 480 nm which grows up to 500 ps in addition to a large red band showing a maximum at 620 nm. This red band grows to reach a maximum at 10 ns. The kinetic analysis of the growth of the transient at 625 nm gives a first order rate constant of $5,8 \times 10^8\ s^{-1}$ (Fig. IV.8).

The analysis of six other preparations containing $CuPcTS^{4-}$ gave an average rate constant of $8 \pm 6 \times 10^8\ s^{-1}$. The large error between the different samples is due to the noise created by the scattering of light in the suspension and also it is due to the difficulty of attributing a value to the other transient absorption contributions at 625 nm.

The rate constant does not seem to change with the concentration of the dye, but it changes slightly with the preparation (size of the particles), although it was not possible to define this change quantitatively.

c) TiO_2 - $RuPPS^{4-}$ system:

In a suspension containing 4 g/l of TiO_2 and $2,5 \times 10^{-5}$ M of $RuPPS^{4-}$, the ruthenium dye had an absorbance of 0,03 at 355 nm whereas the TiO_2 had a band gap absorbance of 0,2 in the 2 mm cell. Flashing this suspension at 355 nm gives the transient spectra shown in Figure IV.9. At 20 ps, we can observe the transient absorption due to the absorption of the pump pulse by TiO_2 that we have described previous-

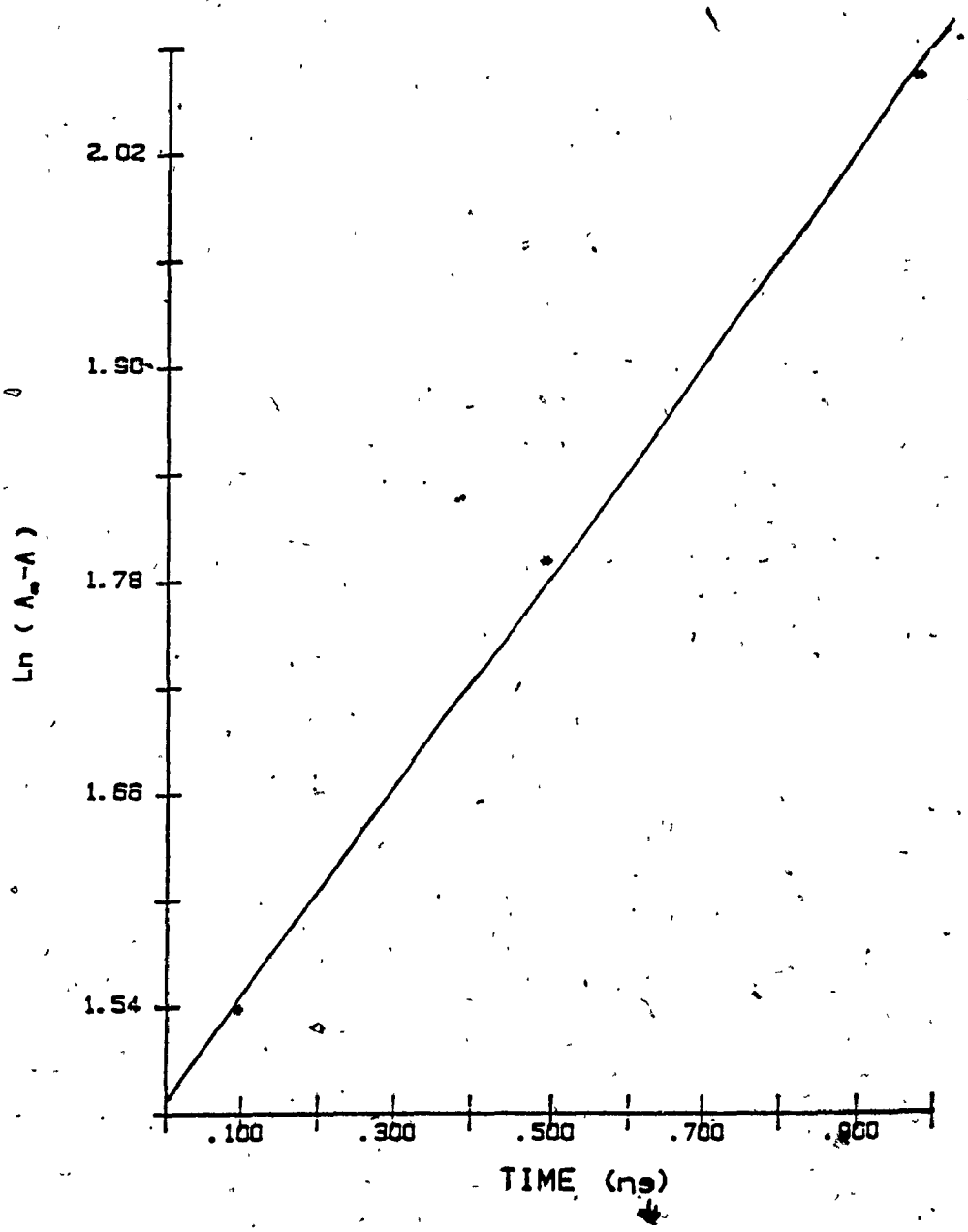

Figure IV.8 Kinetic analysis of the picosecond flash photolysis of a solution of TiO_2 and $CuPcTS^{4-}$. The conditions are the same as Figure IV.7. Δa was taken at 10 ns and the monitoring wavelength was 625 nm.

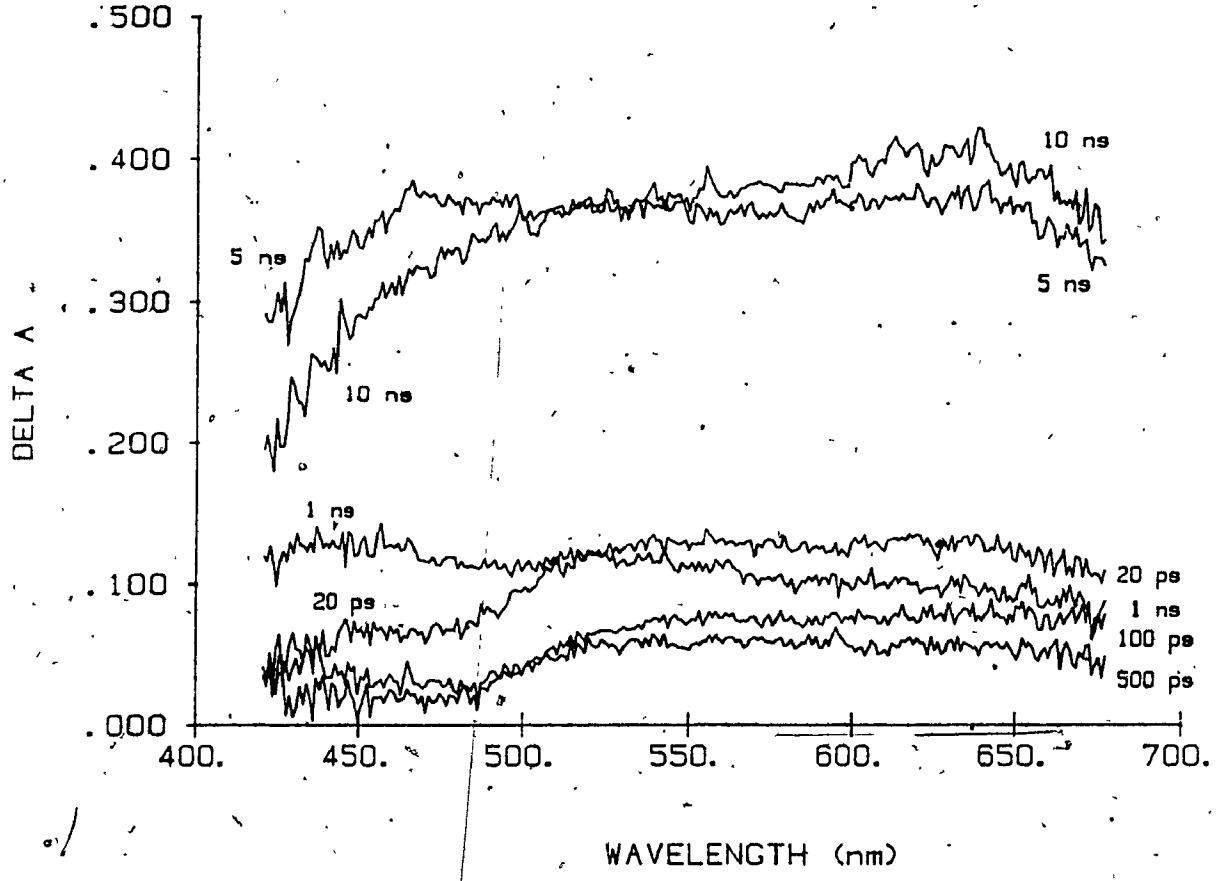

Figure IV.9 Picosecond flash photolysis of a solution of TiO_2 and $RuPPS^{4-}$. The concentration of TiO_2 was 4 g/l and the concentration of the $RuPPS^{4-}$ was $2,25 \times 10^{-5}$ M. The excitation wavelength is 355 nm.

ly. This direct excitation of TiO_2 decays rapidly so that at 500 ps, it has practically vanished.

After 500 ps, growth of a new transient becomes evident; one part in the blue side of the spectrum having its maximum at 460 nm, and the other part in the red side of the spectrum with a maximum at 630 nm. The blue transient grows up to 1 ns where it starts to decay. At 10 ns, this blue transient seems to have vanished. The red transient grows slowly up to 10 ns where it seems to reach a maximum.

The kinetic analysis of the red transient at 625 nm (Fig. IV.10) gives a first order rate constant of $3,1 \times 10^8$ s^{-1}. For four samples of colloids sensitized with the $RuPPS^{4-}$ complex, the average rate constant was $6 \pm 3 \times 10^8$ s^{-1}. The same behavior as described previously for the TiO_2 - $CuPcTS^{4-}$ system has been observed for this rate constant.

A suspension containing 4 g/l of TiO_2 and $2,5 \times 10^{-5}$ M of $RuPPS^{4-}$ was flashed using the second harmonic of the laser. At this wavelength, 532 nm, the TiO_2 shows no absorption whereas the $RuPPS^{4-}$ has an absorbance of 0,03 in a 2 mm cell. The only features in the transient spectra is a dip at 460 nm due to the bleaching of the dye and a slight absorption at 500 nm, characteristic of the $RuPPS^{4-}$ excited. No other transient signal was observed at any time scale.

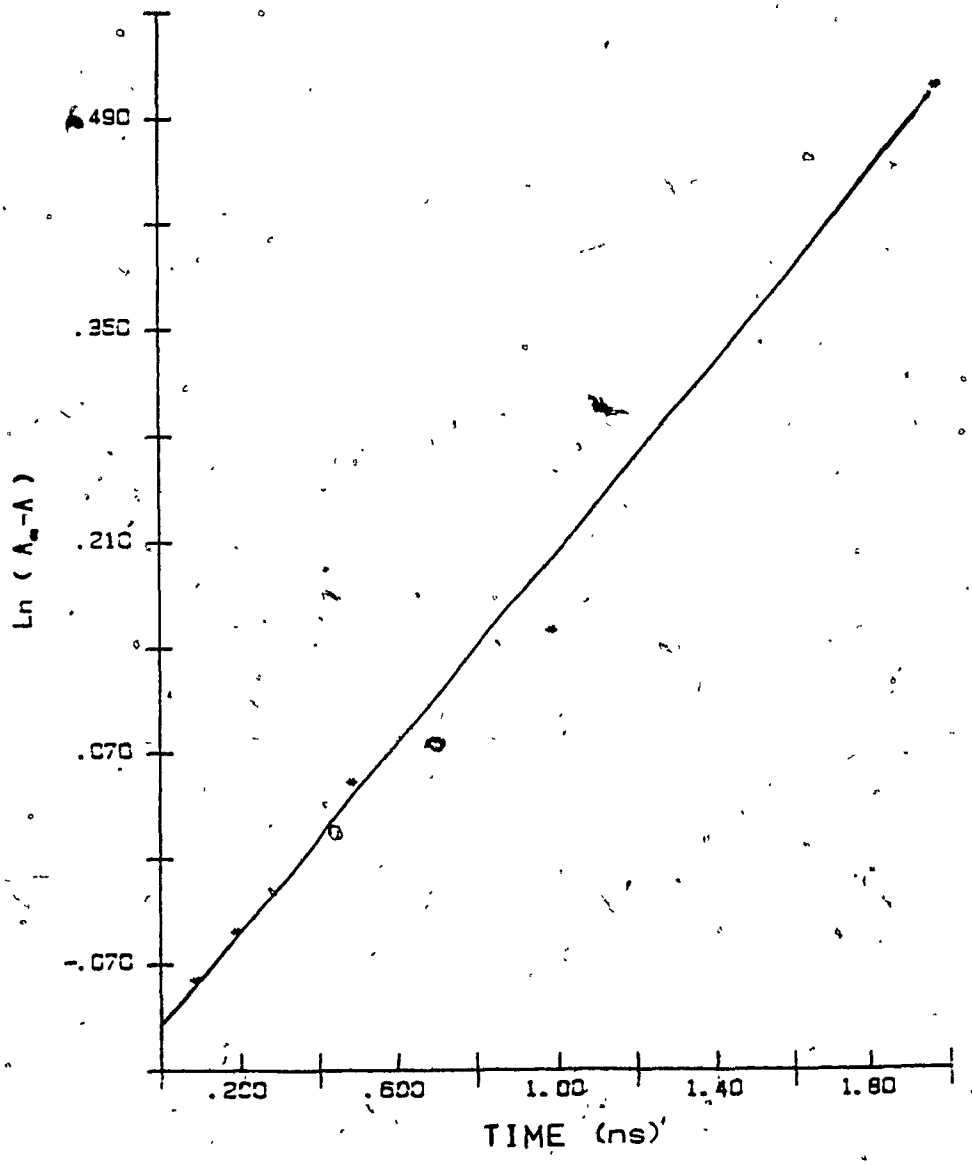

Figure IV.10 Kinetic analysis of the pico-second flash photolysis of a solution of TiO_2 and $RuPPS^{4-}$. The conditions are the same as Figure IV.9. a is taken at 10 ns and the monitoring wavelength is 625 nm.

d) TiO_2 - erythrosin system:

Figure IV.11 shows the transient behavior of a suspension containing 4 g/l of TiO_2 and 1,2 x 10^{-6} M of erythrosin. The transients observed are very similar to the ones observed in the TiO_2 - $RuPPS^{4-}$ system. The band gap excitation of TiO_2 at 20 ps cannot be clearly observed since the erythrosin has a strong bleaching in the middle of the spectra. A blue transient with a maximum around 450 nm and a red transient with a maximum at 630 nm compose the overall spectra at longer time. The kinetic analysis gave a rate constant of 5,5 x $10^8 s^{-1}$. Only one experiment has been done on the erythrosin - TiO_2 system.

e) pH effect:

A decrease of the pH by the addition of HCl can have two different effects in the suspension. First, it decreases the size of the particles by increasing the charge at the surface of the particles. This can be seen by looking at the "disappearance" of particles in suspension when HCl 1N is added. Also, the addition of HCl 1N, bringing the pH to 0, protonates some sulfonate groups on the dyes. Negative charge on the dyes is reduced as is the tendency to be bound onto the colloid surface. Due to these two phenomena, the signal observed for a suspension containing TiO_2 and a dye is reduced drastically by the addition of HCl (1N).

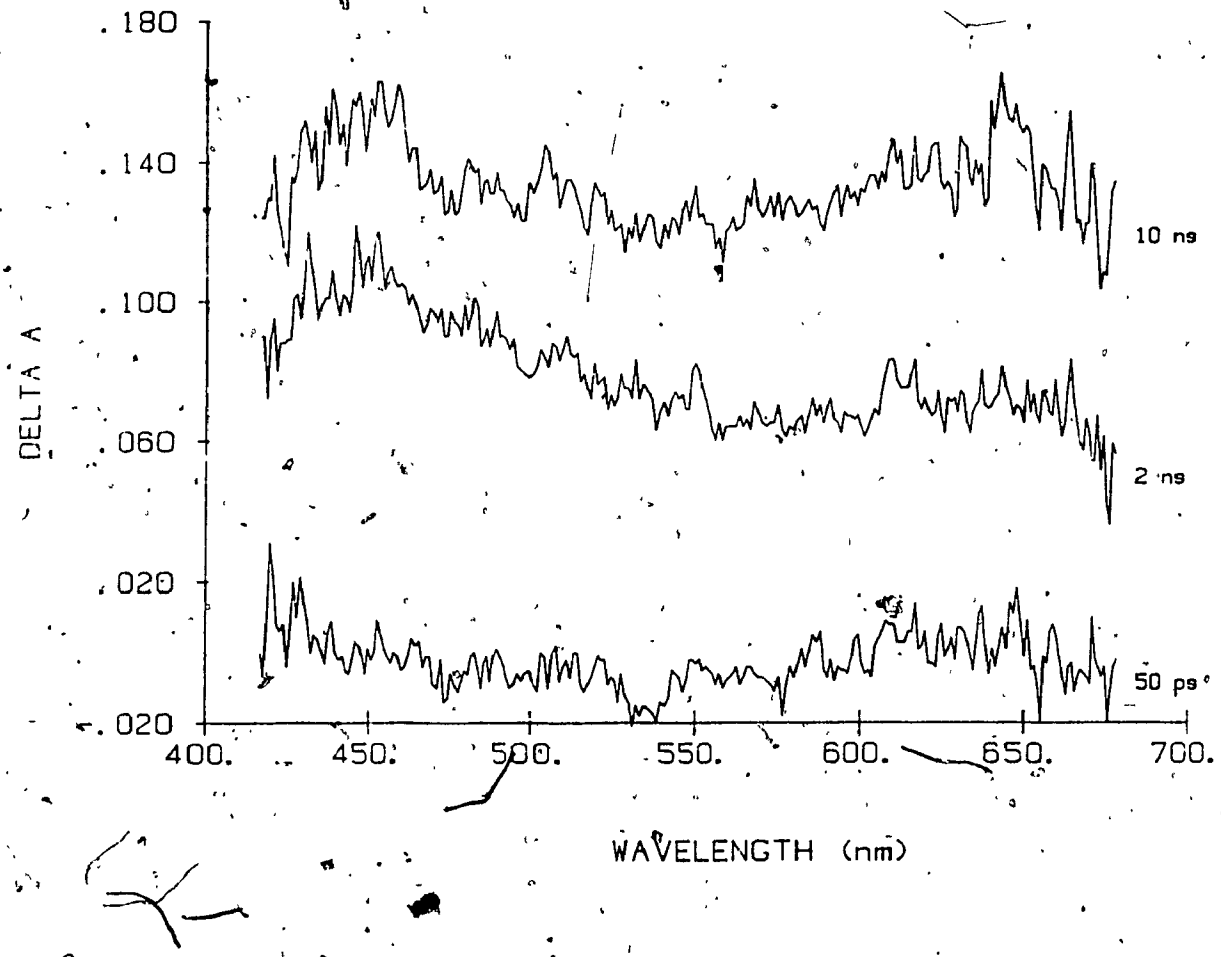

Figure IV.11 Picosecond flash photolysis of a solution of TiO_2 and erythrosine. The concentration of the TiO_2 is 10 g/l and the concentration of the erythrosine is $1,2 \times 10^{-6}$ M. The excitation wavelength was 355 nm.

On the other end, an increase of the pH of the suspension by dialysis increases the size of the TiO_2 particles and should increase the number of electrons and holes produced in TiO_2. Contrary to what is expected, there is a net decrease of the transient absorption at time delay longer than 5 ns.

f) Concentration effects:

As we have mentioned previously, there is no evident change of the rate constant with a change of the TiO_2 concentration or a change in the dye concentration. Nevertheless, there is a large change in the intensity of the transient with a change of the concentration of the dye. The absorbance increases initially in proportion to the concentration of the dye and reaches a plateau at a concentration of $2,5 \times 10^{-5}$ M of $RuPPS^{4-}$. The same trend has been observed for the $CuPcTS^{4-}$ but with a plateau at 2×10^{-4} M.

There is also an increase in the transient absorption when the concentration of TiO_2 is increased. This cannot be analyzed quantitatively because of the fact that an increase in the concentration of TiO_2 also means an increase of the particle size.

g) Temperature effect:

The transient absorption of a suspension containing 10 g/l of TiO_2 and $2,5 \times 10^{-5}$ M $CuPcTS^{4-}$ was taken just after

the suspension was removed from the refrigerator. This transient spectrum is shown in Figure IV.12 (curve a). After flashing for 10 minutes, the transient spectra decreased considerably (curve b). We continued to flash the same suspension for another 10 minutes and the transient decreased further. To test that this was a temperature effect, the suspension was returned to the refrigerator to cool it down. The signal was restored to the initial value (curve c) by this chilling. The transient started to go down again on repeated flashing as observed initially.

h) Energy effect:

Both TiO_2 - $CuPcTS^{4-}$ and TiO_2-$RuPPS^{4-}$ systems show an energy dependence of their transient absorption spectra. This energy dependence cannot be quantified easily due mainly to the fact that it varies from one preparation to another. Nevertheless, some trends can be observed and they will be discussed later.

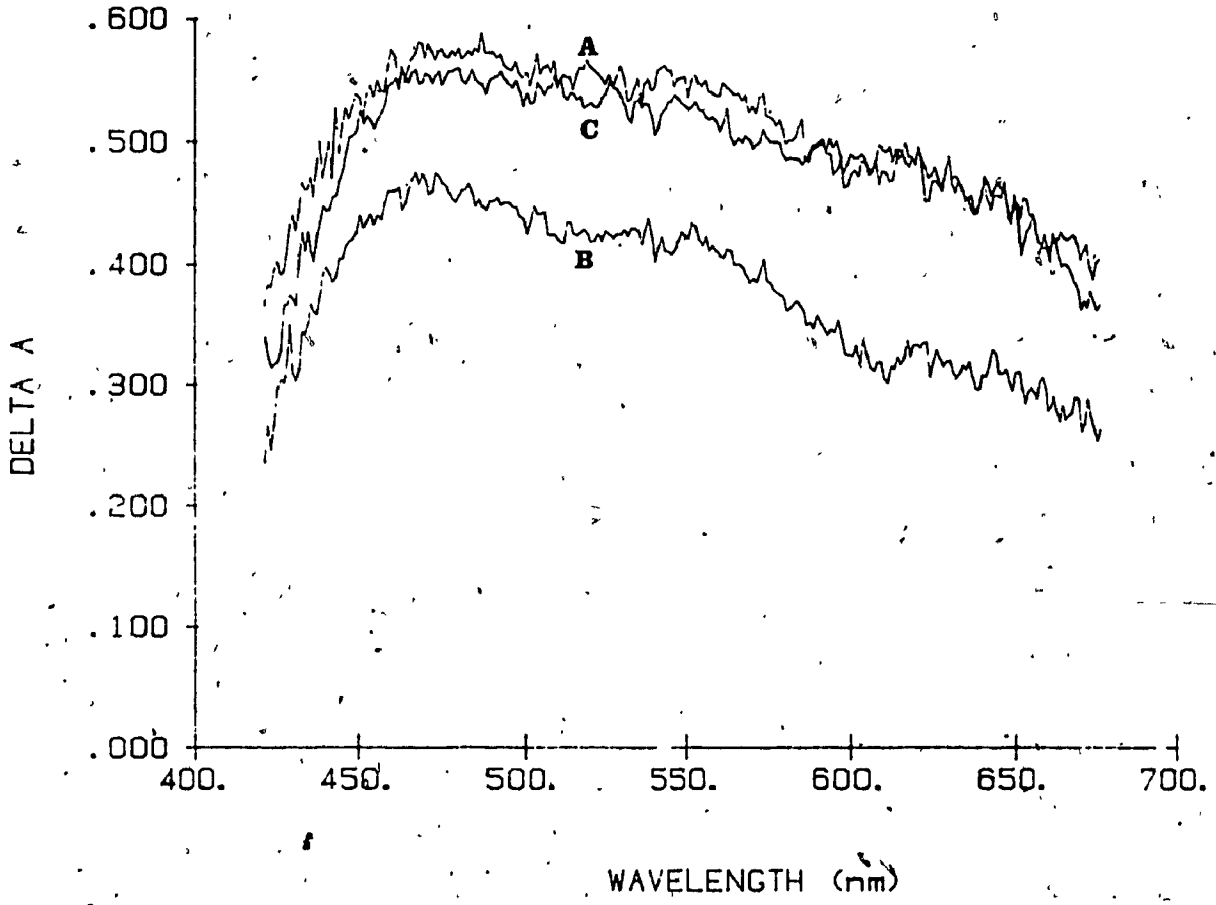

Figure IV.12 Picosecond flash photolysis of a solution of TiO_2 and $CuPcTS^{4-}$ at different temperatures. The concentration of TiO_2 is 10 g/l and the concentration of the dye is $2,5 \times 10^{-5}$ M. (A) Spectra taken after the solution was removed from the refrigerator. (B) After flashing for 10 min. (C) After cooling down. The delay was 5 ns and the excitation wavelength was 355 nm.

V. DISCUSSION

V.1. The colloidal particles of TiO_2:

The absorption spectrum of colloidal TiO_2 is a faithful representation of the particle size of the TiO_2. We have estimated the particle sizes to vary between 20 Å for the smallest particle to approximately 250 Å for the particles showing no further red shift in the absorption edge. Using the model developed by Brus (1984), one should be able to determine the diameter of the 1S exciton of TiO_2 with the equation I.3. By taking the value of 173 for the dielectric constant and 30 m_0 for the electron mass in TiO_2 (Yana, 1963), we obtain a diameter of 3 Å for the first exciton in TiO_2. We see immediately that this value is far from reality since 3 Å is approximately the size of a Ti^{3+} ion.

This small diameter can be explained if we look at the values used in this calculation. The value used for the mass of the electron in TiO_2 is 30 m_0 which is at least 20 times higher than the mass used in any other semiconductor. This high value of the mass of the electron in TiO_2 can be explained by looking at the molecular orbitals of TiO_2.

The valence band of TiO_2 is composed of the s and p orbitals of the oxygen which make σ and π bonding systems with the s, p and d orbitals of the titanium. The conduc-

tion band is composed primarily of the d orbitals of the titanium atoms. These d orbitals have a very poor overlap giving a very narrow band for the semiconductor conduction band. This narrow band restrains the movement of the electrons in the semiconductor which is reflected by a high effective mass of the electron. The poor overlap between the d orbitals comes from the fact that by taking the rutile lattice arrangement, TiO_2 minimizes the interaction between the titanium atoms.

Since small colloidal particles do not exhibit a high degree of rutile arrangement, it is possible to have a larger overlap between the d orbitals of the titanium, thus decreasing the mass of the electron by a significant factor. On the other hand, the value used for the dielectric constant of TiO_2 (173) is very high compared to other semiconductors. This value will also be decreased if we consider the low degree of order shown by the particles. This effect should be smaller than the previous one since the polarizability is less dependant on the lattice arrangement.

Nevertheless, we will not obtain a value of 200 Å for the exciton radius, but none of the semiconductors studied show an exact exciton radius matching with the experimental value of the minimum radius for bulk material. Brus (1984) suggests that in order to be more accurate, the charge density will have to be considered instead of a resort to

the effective mass approximation.

The absorption coefficients measured for these particles show clearly the band edge shift related to the particle size. It is evident that it is not possible to give a unique absorption coefficient for the TiO_2 colloids. Instead, an absorption coefficient corresponding to the radius of the particle must be adopted and also, its evaluation will permit the determination of the size of the particles without having to resort to transmission electron microscopy or dynamic light scattering analysis for every suspensions prepared.

Gratzel and Moser (1983) have reported an absorption coefficient of 0,785 g^{-1} l cm^{-1} at 347 nm for suspensions of TiO_2 in which they have measured a radius of 50 Å for the colloids. This value is higher than observed here for any preparation. Two reasons can be given to explain the discordance of these results. First, it is possible that we are overestimating the size of the particles such that all our particles have a radius lower than 50 Å. It is also possible that Gratzel and his group have measured the absorption spectra of their colloids after dialysis which would have considerably increased the size of the particles. It is very plausible that we are overestimating the size of our particles, but not to a point where the size of the particles of the 4 g/l suspension will be less than 10 Å. Thus, the second explanation is likely. This reference

is not specific on the essential point but is consistant with our interpretation.

The nature of the species giving rise to a transient absorption upon band gap excitation of TiO_2 cannot be identified unambiguously. This transient can be due to the absorption of an electron. Rothenberger et al. (1985) were the first to report this transient absorption and they attribute it to the absorption of an electron in a trap site in accordance with the large red region absorption observed in n-type TiO_2 or when a hole scavenger is present at the surface of TiO_2 (Kolle et al., 1985).

We think that this attribution is oversimplified since the transient is present within the arrival of the pulse whereas a trapping process is expected to require some induction time to permit the electron to encounter the trap site. Also, the fast disappearance of the transient is difficult to reconcile with the fact that the blue color induced in TiO_2 with hole scavengers can be observed for a long period (minutes for deoxygenated suspensions).

We attribute this absorption to an electron in the conduction band because of the disappearance of that transient when a dye is present as we will see later. The decay process is due to the recombination of the hole and the electron. The number of electrons created per particle can be calculated assuming that each photon absorbed creates an electron in the conduction band. With an energy

of 2,5 mJ in a 6,28 x 10^{-6} l volume and a size particle of 200 Å (6,3 x 10^{12} particles), we obtained 260 electrons per particle. This value gives an absorption coefficient of 2200 M^{-1} cm^{-1} which is 2 times higher than the value reported by Kolle et al. (1985) for a trapped electron.

The kinetic analysis showed a second-order process for the decay of the transient observed. The rate constant was dependant upon the initial absorbance of TiO_2 and for four different suspensions of TiO_2, values between 2,0 x 10^{-10} n_e^{-1} s^{-1} and 4,0 x 10^{-10} n_e^{-1} s^{-1} were obtained. If 1 electron is created in the conduction band of each particle the most probable lifetime is 3 ± 2 ns.

With the value of the rate constant for the decay of the transient, we have a direct measurement of the rate of recombination of the hole-electron pair and since the time necessary for an electron to diffuse to the surface is approximately 2 ps, a scavenger at the surface will have plenty of time to scavenge the electrons if the interfacial electron transfer is fast enough.

There is always a residual absorbance in the transient even after a long time (10 ns). This is probably originating with electrons that have been trapped and detrapped from shallow traps.

The large error in the rate constant is mainly due to the absorbance error, but it also results from a change in particle size. The blue shift of the absorption edge

decreases the absorption of the smaller TiO_2 particles. In addition, an increase of the rate constant is observed for smaller particles. This is mainly due to the fact that in a smaller particle, electrons and holes can encounter more often, increasing the chances of charge recombination.

V.2 The TiO_2-dye systems:

V.2.1 Absorbance and excited species

Table V.1 gives the absorbance of the dye and the TiO_2 at 355 nm for every system before and after they are mixed. We can see that the absorbance of the TiO_2 increases a great deal during the mixing process.

Table V.1 Absorbance of the TiO_2 and the dye at 355 nm before and after mixing.

	Absorbance			
	TiO_2	$CuPcTS^{4-}$	TiO_2	$RuPPS^{4-}$
Before	.02	.34	.08	.03
After	.26	.34	.20	.03

The only reason for this phenomenon is the increase in the size of the particles and it can also be seen by the red shift of the absorption edge of the TiO_2 dye mixture with respect to the TiO_2 alone.

The number of photons in a 2.5 mJ pulse at 355 nm is $4,46 \times 10^{15}$ photons. For a TiO_2-dye suspension where the

TiO_2 has an absorbance of 0,2 in a 2mm cell, $1,65 \times 10^{15}$ photons will be absorbed by the TiO_2 leaving approximately $2,81 \times 10^{15}$ photons for the dye molecules. The typical concentration used for the dye is $2,0 \times 10^{-5}$ M so that a maximum of $7,6 \times 10^{13}$ molecules will be in the volume of the excitation pulse ($6,3 \times 10^{-6}$ l). Since all the dyes have an absorbance over 0,03 at 355 nm, the number of photons absorbed by the dye will be $8,31 \times 10^{13}$ giving an excitation of practically 100% of the dye molecules in the excitation volume. This means that a typical concentration $4,4 \times 10^{-4}$ M of electrons will be excited in the TiO_2 and at the same time, all the molecules of the dye will be excited. The details of the calculations and a table of these values is given in Appendix D.

V.2.2 Fate of the carriers:

a) Proposed mechanism:

The fact that both the TiO_2 and the dye are excited at the same time in the suspension can lead to many energetically possible mechanisms. Electron transfer from the dye to TiO_2 or from TiO_2 to the dye, hole transfer from the dye to TiO_2 or from TiO_2 to the dye are some of the various possibilities. In this thesis, a mechanism is proposed that takes into account all the observed results. Other mechanisms fail to accommodate all aspects. Moreover, one mechanism is proposed for all the systems studied and we

will see below how every different system fits into that mechanism.

The mechanism (represented in ~~Figure~~ V.1)' is as follows: upon band gap excitation ($h\nu_{BG}$) an electron is excited into the conduction band and a hole is left in the valence band. At the same time, a dye molecule is excited giving an electron in the LUMO and a hole in the HOMO. As we have seen before, the electron and hole can recombine, but since there is a scavenger at the surface, the electron will be transferred from the C.B. into an empty orbital of the dye. The result of this electron transfer will be a hole left in the valence band and a reduced dye. The hole in the valence band will later be trapped in a p-site whereas the reduced dye can reduce a species present in the solution or at the interface.

The proposed mechanism is then an electron transfer from the TiO_2 into the excited dye and the trapping of a hole inside or at the surface of the TiO_2 particle. We will now follow each step of this mechanism and see how they are related to the transients observed in the different systems.

b) TiO_2 - Cu Pc TS^{4-} system:

At 20 ps, the excitation of the TiO_2 - $CuPcTS^{4-}$ system shows the transient of the electrons in the conduction band reported above. This transient is screened in the red side of the spectra by the bleaching of the dye. If we compare

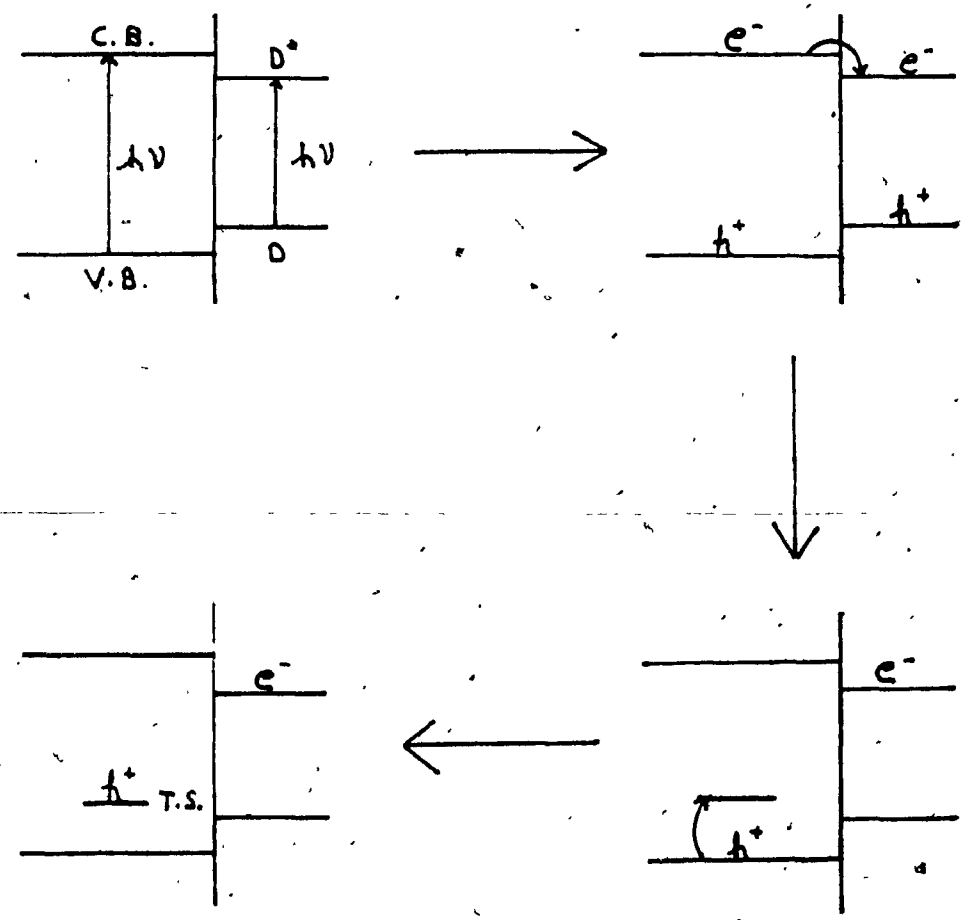

Figure V.1 Proposed mechanism for the interpretation of the picosecond flash photolysis results. (A) The TiO_2 and the dye are excited after the absorption of two photons. (B) Electron transfer (E.T.) from the conduction band (CB) of the TiO_2 to the dye. (C) Hole trapping (h^+ tr) of the hole left in the valence band (V.B.) of the TiO_2.

this spectrum with a spectrum of the excitation of the $CuPcTS^{4-}$ alone at 20 ps (Figure V.2), we can see that on TiO_2, the excited state absorption of the dye and the bleaching of the dye are already partially depleted at 20 ps.

At 100 ps, the transient spectrum of the system shows no feature except residual bleaching of the dye. Nevertheless, at 500 ps, a new transient has grown and this transient is characteristic of some reduced metallophthalocyanine dyes. We have attributed this transient to the species $Cu(I)PcTS^{5-}$ following the comparison of this transient with transients of reduced porphyrine and phthalocyanine derivatives (Nevin et al., 1986 and Neta, 1981). Table V.2 shows the position of the maxima for different reduced dyes and the maimum absorptions of the transient observed in this study.

Table V.2 Absorption maxima of reduced porphyrines and phthalocyanines and the transient observed for the TiO_2-$CuPcTS^{4-}$ system.

	max (nm)	
ZnTPPS	450	640
CoTPPS	500	650
CoPcTS	465	645
Transient	480	640

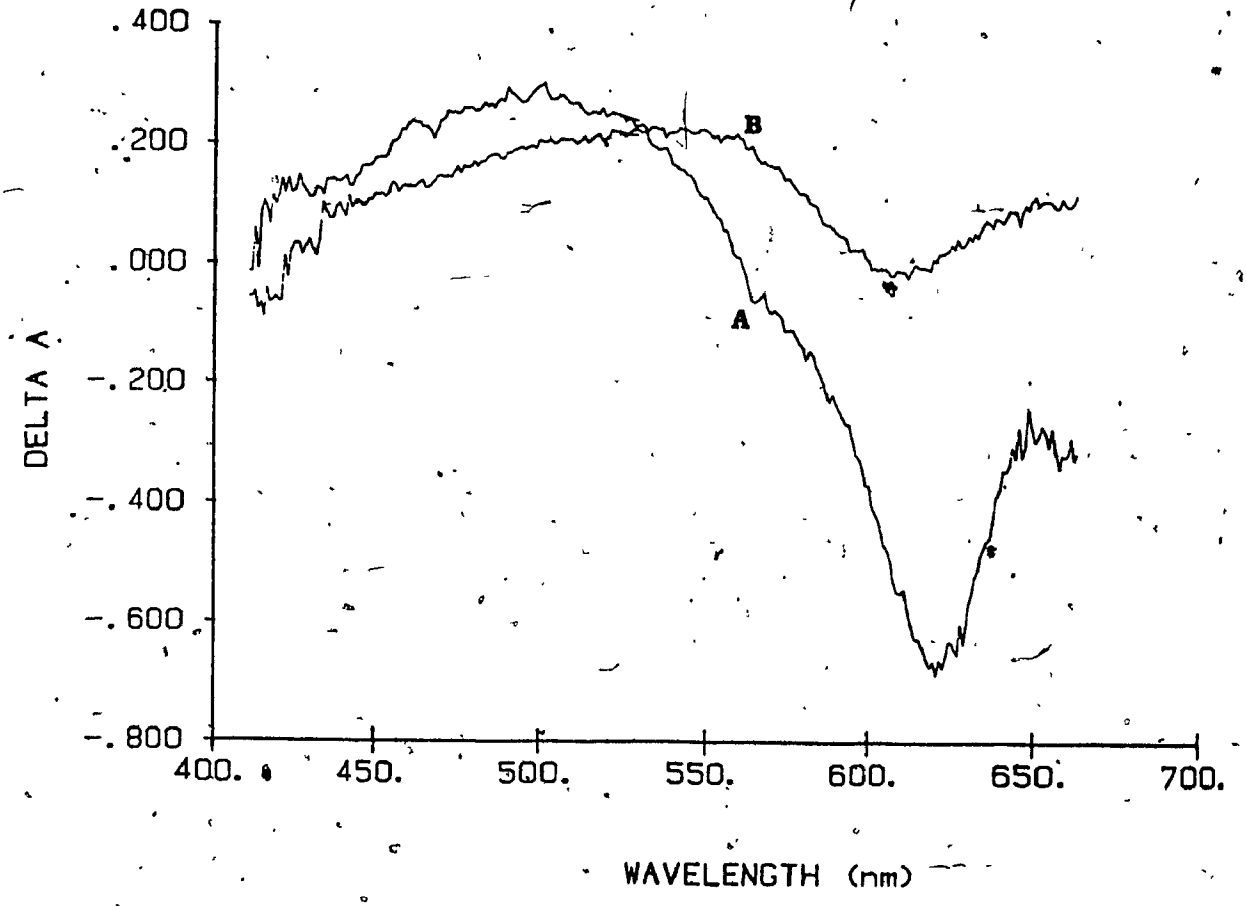

Figure V.2 Picosecond flash photolysis of a solution of TiO_2-$CuPcTS^{4-}$ and a solution containing only $CuPcTS^{4-}$. (A) Spectra of a solution containing 6,65 x 10^{-5} M of the $CuPcTS^{4-}$. (B) Spectra of a solution containing 1,3 g/l of TiO_2 and 6,65 x 10^{-5} M of $CuPcTS^{4-}$. The delay is 20 ps and the excitation wavelength is 355 nm.

We have attributed the transient absorption to a reduced form of the dye following this matrix comparison: 1) There is no large effect by changing the central atom on the position of the bands for reduced porphyrines (CoTPPS vs ZnTPPS) and 2) A change in the ligand does not show a significant change in the position of the bands since PcTS is similar to TPPS (CoPcTS vs CoTPPS). This means that the spectrum of the reduced CuTPPS should be similar to the spectrum of the CoTPPS. Also, since a change in the ligand has no significant effect, the spectrum of the reduced CuPcTS should be similar to the spectrum of the reduced CuTPPS.

By combining these relations, we can assume that the spectrum of the reduced CuPcTS is similar to the spectrum of the reduced CoPcTS. On the assumption of an absorption coefficient of $4,5 \times 10^4\ M^{-1}\ cm^{-1}$ at 480 nm (from Co(I) $PcTS^{5-}$), we obtained a concentration for the reduced dye of $6,2 \times 10^{-5}$ M which is 93% of the initial dye concentration, in agreement with the above argument for the quantity of dye excited.

At 10 ns, the transient is a large band with a maximum at 630 nm and a shoulder at 480 nm. This shoulder is due to the reduced species observed at 500 ps. By subtracting the transient at 500 ps from this transient (Figure V.3), we obtain the spectrum of the hole trapped in TiO_2 which has a maximum at 630 nm. The absorption coefficient at 630

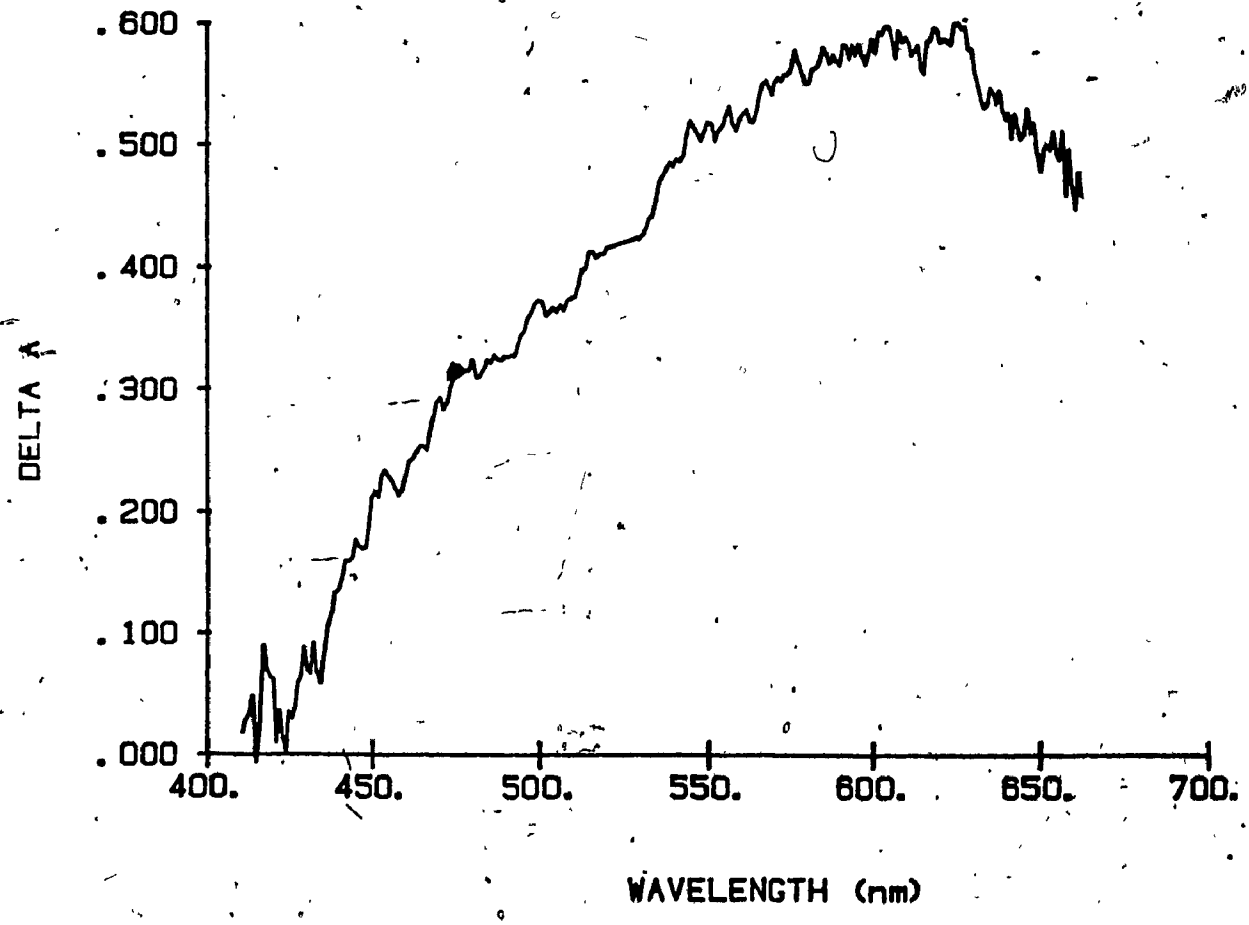

Figure V.3. Subtraction of the transient observed at 500 ps from the transient at 10 ns for a solution of TiO_2-$CuPcTS^{4-}$. Same conditions as Figure IV.7.

nm calculated by taking the hole concentration equal to the reduced dye concentration ($6,2 \times 10^{-5}$ M) is $4,2 \times 10^{4}$ M^{-1} cm^{-1}.

The transients observed for the TiO_2-$CuPcTS^{4-}$ are in agreement with the mechanism proposed except at short time delay (20 ps to 100 ps). At 100 ps, following our mechanism, we should see a spectrum which will be the combination of the absorption of the electrons not yet transferred to the dye (still in the TiO_2), the absorption of the reduced dye molecules, the absorption of the non-reduced excited dye molecules, and the bleaching of the non-reduced ground state dye molecules. It is not clear that we can account for the spectrum observed at 100 ps by any combination of these transients.

Nevertheless, the behavior can be explained by looking at the energy levels involved in the reduction process of the dye. The electron is transferred from the TiO_2 to the π orbital of the phthalocyanine ring. This is removing the absorption of the excited state level and also the bleaching of the ground state since the HOMO orbital will be filled exactly as in the ground state. In addition, the transient of the reduced dye will not be seen since the electron is in the π^* orbital and not yet in the copper orbital $d(x^2-y^2)$. The reduced dye species responsible for the transient absorption at 500 ps is not yet formed. The first reduced species is $(Cu(II)PcTS(7-))^{5-}$. The electron

is later transferred to the copper ($Cu^{II} + e \rightarrow Cu^{I}$) to give the $(Cu(I)PcTS(6-))^{5-}$; the transient spectrum at 500 ps results. We can now account for the spectra observed at 20 ps and 100 ps by a combination of the very small amount of excited state absorption and ground state bleaching of the non-reduced excited dye molecules. The reduced dye and the trapped holes do not yet give any contribution to the overall spectra observed at those times.

The energy levels show that this mechanism is the favored one. Figure V.4 shows the redox potential of the different couples involved in the mechanism. The energy level of the $^{*}CuPcTS^{4-}/CuPcTS^{5-}$ is at 0,89 V more positive than the conduction band so that electron transfer from TiO_2 is energetically very favorable. Furthermore, the $CuPcTS^{4-/5-}$ couple is 0,65 V more negative than the Cu^{2+}/Cu^{+} couple. Figure V.5 shows part of the order of the molecular orbitals of the $CuPcTS^{4-}$. We have assumed that due to the presence of an electron in the $d(x^2-y^2)$ orbital, this orbital will come down to the level of the HOMO of the phthalocyanine ring. ESR experiments (Guzy et al., 1969) have shown that the HOMO of the CuPc has 70% of metal character. The LUMO is a π^{*} orbital of the phthalocyanine ring. The electron will be transferred from the conduction band of the TiO_2 to the LUMO orbital of the $^{*}CuPCTS^{4-}$ to give the species $(Cu(II)PcTS(7^{-}))^{5-}$. The electron from the LUMO will later relax to the HOMO orbital

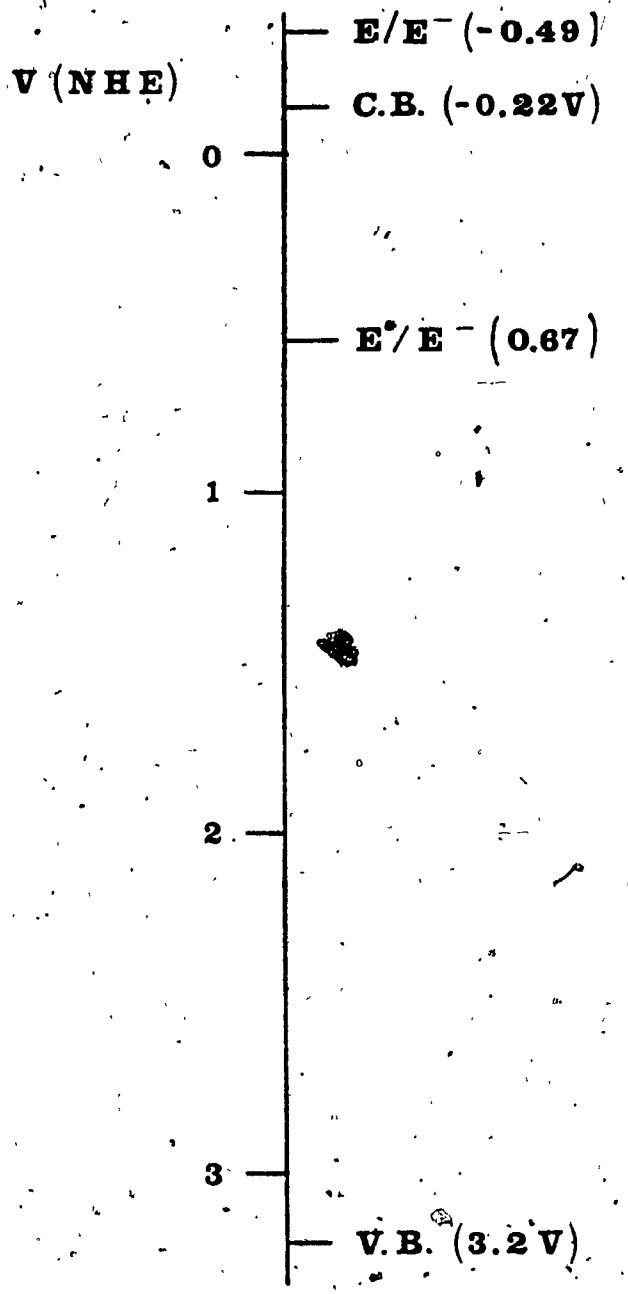

Figure V.4 Energy levels for the reduction of the $^{*}CuPcTS^{4-}$ by the conduction band of the TiO_2. The potentials are given on the NHE scale.

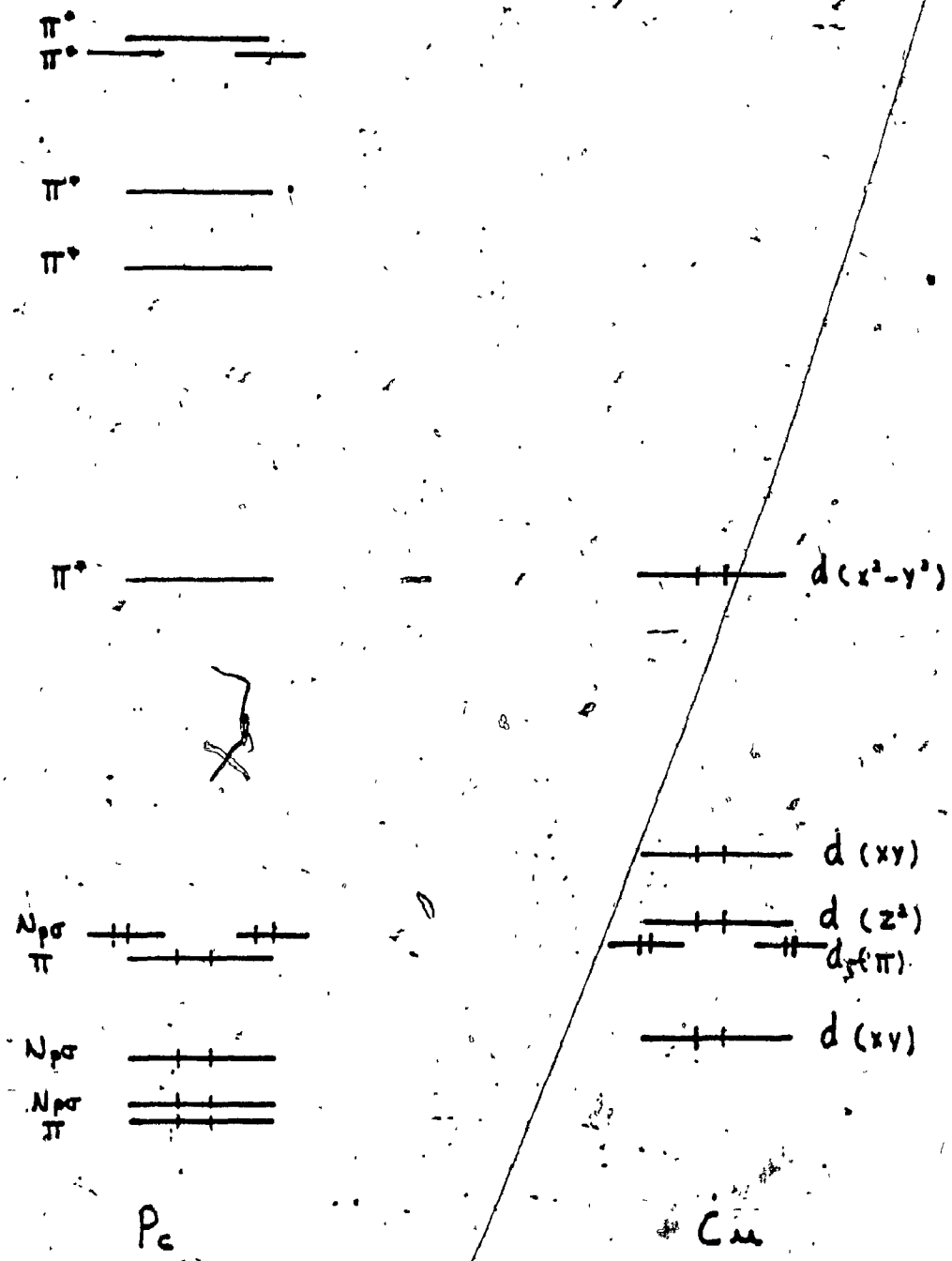

Figure V.5 Molecular diagram of the CuPc. It is assumed that due to the presence of electrons in the $d(x^2-y^2)$ orbital, this orbital will come very close to the HOMO orbital of the Pc.

which has 70% metallic character to give the species (Cu(I) PcTS(6^-))$^{5-}$ giving the spectra observed at 500 ps. The reduction of the metal has also been observed in the case of the CoPcTS^{4-} (Nevin et al., 1986).

c) TiO_2-RuPPS^{4-} system:

Even though the RuPPS^{4-} complex has an absorbance of only 0,03 at 355 nm, at pump beam energies of 2,5 mJ, all the molecules inside the volume of the pump pulse will be excited (see calculations in Appendix D). This produces, again, a system with 2 photons absorbed. Two redox reactions are thus possible: the oxidation of the ground state of the Ru(II)PPS^{4-} to give Ru(III)PPS^{3-} or the reduction of the excited state to give Ru(I)PPS^{5-}. These two species are easily resolved by their absorption spectra. The Ru(I) complex shows an absorption maximum at 480 nm, with an extinction coefficient of approximately 1,4 x 10^4 M^{-1} cm^{-1} whereas the Ru(III) has absorption maxima at 420 nm and 680 nm. The absorption coefficient is so low (3,3 x 10^3 M^{-1} cm^{-1} for 420 nm) that the band is not usually observable (Watts, 1983).

At 20 ps, in addition to the transient absorption of the electrons in the TiO_2 conduction band, we can clearly observe the bleaching of the dye and the start of a growth of a new transient in the red side of the bleaching dip. At 100 ps and 500 ps, this transient is not fully resolvable since it is partially superimposed on the bleaching of

the dye.

After 500 ps, the same broad transient as the one observed with the $CuPcTS^{4-}$ starts to grow and we can clearly see its shape at 10 ns where the transient absorption of the dye is reduced. We attribute the transient of the dye to the reduced form of the dye ($RuPPS^{5-}$) which has an absorption maximum at 480 nm with an absorption coefficient of $1,4 \times 10^4\ M^{-1}\ cm^{-1}$. This gives us a concentration of the dye reduced equal to $4,3 \times 10^{-5}$ M. The large band has a maximum at 630. By assuming that for each molecule of dye reduced there is a hole trapped, we obtain an absorption coefficient of $4,5 \times 10^4\ M^{-1}\ cm^{-1}$. This is exactly the same value as the one obtained for the $CuPcTS^{4-}$ dye.

We observed the same redox reactions for this dye as when the copper phthalocyanine dye is used. The $RuPPS^{4-}$ dye and the TiO_2 are excited at the same time, an electron is transferred from the conduction band of the TiO_2 to the dye at the surface giving a reduced dye and a hole is left in the valence band. This hole is later trapped to give the broad transient observed. The potential for the reduction of the excited state of the $^*RuPPS^{4-}$ is +0,82 V so this reaction will be favored thermodynamically.

d) TiO_2 - Erythrosin system:

The TiO_2- erythrosin system shows exactly the same features as the other two systems. The reduced erythrosin

has an absorption at 410 nm with an absorption coefficient of 3,4 x 10^4 M^{-1} cm^{-1}. In our case, the band appears to have a maximum near 440 nm, but as mentioned previously, the continuum generated is "peaked" so that continuum subtraction has probably shifted peaks. The concentration of reduced dye measured is 1,5 x 10^{-5} M. On the same assumption that for every reduced dye molecule produced there is a hole trapped, we obtain an absorption coefficient of 4,76 x 10^4 for the trapped hole.

e) Overall reaction scheme:

For all the three cases studied here, we can draw an overall scheme representing the fate of the electrons and holes in each system (Figure V.6). Upon band gap excitation, and excitation of a dye molecule (a), an electron is transferred from the conduction band of the TiO_2 to an excited dye molecule (b). The hole left in the valence band is trapped (c) giving the large band observed after 500 ps. The absorption coefficient measured for the trapped hole in all three systems presented here is 4,6 ± 0,1 x 10^4 M^{-1} cm^{-1} at 630 nm. For 12 different suspensions containing one of the dyes studied, the absorption coefficient was 4,5 ± 0,5 x 10^4 M^{-1} cm^{-1}.

This mechanism of electron transfer from the TiO_2 to the excited dye cannot be generalized for the other systems studied elsewhere because in our case consideration must be given to the two photon process which happens only when the

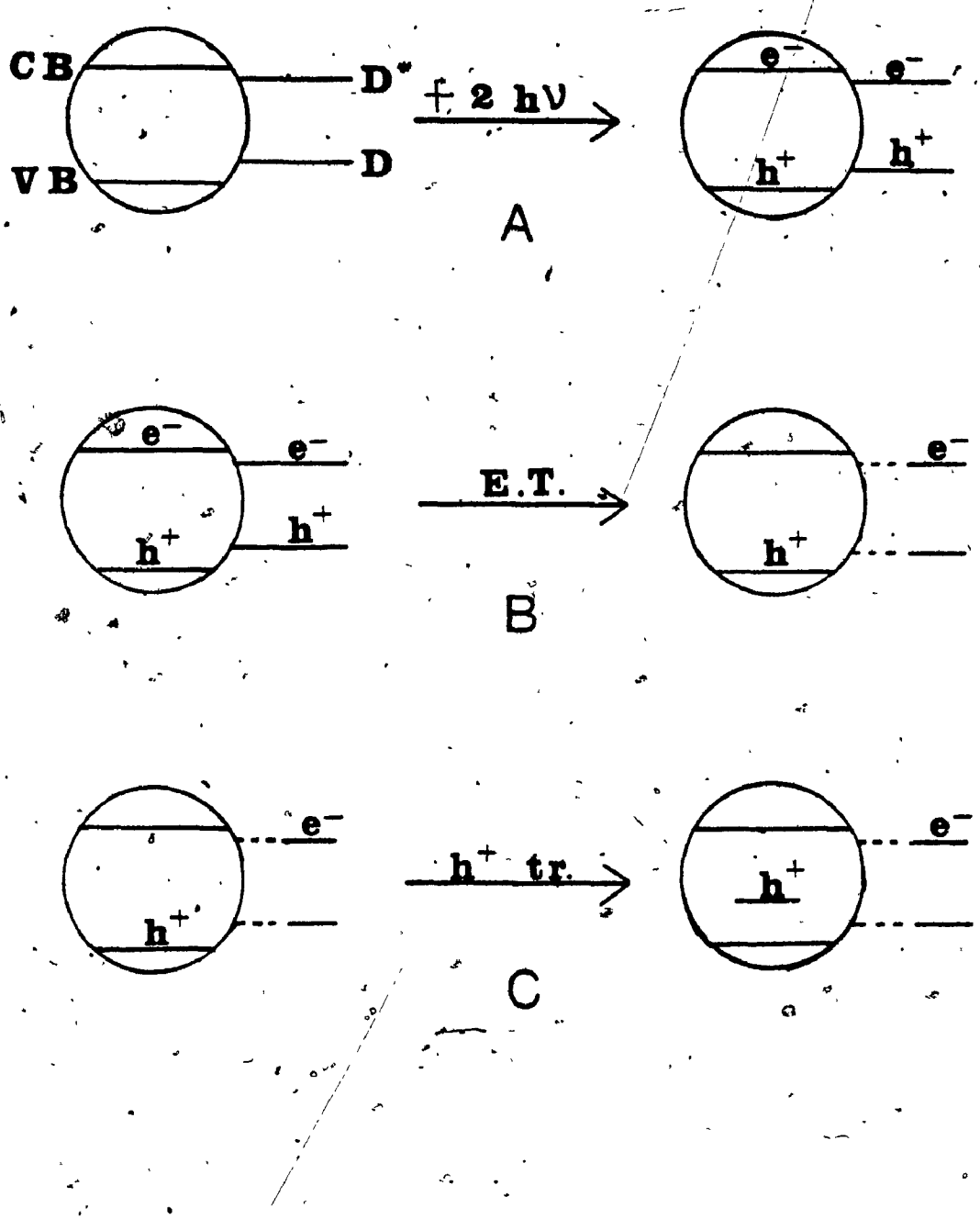

Figure V.6 Schematical representation of the overall process. A) Excitation of the TiO_2 and the dye by the absorption of two photons. B) Electron transfer from the conduction band (CB) of the TiO_2 to the dye. C) Trapping of the hole left in the valence band (VB) of TiO_2.

density of photons is fairly high. For systems where the density of photons is low, the excitation of both the TiO_2 and the dye will not be possible and the process will be completely different.

It is not possible to explain our results with any other mechanism because we always observe the presence of the reduced dye which cannot be thermodynamically formed from the ground state.

The broad band observed at time delay longer than 500 ps is very similar to the one already observed by many authors[2]. They have attributed this band to an electron trapped in TiO_2. Our attribution of a hole trapped is not in contradiction with these authors since it is evident that both a hole and an electron can be trapped in TiO_2. The fact that the two bands have a similar shape is not surprising since the two processes giving rise to the transient arise from a wide band: the valence band in the case of the trapped hole transient and the conduction band in the case of the trapped electron transient.

The two broad bands seem to show a maximum at approximately 650 nm, but this is probably only a coincidence since there is no relation between the levels involved in the observation of these two bands. In fact, it may be an artifact of the spectral distribution of the probe pulse

---

[2] As an example, see Henglein (1982) and Bahneman et al. (1984).

used in the Nd:YAG picosecond spectroscopy. Nevertheless, one possibility can make them look similar and it is the fact that they both involve nearly-free electron transitions. Both spectra look like the spectra of a solvated electron, but this attribution has to be rejected since the lifetime of this transient is much longer than the lifetime of a solvated electron (approximately 1 ns at pH of 1,5) (Hart, 1965).

f) Nature of the trapped state:

The most difficult part in the study of the carriers in undoped semiconductors is the determination of the nature of the trap sites. For the electron trapped sites in TiO_2, much evidence like the ESR experiments (Howe and Gratzel, 1985) has led to the conclusion that the nature of the trap site was a Ti^{3+} atom. The location is still unclear, but a fair amount of evidence supports assignment to surface Ti^{3+} atoms.

Since the TiO_2 is a better oxidizing agent than reducing agent, fewer experiments have been conducted to scavenge the electron in order to be able to observe the hole trapped. In this study, it was not possible to determine the exact nature of the hole trapped. Nevertheless, three possibilities can be pointed out. The preparation of our colloidal particles can lead to different defects and impurities in the particles. The rapid formation of TiO_2 by the hydrolysis of $TiCl_4$ can provide

Ti-Cl bond impurities in the lattice due to the partial or non-hydrolysis of a $TiCl_4$ molecule. The Cl^- species can result in a hole trapped by the formation of a Cl radical (atom) ($Cl^{\cdot}$).

Other species that can act as hole trapping are hydroxyl radical ($OH^{\cdot}$) formed at the surface of the particles or oxoradicals (O^-) which will be site defects in the interior of the particles. These two possibilities cannot be neglected since the major species at the surface will be hydroxyl groups at the pH of our particles. Also, since the particles are very small, defects in the particles will be very frequent so that oxo groups which are point defects in the particles will be numerous.

In this study, it was not possible to differentiate between these three possibilities since no other methods were used to track down the species responsible for the broad absorption. ESR experiments should probably give good indication of the nature of that species. As we will see later, changing the conditions of the experiments did not permit us to exclude any of the three possible hole traps.

g) Effects on the transient absorption:

By changing the different experimental conditions, we have tried to explore the characteristics and the nature of the trapped hole. No conclusive results were obtained due mainly to the fact that the change of one condition of the

experiment had more than one effect on the particles. Nevertheless, it is still important to list these effects in order to provide a better understanding of these experiments and their delicacy.

i) Effect of temperature (4-25 C):

The most obvious effect observed on the transient is a decrease of the signal intensity with an increase of the temperature. The absorption spectra of a suspension at raised temperature indicated the growth of the particles. However, the particles do not recover their initial size by cooling so that the decrease of transient intensity observed is probably not due to a change of size as it is reversible. Probably, increasing the temperature of the suspension, increases the mobility of the holes and electrons in the particle and the recombination rate will increase. Since the electron transfer is in competition with the recombination, an increase in the recombination rate should decrease the number of electrons transferred decreasing the intensity of the transient observed. This effect will be proportional to temperature not exponential in temperature, since an activation energy is not involved.

ii) Effect of pH:

As mentioned previously, (sec. V.2.e), the decrease or the increase of pH causes a decrease in the signal of the transient absorption. The decrease of the signal due to a

decrease of the pH can be explained by the detachment of the dye from the surface of the particles at pH lower than the pK_a of the dye molecule. For the same reason, an increase of the pH should decrease the intensity of the transient since the charge at the surface of the particle is reduced decreasing the affinity of the dye for the surface of the particle.

As well, the reduction in transient intensity may be caused by an increase of the size of the particle decreasing the possible number of defect sites in the lattice. Also, an increase in the pH decreases the number of OH groups at the surface which have been previously assigned as a possible trap site of the holes. In summary, the influence of dye binding cannot be separated from the influence of changing hole sites.

iii) Effect of energy:

No quantitative results were obtained which show the dependence of the transient signal intensity on the incident energy. This is mainly due to the difficulty of disentangling two photon processes. The process does not depend directly on the energy as observed for a one photon process. However, it does not exhibit a simple square dependence on energy observed for a two photon process where saturation is not occuring.

The dependence on energy observed in the case of our systems varies with the concentration of each species and

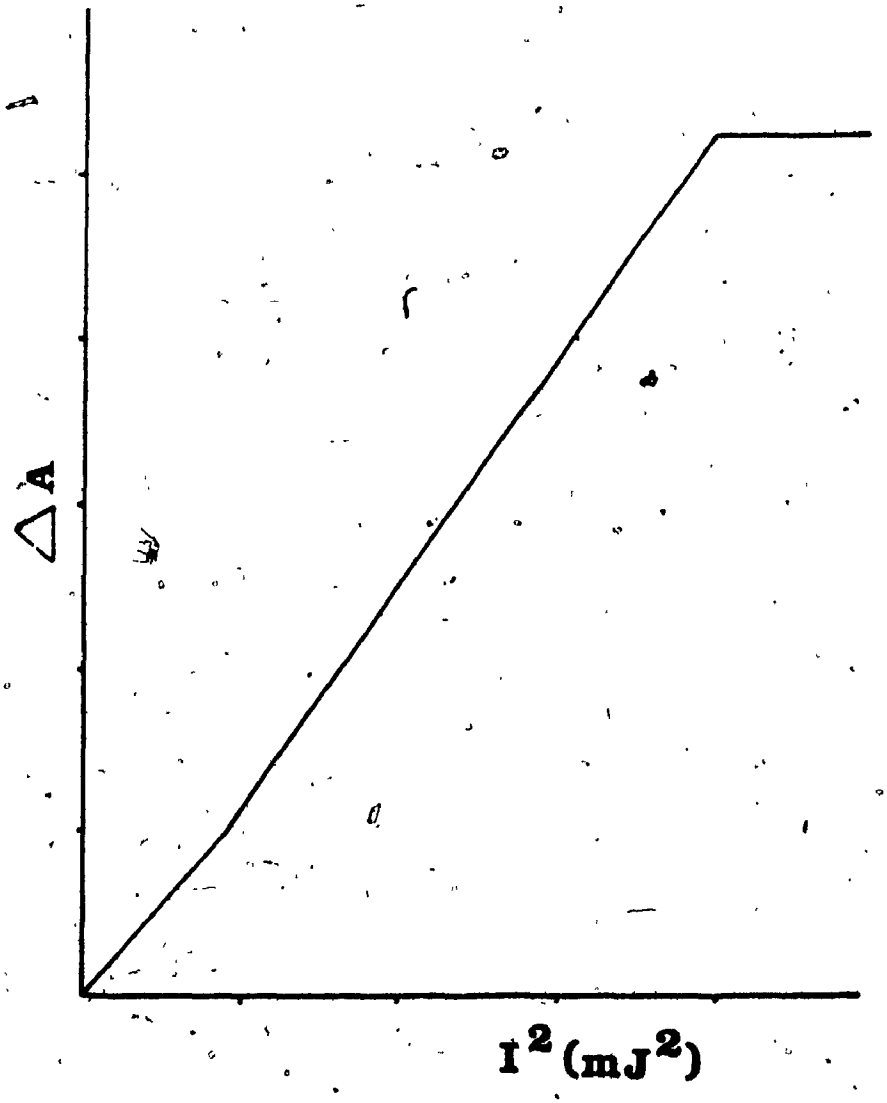

Figure V.7 Schematical representation of the transient signal as a function of the energy squared. The saturation energy is approximately 4 mJ.

also on the size of the TiO_2 colloids. This dependence is schematically represented in Figure V.7. The first growth of the signal is not linearly dependant on the square intensity since most of the photons are absorbed by the TiO_2 so that the dye molecules are not excited and the electron transfer is suboptimal. When there are enough photons to excite both the dye and the TiO_2, we can observe a square dependence of the signal on the energy. This relation is valid up to saturation where all the dye molecules and TiO_2 are excited.

The first behavior is observed for energies up to 2 mJ depending on the concentration of the TiO_2 and the size of the particles. When the particles were very small, this first part of the curve was absent and we were able to observe a direct relation between the energy of the pump beam and the intensity of the signal. To our knowledge, it is the first time that this behavior has been observed in this short time scale. It is caused mainly by the fact that this case is a simultaneous two photon process where one of the species is in excess.

iv) Effect of the concentration of the dye:

The intensity of the transient observed is proportional to the concentration of the dye up to a level where there is a plateau observed. This plateau must occur when there is one layer of dye molecules at the surface of the particles. If we take as an example the TiO_2 - $CuPcTS^{4-}$

system, a concentration of 4g/l of TiO_2 with a radius of 100 Å will give a total surface of 283 m^2/l. The $CuPcTS^{4-}$ has an approximate dimension of 400 $Å^2$ which means that it will take a concentration of $1,2 \times 10^{-4}$ M to cover all the TiO_2. The value obtained is 2×10^{-4} M which is very close to that value. The same behavior is also observed for the TiO_2 - $RuPPS^{4-}$ system.

V.2.3: Kinetic considerations

This study has been motivated by the possibility to answer two important questions. What is the fate of the carriers generated in TiO_2 and what is the rate of interfacial charge transfer? We now have the tools to answer those questions. The general scheme will follow the steps described in scheme A.

Upon band gap excitation of TiO_2, an electron will be produced in the conduction band and a hole will be left in the valence band (eq. A.1). If there are no scavengers at the surface, the electron and the hole will recombine to give heat (eq. A.2). This back reaction happens with a rate constant of 2×10^{-10} n_e^{-1} s^{-1} as measured by the flash photolysis of TiO_2 alone. If there is a scavenger at the surface of the particle, the electron or the hole will be removed leaving the other species in the semiconductor (eq. A.3a and A.3b). This interfacial charge transfer, to be efficient, needs to be faster than the recombination rate ($k_{CT} > k_r$) so that k_{CT} will be equal or larger than 1 x

SCHEME A

$$TiO_2 \xrightarrow{h\nu} TiO_2\,(e^-_{c.b.} \cdots h^+_{v.b.}) \qquad 1$$

$$e^-_{c.b.} + h^+_{v.b.} \xrightarrow{k_r} HEAT \qquad 2$$

$$D + h^+ \xrightarrow{k_e} D^+ \qquad 3a$$

$$A + e^- \xrightarrow{k_e} A^- \qquad 3b$$

$$h^+_{v.b.} \xrightarrow{k_{eT}} h^+_t \qquad 4a$$

$$e^-_{c.b.} \xrightarrow{k_{eT}} e^-_t \qquad 4b$$

10^{10} s^{-1}.

In all the cases studied here, we have observed a quantum yield of interfacial charge transfer very close to 1 so that the rate constant k_{CT} was large compared to the value of 2×10^{-10} n_e^{-1} s^{-1} for the recombination rate.

The charge carrier left in the semiconductor (a hole in these experiments) will have a long lifetime since there is no longer a species to react inside the semiconductor. We have observed that this species undergoes a trapping process (eq. A.4a and A.4b) due to the presence of defect sites or impurities. This trapping process occurs with a rate constant of 5×10^8 s^{-1} and the species trapped has a very long lifetime. This species can later react to close the oxydo-reduction cycle necessary for a catalyst.

This mechanism is valid for the small colloids studied (< 1000 Å), but it will be rather different for bulk material, mainly due to the difference in the electronic properties of the two systems. The first striking difference between the two is the fact that for bulk material, the scavenger does not have to be at the surface of the semiconductor to be efficient. This shows a large difference between the lifetime of the carriers in the bulk material compared to the colloidal particles. Contrary to the colloidal particles where the lifetime of the carriers is approximately 500 ps, in the bulk material, the lifetime of the carriers is larger than the diffusion time of the

scavengers to the surface of the semiconductor. This difference is mainly due to the presence of a band bending in bulk material which separates the charges and prevents the recombination.

Another difference between the two systems is in the attribution of the role played by the defect and impurity sites. In the bulk material the trap sites act as promoters of recombination by removing the charges from the band bending field. In small particles, the trap sites do not play that role since there is no band bending and since the trapping rate is smaller than the recombination rate.

Since it is believed that the charge carriers are trapped before recombining in large materials, the trapping rate measured in these small particles may be seen as a direct measurement of the recombination rate in bulk material. Even if the value obtained (2 ns) is similar to observed lifetimes in bulk materials, this relation may not be justified since the concentration of defects in small semiconductors is large compare to bulk materials.

VI. RESULTS AND DISCUSSION ON PHOTOACOUSTICS

VI.1. The signal:

As described in the experimental section, the signal obtained is the intensity of the acoustic pulse reaching the wall of the piezoelectric as a function of time. Figure VI.1 shows a typical signal obtained for a solution of potassium dichromate on a long time scale. As one can see, the photoacoustic signal becomes incoherent so that it is not possible to relate the signal observed to an acoustic wave on a long time scale.

In fact, the signal is a sum of many acoustic waves reaching the wall of the piezoelectric in a nonsynchronous fashion. Only the first maximum and minimum represent a pure acoustic wave. Afterwards, the signal is the sum of echoes of the acoustic wave and since the traveling time of the acoustic wave is not the same at every place inside the cell, the remaining signal is not useful for analysis. The positioning of the cell so that the laser pulse arrives exactly in the middle does not remove the incoherence of the signal, but it is important in order to increase the resolution of the first wave. The only way to increase the coherence of the echoes is to use an elliptical cell as described by Heritier (1983). where the piezoelectric is positioned at one focal point and the laser is focused on

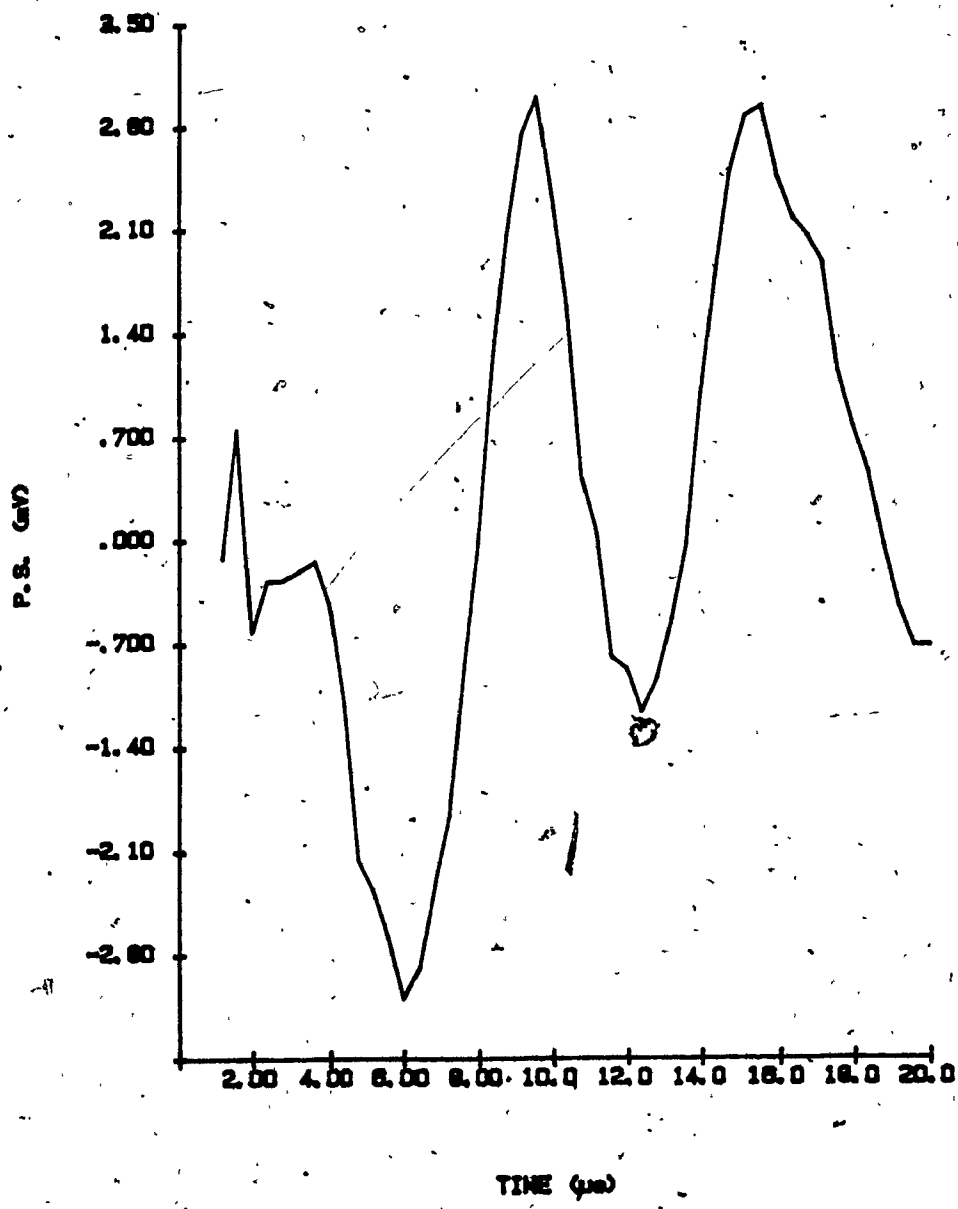

Figure VI.1 Photoacoustic signal of a solution of $K_2Cr_2O_7$ as a function of time. A value of the signal was taken every 0,4 μs. The signal is incoherent after the first photoacoustic wave.

the other focal point. All the echoes are then traveling the same distance so that they are coherent.

By increasing the time resolution, we can focus on the first wave arriving on the wall of the piezoelectric. If the laser pulse is perfectly centered, the signal obtained corresponds to a pure acoustic wave since the piezoelectric is round and the acoustic wave reaches every place on the wall at the same time. Figure VI.2 shows the first acoustic wave impulse for a solution of $K_2Cr_2O_7$.

The time of arrival of the first pulse and the subsequent pulses depends on the speed of the acoustic wave in the solvent. The frequency of the signal is then a direct measure of the sound speed in the solvent. The value obtained by dividing the radius of the cell with the time difference between the first minimum and the first maximum is $1,67 \times 10^5$ cm/s which is close to the value of $1,48 \times 10^5$ cm/s for the speed of sound in water.

VI.2. Relation between signal and absorbance:

As we have mentioned before, only the first acoustic pulse can be used for the signal analysis. To cancel any drift in the baseline, the intensity of the acoustic signal was measured by taking the difference between the minimum value and the maximum value of the first pulse following the relation:

$$P.S. = V_{min} - V_{max} \quad \text{(volts)} \qquad \text{(VI.1)}$$

where V_{min} and V_{max} is the voltage measured at the minimum

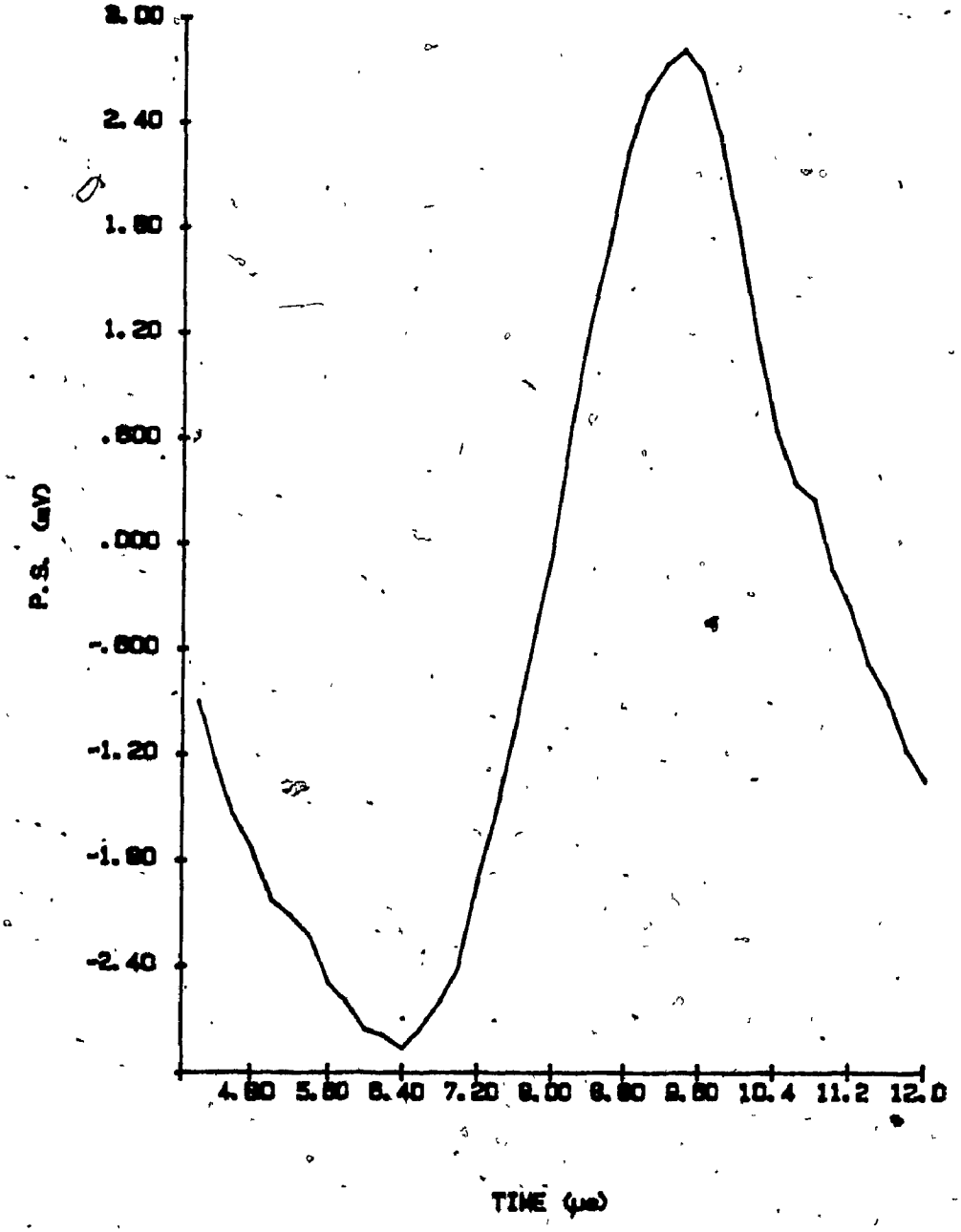

Figure VI.2 First photoacoustic pulse of a solution of $K_2Cr_2O_7$. A value of the signal was taken every 0,2 μs.

and maximum respectively. This corrects for any change in the baseline during successive runs without adding any noise.

All the photoacoustic signals were measured by subtracting the water signal as the background. This allows the removal of electronic noise, the signal from water as well as the signal coming from absorption by the wall of the cell or the base of the cell (window and support).

As we have seen in the introduction (Chapter II), the photoacoustic signal is directly proportional to the energy absorbed by a solution following the equations II.9 and II.10. If the sample is optically thin, the following relation can be valid:

$$(1 - e^{-\beta l}) \simeq \beta l \qquad \text{(VI.2)}$$

so that equation II.10 can be written as

$$E_a = E_i \beta l \qquad \text{(VI.3)}$$

and the photoacoustic signal is

$$V = A E_i \beta l \qquad \text{(VI.4)}$$

For constant incident energy, the photoacoustic signal measured will be directly proportional to the absorption of the solution

$$P.S = A a \qquad \text{(VI.5)}$$

Figure VI.3 shows the photoacoustic signal measured as a function of the absorbance for different concentrations of $K_2Cr_2O_7$. The curve is linear up to an absorbance of

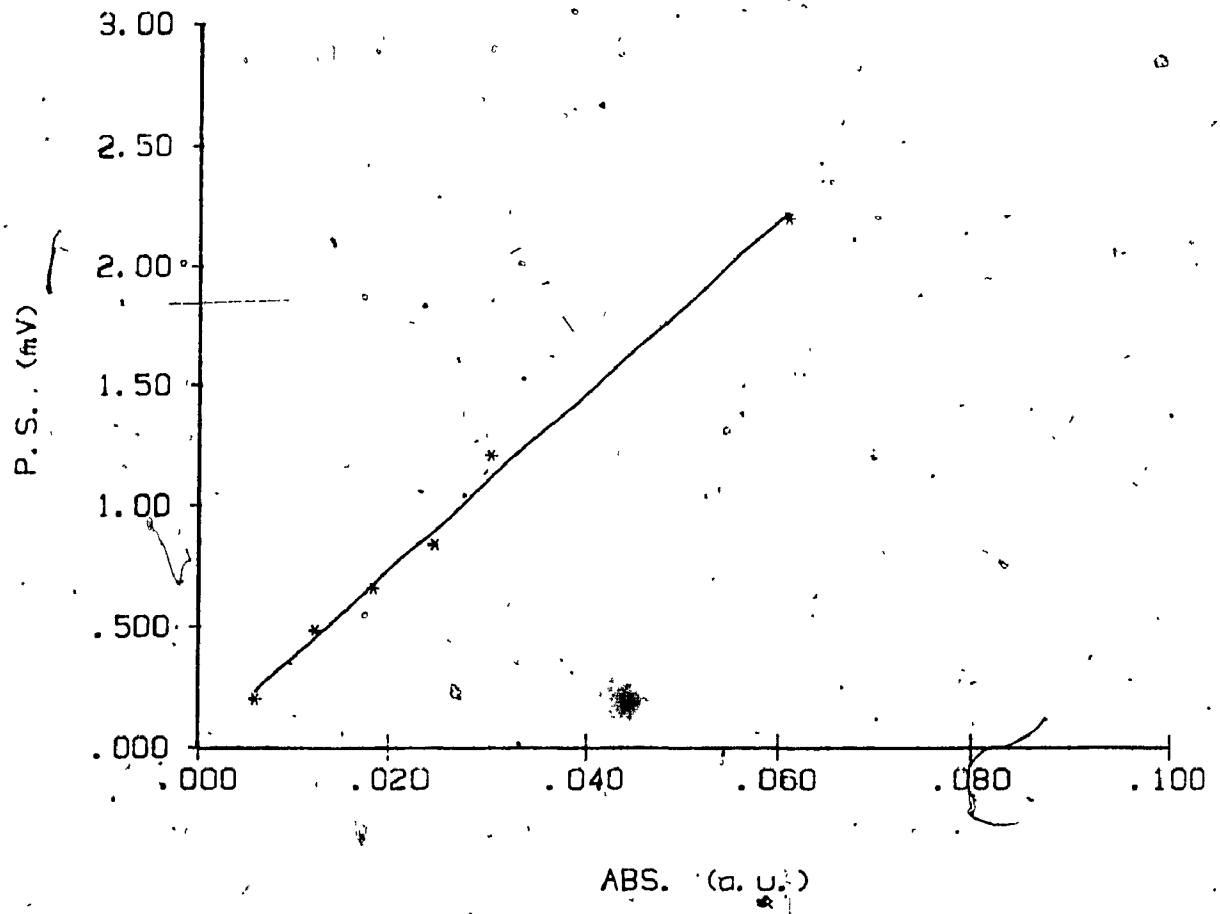

Figure VI.3 Photoacoustic signal as a function of the absorbance of solutions of $K_2Cr_2O_7$. The photoacoustic signal was obtained by taking the difference between the maximum and the minimum value of the first photoacoustic pulse.

approximately 0,1 beyond which a large deviation starts to occur. This deviation is due to the fact that for larger values of absorbance relation VI.2 is no longer valid. The relation can be approximately linearized by taking the logarithm of the signal as a function of the absorbance.

From the slope of the Figure VI.3, the minimum detectable signal calculated corresponds to an absorbance of 6×10^{-3}. At this absorbance, the signal to noise ratio was 2. The linearity was good. Least square fitting gives a regression coefficient of .9978.

These results establish a direct relation between the signal and the absorbance so that a value for the constant A, equation VI.5, can be extracted. The slope of the curve in Figure VI.3 is $3,4 \times 10^{-2}$ V for an input energy of 20μJ so that the equation (VI.4) can be written as

$$PS = 1,7 \times 10^{3} E_i a \quad (V) \quad (VI.6)$$

We can extract the energy output in the photoacoustic wave with the equation (VI.3):

$$E_{ps} = \frac{P.S.}{1,7 \times 10^{3}} \quad (J) \quad (VI.7)$$

The overall energy of the excited "trapped" state is the energy absorbed minus the energy released in the photoacoustic wave so that by difference we measure the energy stored in the "trapped" state by the equation:

$$E_{T.S.} = E_i a - (PS/1,7 \times 10^{3}) \ (J) \quad (VI.8)$$

If the intersystem quantum yield (ϕ) for the transfer of

the excited molecules to the trapped states is not 1, we will have:

$$E_{T.S.} = \frac{E_i a - (PS/1,7 \times 10^3)}{\phi} \quad (J) \quad (VI.9)$$

The energy of one trapped state is the total energy divided by the number of molecules in the trapped states:

$$E_{T.S.} = \frac{E_T}{n_{T.S.}} \quad (V.10)$$

where

$$n_{T.S.} = \phi\, n_p = \phi\, E_a/E_p \quad (V.11)$$

E_a is the energy absorbed ($E_i a$) and E_p is the energy of a photon which is equal to $5,9 \times 10^{-19}$ J at 337 nm. The energy of one "trapped" state is then equal to:

$$E_{T.S.} = \frac{5,9 \times 10^{-19} - 3,47 \times 10^{-22}\ P.S./E_i a}{\phi^2} \quad (V.12)$$

This equation gives a direct relation between the photoacoustic signal, the absorbance of a compound and the energy of a "trapped state" in the compound.

VI.3 Sensitivity

The sensitivity obtained does not look very impressive, but if we consider that the energy of the pulses was only 20μJ, this value is respectable since it gives a relative sensitivity of $7,5 \times 10^{-10}$ if pulses of 1 J were used. This is in good agreement with values reported for experiments using more powerful lasers (Voigtman et al., 1981).

There are two major factors affecting the sensitivity

of the system. The first one is the electronic noise which arises mainly from the laser. The laser uses a spark to initiate the lasing and the spark initiation requires a large voltage which is also transmitted through all the power lines of the room. The use of boxcar integration cannot get rid of this noise because it is not random since it is correlated to the trigger.

The second major factor decreasing the sensitivity of the apparatus is the absorption of a part of the pulse by the water and the cell itself. The noise arises mainly from the absorption by the support of the cell which affects the first part of the signal. Even using an isolating part between the support and the cell leaves a part of the acoustic wave which comes from the support and reaches the wall of the piezoelectric.

VI.4. Time resolution:

The development of this apparatus was not primarily to obtain a very sensitive photoacoustic system, but to be able to perform time resolution photoacoustic experiments. There is nothing in the theory of photoacoustic phenomena which prevents work at high time resolution. The acoustic pulse is formed by the deactivation of the excited molecules through heat transfer to the surroundings. This process is only limited by the deactivation time which is often in the order of picoseconds. The time limitation is not set by the photoacoustic process, but by the experimen-

tal set-up.

An important parameter which limits the time resolution of the photoacoustic apparatus is the response time of the microphone used for detection. The piezoelectric is not limiting since its response is "instantaneous" on the scale of these experiments. Only two factors can limit the response. The minimum detectable time is determined by the duration of the laser pulse or the traveling time of the acoustic wave in the illuminated area, depending on which is the larger.

In our experimental set-up, the pulses of the laser have a duration of 300 ps. The traveling time of the acoustic pulse in the illuminated area is equal to:

$$t = w_0/v \qquad \text{(VI.13)}$$

where w_0 is the beam waist, and v is the sound velocity in water. It is not possible to have a beam waist smaller than 1 mm since the laser has a very large divergence. Our limitation is then set to approximately 1 µs due to the beam waist. If we look at the width of the acoustic wave in Figure VI.2, we obtain a time resolution of 2,3 µs which corresponds to a beam waist of 3,5 mm. This is not due to a poorly focused beam, but rather to the fact that the beam is passing through 1 cm (the length of the cell). This value represents the largest relevant beam diameter inside the cell.

The only way to improve the time resolution of the

apparatus will be to use a two pulses (pump-probe) system similar to the one used in the picosecond experiments described earlier. The time resolution will then be limited only by the pulse duration which can be decreased to 20 ps by the use of a dye laser. A good example of this type of system has been given in the introduction.

VI.5 Energy level measurements:

Since the resolution of the system is in the order of 1 μs, it can be used to determine the energy level of states which have at least a 10 μs lifetime. For states which have a lifetime of 1μs, there will already be a large contribution from the decay of those states in the energy output. In order to test the possibility of using this instrument to measure the energy of triplet states of some molecules, we have tried to measure the energy of the triplet state of the zinc tetraphenylporphyrine sulfonated ($ZnTPPS^{4-}$).

The $ZnTPPS^{4-}$ is a good candidate for photoacoustic experiments since the quantum yield of fluorescence is only 0,043. In addition, it is a good choice for these experiments since it has a high quantum yield of intersystem crossing (0,84) and a triplet lifetime of 1,4 ms (Darwent et al., 1982) which is long enough to avoid a large contribution to the signal.

Figure VI.4 shows the signal from a solution of $ZnTPPS^{4-}$ compared to the signal from a solution of

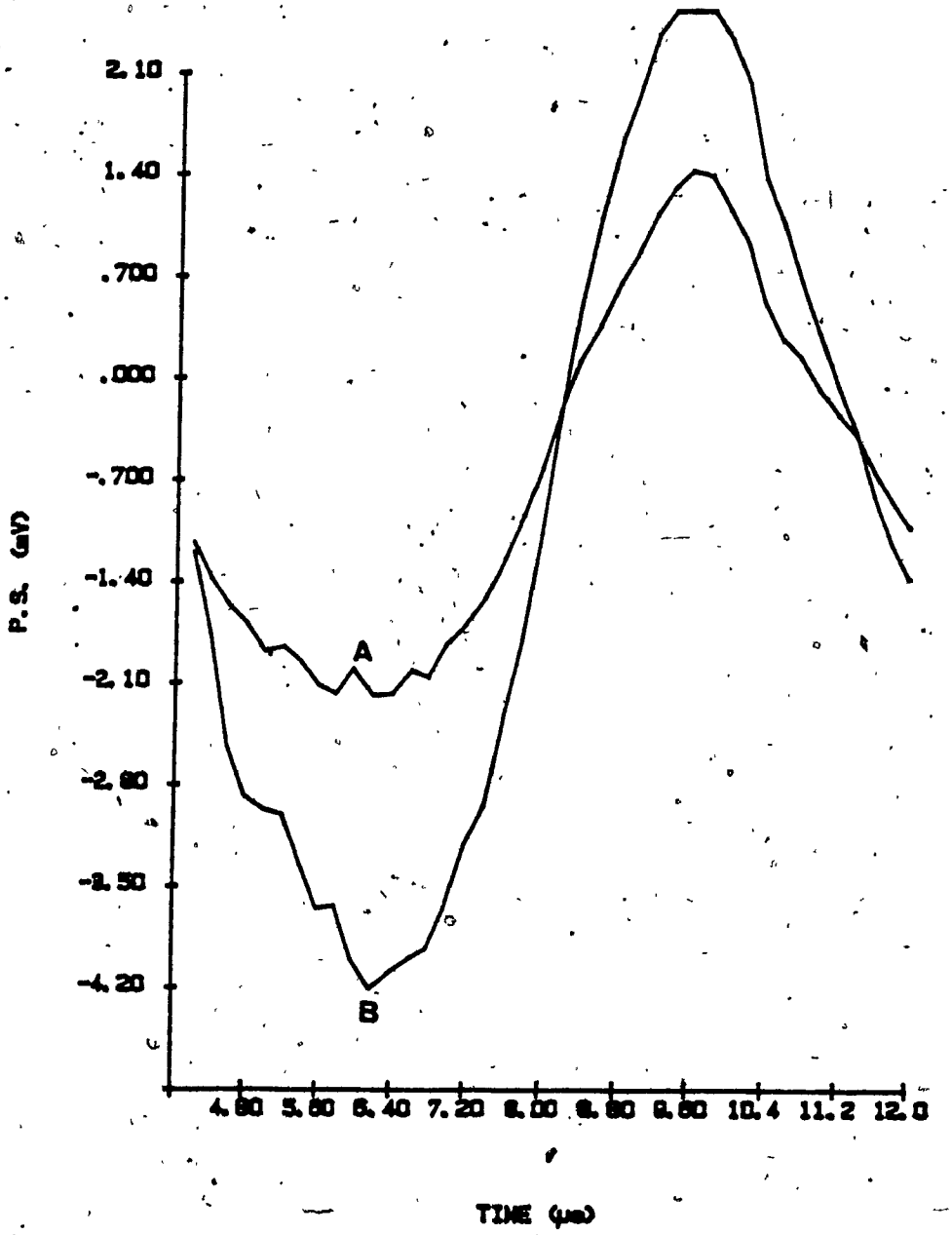

Figure VI.4 Photoacoustic sighal of a solution of $ZnTPPS^{4-}$ and a solution of $Fe(phen)^{2+}$. The absorbance of the solution of $ZnTPPS^{4-}$ (A) is 0,0743 whereas the absorbance of the solution of $Fe(phen)_3^{2+}$ (B) is 0,0759.

$Fe(phen)_3^{2+}$ having approximately the same absorbance. We can see that the signal coming from the $ZnTPPS^{4-}$ is half the signal of the $Fe(phen)_3^{2+}$ even if they have the same absorbance.

By the use of equation (VI.12), we have calculated the energy of the triplet of the $ZnTPPS^{4-}$ to be 1,4 eV. The major source of errors comes from the difficulty of measuring accurately the energy of the laser pulse. The error in this measurement is estimated to be approximately 10%. Other sources of errors come from the measurement of the photoacoustic signal and also from the fact that even if the $ZnTPPS^{4-}$ triplet state has a long lifetime, there is still a contribution to the photoacoustic signal from the decay of a part of the triplet state molecules. If pulse energy error is limiting, the value obtained is (1,4 ± 0,2) eV. This just agrees with the value of 1,61 eV reported by Darwent et al. (1982).

VI.6 Energy of trapped states of TiO_2:

Having proven that it was possible to measure the energy levels of triplet states with this apparatus, it seems useful to try to measure the energy level of trapped states in TiO_2. Figure VI.5 shows the photoacoustic signal obtained for a suspension containing 0,1 g/l of TiO_2 colloids and $4,0 \times 10^{-6}$ M of the $RuPPS^{4-}$. The photoacoustic signal is plotted with the photoacoustic signal of a solution of $Fe(phen)_3^{2+}$ which has approximately the same

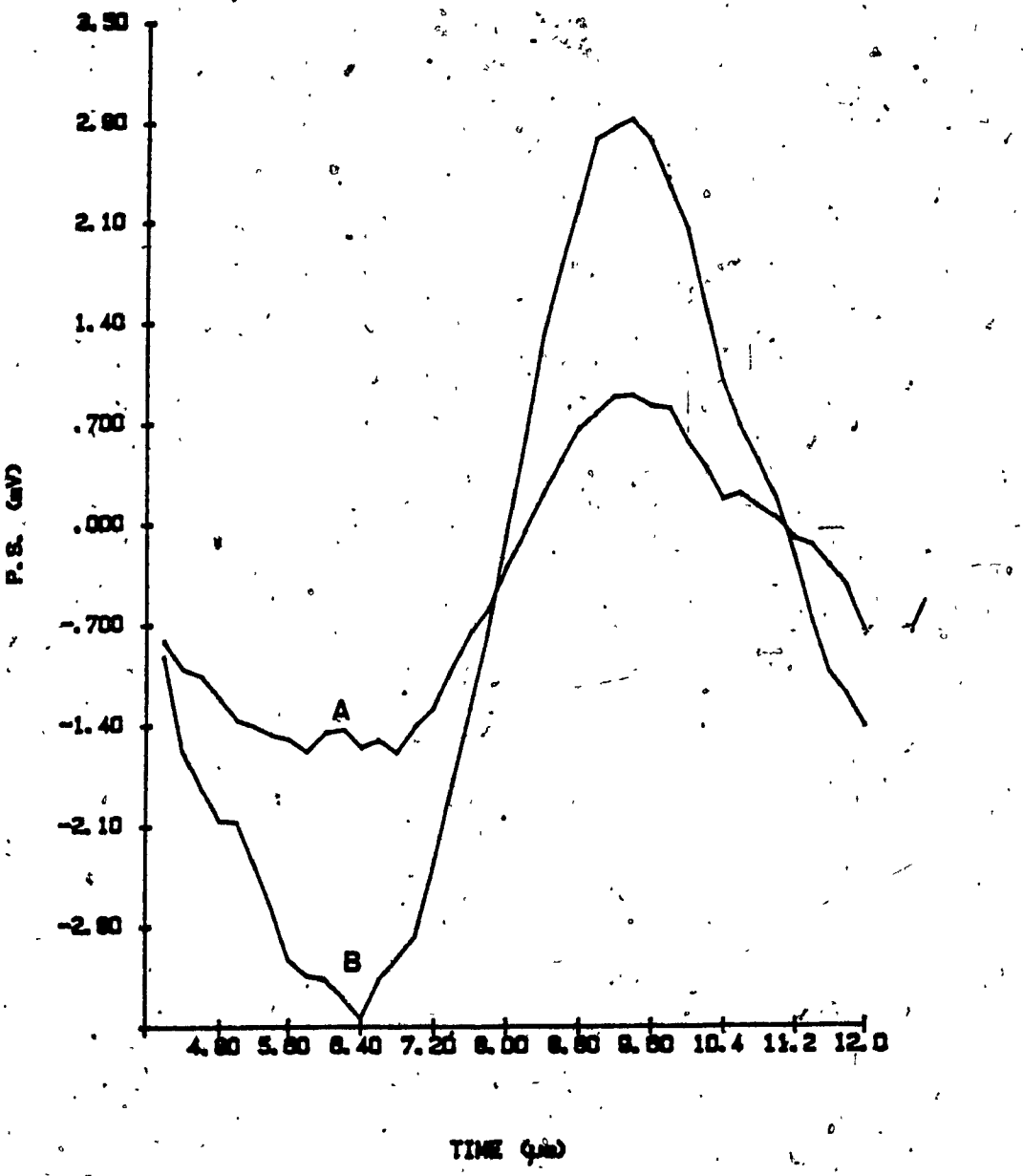

Figure VI.5 Photoacoustic signal of a solution of TiO_2-$RuPPS^{4-}$ and a solution of $Fe(phen)_3^{2+}$. The absorbance of the solution of TiO_2-$RuPPS^{4-}$ (A) is 0,0981 and the absorbance of the solution of $Fe(phen)_3^{2+}$ (B) is 0,0811.

absorbance (0,0811 compared to 0,0981 for the TiO_2 suspension). We can observe the large width of the signal due to slow decay processes in TiO_2 which are longer than the formation time of the photoacoustic pulse.

By using the equation (VI.12), we have obtained a value of 1,25 eV for the energy of the trapped states in TiO_2. This means that the trapped states are 1,25 eV higher than the valence band or, for a better understanding, 2,0 eV lower than the conduction band. This is very close to the value of 1,91 eV reported for the blue color of n-doped TiO_2 (Ghosh et al., 1969). The difference between the two values is much less than the estimated instrumental uncertainty of $\geq$ 10%.

Also, there is a point here that needs some comments. The energy measured by photoacoustics is the energy between the average energy level of the trap sites and the bottom of the conduction band. In absorption spectroscopy, the energy value given is usually the energy at the maximum absorption which represents the transition from the average trap state to a level in the conduction band where the density of states is the largest. This level is not necessarly the bottom of the conduction band.

The bottom of the conduction band is very difficult to estimate due to the presence of long tails in the absorption edge of the spectra of semiconductors. The value reported by absorption spectroscopy is then the maximum

energy value of the average trap state.

VI.7 Comparison with picosecond experiments:

The aim of this photoacoustic study of TiO_2 was to try to compare these results with the ones obtained by the picosecond experiments. Even if we have observed an absorption due to trapped states at 630 nm (<1,98 eV) which is very close to the value obtained in photoacoustic experiments, there is absolutely no relation between the two results.

The picosecond experiment results reflect a process involving two photons whereas the photoacoustic experiments involved only one photon. The energy of the trapped state measured in picosecond experiments has been attributed to a hole trap site which means that the trap state is at most 1,98 eV above the valence band edge. The energy of the trap sites is probably lower but it cannot be determined exactly due to the difficulty of determining the valence band edge. In the photoacoustic experiments, an electron of the valence band is excited into the conduction band and after the scavenging of the hole by the dye, this electron is trapped in a trap-site which is 2,0 eV below the conduction band.

There is no relation between the two sets of experiments since the trap sites studied are completely different. Nevertheless, the results obtained with the photoacoustic experiments correlate very well with the observa-

tion of the large band at 650 nm in TiO_2 (Henglein, 1982 and Bahneman et al., 1984).

VII. Conclusions

VII.1 TiO_2 particles:

The TiO_2 colloidal particles show a quantification size effect which can be seen by the shift in the edge of the absorption band of TiO_2. This shift may also be used for the direct determination of the size of the particles. The size of those particles give them very different electronic properties compared to the bulk material due to the absence of band bending and a permanent interaction between the hole and the electron.

The increase of photoreaction on these small particles is probably not to be explained by the change in electronic properties, but rather by the fact that there are more defect sites and impurities in small particles. These defect sites and impurities function to prevent recombination of the hole and electron and extend their lifetimes. This extension of lifetime is evidenced by the long transients for trapped species.

VII.2 Picosecond experiments:

The picosecond flash photolysis ~~of~~ TiO_2 suspensions alone gives a direct measure of the lifetime of the carriers in the particles when trapping is not promoted. The average lifetime is 500 ps for the particles studied.

The absorption coefficient is 2200 M^{-1} cm^{-1} and the

decay follows a second order process giving a direct measurement of the recombination rate of the hole and the electron. We have demonstrated that this transient is not coming from electrons in trapped sites as it was suggested before in another study.

The use of picosecond flash photolysis on TiO_2 suspensions where scavengers designed to adsorb strongly at the surface have been added has permitted the study of the primary events in the photochemical reactions using semiconductor catalysts. The results show that when the scavenger is present at the surface, the quantum yield for rapid transfer of an electron from the TiO_2 to any one of the three excited dyes is approximately 1. The hole left is later trapped with a rate constant of 5×10^8 s^{-1}.

The nature of the p-type trap sites in the TiO_2 colloidal particles has not been identified, but three possibilities suggest themselves: an oxygen vacancy in the lattice, the formation of an O^- or a hydroxyl radical (OH) at the surface of the particles. All these three species can arise in very small particles where there are a large number of defects and impurities.

The mechanism studied involved the transfer of an electron from the conduction band of the TiO_2 to an excited dye. This process involved the use of two photons, but other mechanisms involving only one photon can also be studied using picosecond flash photolysis. As examples,

the system can be used to study the transfer of an electron from an excited dye to the conduction band of the TiO_2 with the scavenging of the hole by a scavenger.

The study of these other mechanisms can be seen as small changes in the experimental conditions. The major reason for the two photon process observed here is the high density of photons in the pump pulse. One photon process can be studied by increasing the size of the pump beam or decreasing the energy of the pulse. Also, the choice of a suitable scavenger or the use of another wavelength can prevent the two species from "double" absorbing.

Many semiconductors (e.g. CdS, ZnO) have been prepared as colloids and they would be good candidates to study the primary events of photochemical reactions by the methods developed in this thesis. CdS looks particularly interesting since it is a p-type semiconductor and it has been studied extensively so its steady state photochemical properties are well known.

VII.3 Photoacoustic experiments:

The first experiments done with this new set-up show that this system can be sensitive, and that it can be very helpful for the measurements of energy levels of simple molecules as well as more complicated systems like the semiconductor particles. Even if those experiments were only preliminary experiments, they demonstrate the promise of the photoacoustic apparatus.

Since this new set-up is at its first stage, many improvements can be proposed. First of all, the system should be completed by adding the dye laser system so that the photoacoustic apparatus can be used at most wavelengths in the visible, and also to pursue the aim of using a double pulse system to achieve a sub-nanosecond resolution. This, with the addition of modulated continuous laser (an Argon laser has already been purchased for this project) will give us a very interesting time domain. The dynamic range will go from the sub-nanosecond time resolution down to the second. It will then be possible to study the full decay time range.

It is probably not useful to try to modify the design of the cell since the sensitivity obtained is sufficient for most of the systems of interest. Nevertheless, it could be interesting to try to decrease the size of the piezoelectric detector in order to increase the time resolution of the system. The factor would be less than 10, but might prove critical.

Also, since this research team is really interested in photochemical processes happening at the surface of electrodes, it will be very useful to have the same kind of photoacoustic system capable of detecting photochemical processes in solid. This can be easily achieved by the replacement of the piezoelectric cell by a piezoelectric detector for solids. No other parts of the system have to

be changed and in addition, it will be possible to scan all the surface of the electrode with the use of the positioning motors.

Another example of simple modifications that can be implemented in that system is to use it to detect at the same time, the radiationless decay by photoacoustics and the luminescence with the use of a photodetector. One can then measure the two complementary deactivation processes of a molecule at the same time with a very good time resolution.

REFERENCES

Anpo, M., Norikazu, A., Yutaka, K., Michel, C., Catherine, L., and Gianello, E., J. Phys. Chem., 89, 5017, 1985.

Bell, A.G., Am. J. Sci., 20, 305, 1880.

Bell, A.G., Philos. Mag., 11, 510, 1881.

Born, M., and Wolf, E., Principles of Optics, 3rd ed., Pergramon, Oxford, 1965, Chapt. 13.

Brus, L.E., J. Chem. Phys., 80, 4403, 1984.

Darwent, J.R., Douglas, P., Harriman, A., Porter, G., and Richoux, M.C., Coordination Chemistry Reviews, 44, 83, 1982.

Dimitrijevic, N.M., Savic, D., Micic, O.I., and Nozik, A.J., J. Phys. Chem., 88, 4278, 1984.

Duonghong, D., Ramsden, J., and Gratzel, M., J. Am. Chem. Soc., 104, 2977, 1982.

Gratzel, M., and Frank, A.J., J. Phys. Chem., 86, 2964, 1982.

Ghosh, A.K., Wakim, F.G., and Addiss, R.R. Jr., Phys. Rev., 184, 979, 1969.

Guzy, C.M., Raynor, J.B., and Symons, M.C.R., J. Chem. Soc., A, 2299, 1969.

Henglein, A., Ber. Bun. Phys. Chem., 86, 241, 1982.

Heritier, J.M., Ph.D. Thesis, Stanford University, 1983.

Howe, R.F., and Gratzel, M., J. Phys. Chem., 89, 4495, 1985.

Kittel, C., Introduction to Solid State Physics, 5th ed., John Willey and Sons, 1976.

Kolle, U., Moser, J., and Gratzel, M., Inorg. Chem., 24, 2253, 1985.

Leugers, M.A. and Atkinson, G.H., Anal. Chem., 56, 925, 1984.

Moser, J. and Gratzel, M., Helv. Chim. Acta, 65, 1436, 1982.

Nevin, W.A., Liw, W., Melnik, M., and Lever, A.B.P., J. Electroanal. Chem., 213, 217, 1986.

Neta, P., J. Phys. Chem., 85, 3678, 1981.

Nozik, A.J., Williams, F., Nenadovic, M.T., Rajh, T., and Micic, O.I., J. Phys. Chem., 89, 397, 1985.

Parker, J.G., Appl. Opt., 12, 2974, 1973.

Rosencwaig, A., and Gersho, A., Science, 190, 556, 1975.

Rossetti, R., Ellison, J.L., Gibson, J.M., and Brus, L.E., J. Chem. Phys., 80, 4464, 1984.

Rossetti, R., Hull, R., Gibson, J.M., and Brus, L.E., J. Chem. Phys., 82, 552, 1985.

Rothenberger, G., Moser, J., Gratzel, M., Serpone, N., and Sharma, D.K., J. Am. Chem. Soc., 107, 8054, 1985.

Royce, G.A., and Kay, R.B., App. Opt., 23, 1975, 1984.

Viengerov, M.L., Dokl. Akad. Nauk. SSSR, 19, 687, 1938.

Voigtman, E., Jurgensen, A., and Winefordner, J., Anal. Chem., 53, 1442, 1981.

Watts, R.J., J. Chem. Educ., 60, 834, 1983.

Yana, Y., Phys. Rev., 130, 1711, 1963.

APPENDIX A

THE PHOTOACOUSTIC SYSTEM

A.1 Mechanical parts:

The cell consisted of the piezoelectric tube on which a quartz window has been glued on one side. The glue needs to be cured for 24 hours under UV light. This glue does not absorb at 337 nm and it can be removed with methylene chloride.

The piezoelectric cell is mounted on the photodiode assembly and separated from it by a rubber o-ring to avoid vibrations and also acoustic waves coming from the absorption of light by the support. The photodiode assembly sits on a rail controlled by two motors for the positioning of the cell.

A.2 Electronic circuit:

Figure A.1 represents the overall electronic circuit used for the photoacoustic experiments. The major part of it is the IBM-PC computer which controls all the steps of the experiment through the A/D interface board (DT-2801 Data Translation). Below, we will describe the different steps of the experiment where the electronic circuit is involved.

a) Positioning of the cell.

Figure A.1 Schematical representation of the electronic circuit used in photoacoustic experiments. J1 is the 50 pin connector of the A/D board (DT-2801). SW1 and SW2 are the switches for the power and the motor selection (M1 and M2) respectively. P.S. is the power supply of the current amplifier (C.A.) which drives the motors. P101 is the 50 pin connector of the boxcar. P.D. is the photodiode used to center the beam in the middle of the piezoelectric cell (P.Z.). The pre-amplifier (P.A.) amplifies the signal from the piezoelectric and from the photodiode.

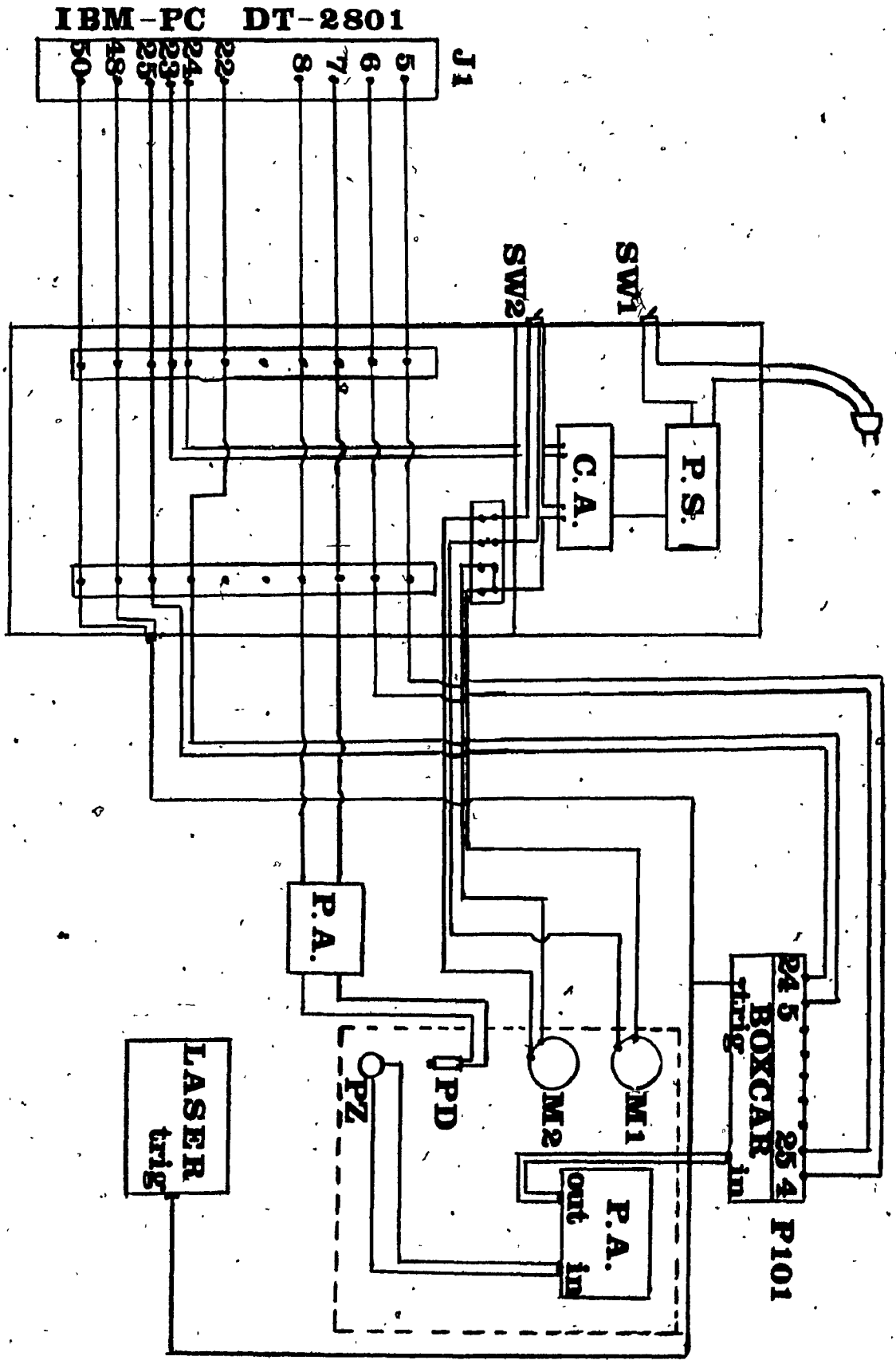
IBM-PC DT-2801
J1
50
48
25
23
24
22
8
7
6
5
SW2
SW1
C.A.
P.S.
P.A.
LASER
trig
PZ
PD
M2
M1
BOXCAR
trig
24 5
25 4
P101
P.A.
out
in

The positioning of the cell is done automatically upon request from the experimentalist. The two motors used (M1 and M2) for the positioning are inexpensive 6V, 120 mA motors. They move gears which are chosen so that the transfer from rotational to translational action is low. The sequence for the positioning is as follows:

i) The experimentalist sets the power switch (SW1) to the on position and the motor switch (SW2) to M1 (motor 1). He then hits a key on the computer to start the process.

ii) The computer reads the value of the photodiode through the pins 7-8 (J1) of the A/D board. Before being sent to the computer, the photodiode voltage is amplified by an amplifier.

iii) The computer sends +6V for a period of half a second through the pins 23-24 (J1) to the current amplifier (CA) which outputs a +6V, 120 mA to the motor M1.

iv) The computer reads again the photodiode and compares the new value with the previous one. If the value is higher or equal, the computer sends another pulse of +6V to the current amplifier. If the new value is lower than the previous one, the computer sends a voltage pulse of -5,5V to the current amplifier.

The same process goes on until the voltage is 0V where it

is stopped. The movement of the motor can be described as follows: the motor moves in one direction until the computer reads a value of the photodiode lower than the previous one. When this value is lower, the motor goes in the other direction a little bit slower until the value of the photodiode is lower. The movement of the motor can be compared to the Simpson approximation in mathematics.

When the positioning of the first motor is finished, the experimentalist is asked to change the motor switch (SW2) to M2 and after he has pressed a key, the same process goes on for the motor 2 which positioned the cell in the other direction.

The current amplifier (CA) and its power supply (P.S.) were designed at the Technical Center of this University.

b) Time setting of the boxcar

The experimental conditions for the boxcar are set by the experimentalist. The only part controlled by the computer is the delay of the aperture. The experimentalist sets up the aperture delay time as well as the starting percentage value. He later enters the delay of the aperture he wants to scan. The computer sends a voltage through the pins 22-25 (J1) to the pins 5-24 (P101) of the boxcar to scan the aperture gate at values specified by the experimentalist. This time process will be explained in Appendix B.

c) Photoacoustic signal

The inside and outside walls of the piezoelectric tube are covered with very thin layers of silver. One electrical wire is positioned on the inside and one on the outside. Upon arrival of an acoustic wave in the inside wall, there is a difference of potential produced between the inside and the outside of the piezoelectric tube. This voltage signal is sent to a pre-amplifier which filters the signal for the desirable frequencies and it also amplifies the signal from 1 to 10,000 times.

When the signal is filtered and amplified it is sent to the boxcar which does the time processing before sending it to the computer. The signal is sent from the pins 4-25 (P101) of the boxcar to the pins 5-6 (J1) of the computer.

A.3 Experimental conditions:

Table A.1 lists the experimental conditions for a typical experiment involving the positioning of the cell and the reading of a photoacoustic pulse.

Table A.1 Typical photoacoustic experimental conditions

Parameters	Cell Positioning	Signal Reading
Laser:		
-frequency	10 Hz	10 Hz
-energy	20-60 µJ	20-60 µJ
Pre-amplifier:		
-high pass filter	1 Hz	3K Hz
-low pass filter	10 Hz	100K Hz
-amplification	50 X	1000 X
Boxcar:		
-integration time (I.T)	-	1 µs
-aperture delay time (A.D.T.)	-	20 µs
-percent of aperture delay	-	15 to 65% (every 1%)
-aperture duration (A.D.)	-	50 ns
-scan time (S.T.)	-	0,1 sec
-time constant (T.C.)	-	1 sec
Computer:		
-input mode	differential	differential
-voltage mode	± 10 V	± 10 V
-A/D gain	3	0
-voltage read	± 1 V	± 10 V

APPENDIX B

TIME PROCESSING OF THE PHOTOACOUSTIC SIGNAL

The experimental conditions for the time processing of the photoacoustic signal are set by the experimentalist and they are usually the same as the one specified in table A.1 for a typical experiment. The time processing starts with each trigger from the laser and it can be represented by a window which is moved along the signal according to a defined pathway. This pathway follows a voltage ramp sent by the computer to the boxcar. The position of the window with regard to the trigger is defined according to the equation:

$$W.T. = \left(\frac{I.D.}{100} + 0{,}1\ V_R\right) A.D.T. \qquad (B.1)$$

where I.D. is the initial percent delay, V_R the voltage sent by the computer, and A.D.T. the aperture delay time. The first position of the window will be at I.D. x A.D.T. since the voltage sent by the computer is 0 V. For a typical experiment (see Table A.1) the first position of the window will be at 3 μs after the trigger. Since the increase is usually 1%, the next position of the window will be at 3,2 μs. The window will then be moved like this along the signal up to the last value (typically 65%) required by the experimentalist. This overall process can be visualized in Figure B.1.

Figure B.1 Time process of the signal in photoacoustic experiments. (A) Acoustic wave produced in the piezoelectric cell. (B) Movements of the window to read the value of the acoustic signal. (C) Voltage ramp emitted by the computer to monitor the movement of the reading window.

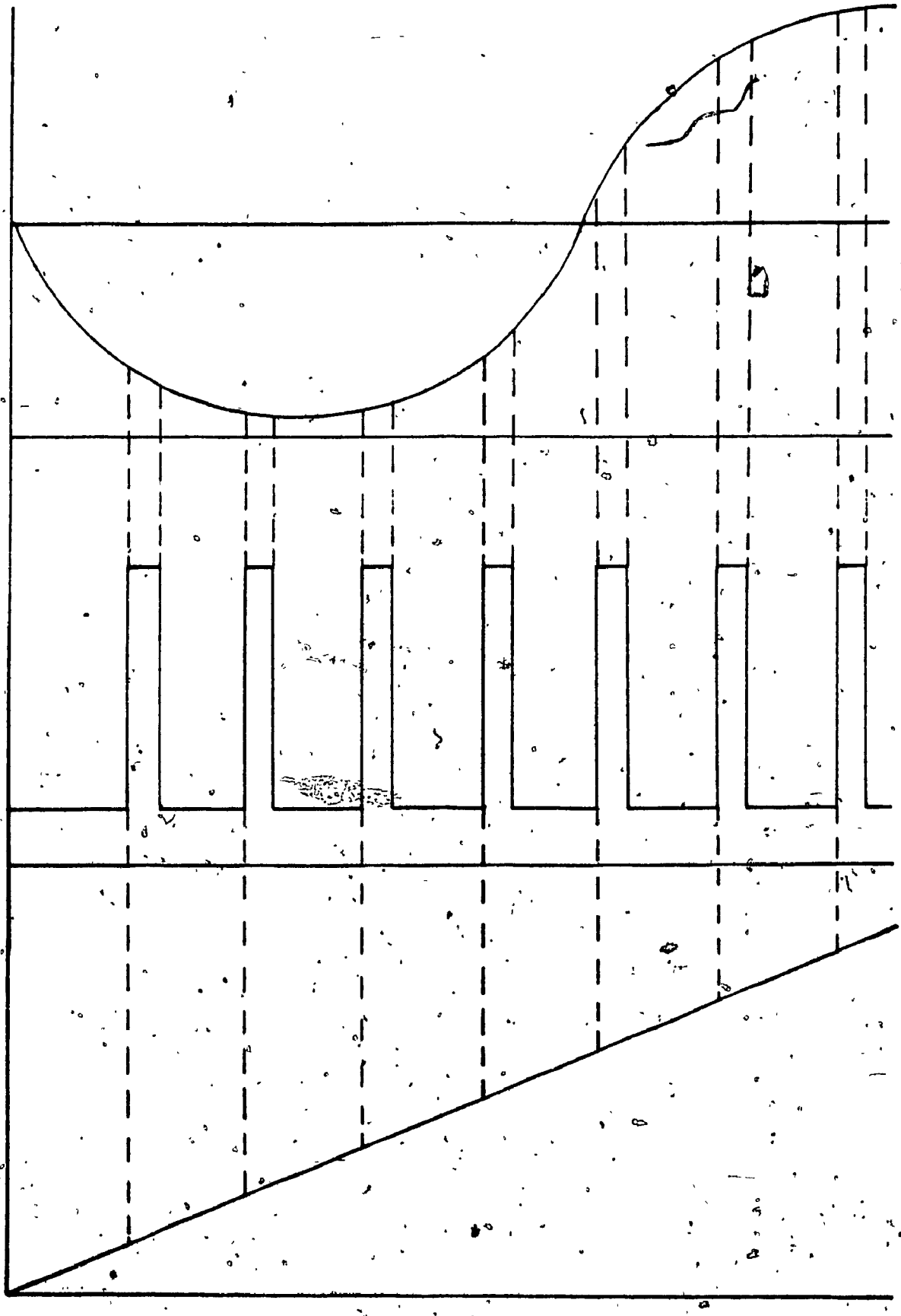

The computer reads the signal coming out from the boxcar at each position of the window. The signal at one position of the window is averaged by the boxcar following an exponential increase. This exponential increase is shown in Figure B.2 as a function of the number of pulses. It represents the charging of a capacitor which reaches approximately 90% of the signal value after 20 pulses (I.T./A.D., see Table A.1). The computer starts to read the value of the signal after approximately 50 pulses and stores 100 values to do an average. This process goes on for every position of the window. The overall signal is then a value for every position of the window which creates the acoustic wave seen on the computer.

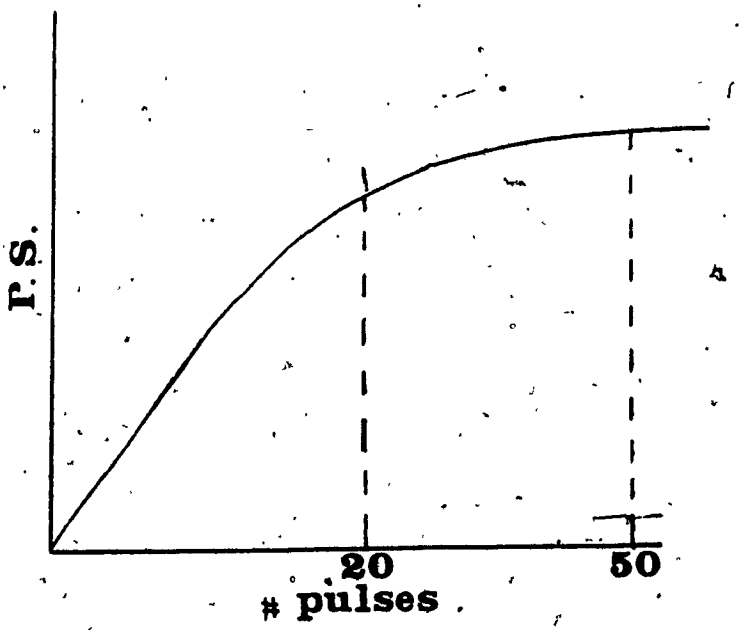

Figure B.2 Photoacoustic signal acquisition with the boxcar. Typical exponential increase of the charge of the capacitor at one position of the reading window. After 20 pulses, the charge on the capacitor is at 90% of its final value. The computer starts to read 100 values after approximately 50 pulses.

APPENDIX C

ACQUISITION AND ANALYSIS PROGRAM

```
/This program does the acquisition and the analysis for
/the photoacoustic system.

REAL SCALAR START.DELAY
     SCALAR SOMX
     SCALAR SOMY
     SCALAR SOMXY
     SCALAR SOMY2
     SCALAR NUMERATOR
     SCALAR DENOMINATOR
     SCALAR R2
     SCALAR STOP.DELAY
     SCALAR INTERVAL.DELAY
     SCALAR OUTPUT.DELAY.1
     SCALAR N.OF.P.2
     SCALAR ABS.2.CORR
     SCALAR ABS.CORR
     SCALAR MAX.VALUE
     SCALAR MIN.VALUE
     SCALAR MIN.DELAY
     SCALAR MAX.DELAY
     SCALAR TEMP
     SCALAR PHOTO.READ
     DIM[ 10 , 100 ] ARRAY CURVE
     DIM[ 1 ] ARRAY SAMPLE.NUMBER
     DIM[ 10 ] ARRAY TOTAL.N
     DIM[ 10 ] ARRAY CONCENTRATION
     DIM[ 10 ] ARRAY RESULTS.1
     DIM[ 5 , 10 ] ARRAY RESULTS
     DIM[ 2 ] ARRAY PARA
     DIM[ 100 ] ARRAY NOISE
     DIM[ 100 ] ARRAY SORT.ARRAY
     DIM[ 100 ] ARRAY S-N.VALUE.2
     DIM[ 100 ] ARRAY RAMP.DELAY.2
     DIM[ 1 ] ARRAY N.OF.P.ARRAY.2
     DIM[ 1 ] ARRAY ABSORBANCE.2
     DIM[ 100 ] ARRAY TAMPON
     DIM[ 1 ] ARRAY ABSORBANCE
     DIM[ 2 ] ARRAY MEAN.V
     DIM[ 100 ] ARRAY RAMP.DELAY
     DIM[ 100 ] ARRAY S-N.VALUE
     DIM[ 64 ] ARRAY FFT.ARRAY
     DIM[ 64 ] ARRAY I.FFT.ARRAY
```

```
INTEGER SCALAR N.OF.P
        SCALAR SAMPLE.NUMBERS
        SCALAR MOTOR
        SCALAR SPEED
        SCALAR N
        SCALAR I.SCAN
        SCALAR SCAN.NUMBER
        SCALAR REJ.NO
        SCALAR DELAY.COUNT
        SCALAR ICOUNT
        SCALAR LASER.FREQ
        SCALAR IRUN
        SCALAR CHOICE
        SCALAR MIN.V
        SCALAR MIN.DELAY.INDEX
        SCALAR MAX.DELAY.INDEX
        SCALAR DELAY.NUMBER
        DIM[ 1 ] ARRAY DELAY.COUNT.ARRAY
        DIM[ 100 ] ARRAY SORT.INDEX.ARRAY
        DIM[ 1 ] ARRAY N.OF.P.ARRAY
        DIM[ 1 ] ARRAY AMP.GAIN
        DIM[ 2 ] ARRAY ICOUNT.ARRAY
        DIM[ 250 ] ARRAY IN.DATA
        DIM[ 20 ] ARRAY PHOTO.IN

13 STRING FILENAME
10. 3. SCI.FORMAT
0 ICOUNT.ARRAY [ 2 ] :=
0 MEAN.V [ 2 ] :=
1 AMP.GAIN :=

/The computer is controlling the acquisition
/through 4 channels of the A/D board.

/Channel 2 = photoacoustic signal

2 2 A/D.TEMPLATE IN.CHNL.2
    IN.DATA TEMPLATE.BUFFER
A/D.INIT

/Channel 0 = boxcar ramp

0 0 D/A.TEMPLATE OUT.CHNL.0
D/A.INIT

/Channel 1 = motor control

1 1 D/A.TEMPLATE OUT.CHNL.1
D/A.INIT

/Channel 3 = photodiode reading
```

```
3 3 A/D.TEMPLATE IN.CHNL.3
    EXT.TRIG
    3 A/D.GAIN
A/D.INIT

: INSTRUCTIONS
  SCREEN.CLEAR
  CR ." <F1> ACQUIRE DATA          <F6> SUBSTRACT 2 CURVES"
  CR ." <F2> PLOT DATA             <F7> FIND MIN/MAX"
  CR ." <F3> SAVE DATA             <F8> FFT OF DATA"
  CR ." <F4> LOAD DATA             <F9> LOAD RESULTS"
  CR ." <F5> PLOT 2 CURVES         <F10> EXIT OF ASYST"
  BELL
;

/Data template

: DEF.FILE.TEMPLATE
  FILE.TEMPLATE
   INTEGER DIM[ 1 ] SUBFILE
   REAL DIM[ 1 ] SUBFILE
   REAL DIM[ 100 ] SUBFILE
    2 TIMES
  END
;

20 0 24 79 WINDOW {BOT}

/Video screen for data plotting

: VIDEO.SET
  GRAPHICS.DISPLAY
  SCREEN.CLEAR
  {BOT}
  0 .20 VUPORT.ORIG
  1 .80 VUPORT.SIZE
;

/Voltage ramp output and
/photoacoustic signal reading

: ACQUIRE.DATA
  IN.CHNL.2 A/D.INIT
   20 CONVERSION.DELAY
  A/D.INIT
  OUT.CHNL.0 D/A.INIT
  OUTPUT.DELAY.1 -10 10 D/A.SCALE D/A.OUT
  100000 LASER.FREQ / MSEC.DELAY
  BEGIN
   A/D.IN>ARRAY
   ?BUFFER.FULL
  UNTIL
```

```
;

/Average of the signal

: FIND.MEAN
  IN.DATA MEAN
  CURVE [ I.SCAN , ICOUNT ] :=
  CURVE [ I.SCAN , ICOUNT ] 2048 - 204.8 /
  CURVE [ I.SCAN , ICOUNT ] :=
;

/Video set for data

: SET.PLOT.POINTS
  VIDEO.SET
  AXIS.DEFAULTS
  HORIZONTAL NO.LABELS
  VERTICAL 0 2 LABEL.POINTS
  HORIZONTAL 0 N.OF.P WORLD.SET
  VERTICAL -10. 10. WORLD.SET
  XY.AXIS.PLOT
;

/Data plot

: PLOT.POINTS
  ICOUNT ICOUNT.ARRAY [ 1 ] :=
  CURVE [ I.SCAN , ICOUNT ] MEAN.V [ 1 ] :=
  DOTTED
  ICOUNT.ARRAY MEAN.V XY.DATA.PLOT
;

/Divide the signal by the amplification

: GET.S-N.VALUE
  S-N.VALUE AMP.GAIN [ 1 ] /
  S-N.VALUE :=
;

/Fourier transform of the data

: FFT.PROG
  FFT
  ZREAL
  FFT.ARRAY :=
  0 FFT.ARRAY SUB[ 1 , 10 ] :=
  0 FFT.ARRAY SUB[ 55 , 10 ] :=
  FFT.ARRAY IFFT
  I.FFT.ARRAY :=
;

: FFT.OF.DATA
```

```
  S-N.VALUE
  FFT.PROG
  0 S-N.VALUE :=
  I.FFT.ARRAY S-N.VALUE SUB[ 1 , 64 ] :=
  INSTRUCTIONS
;

/Find the average curve of the signal

: MEAN.CURVE
  0 S-N.VALUE :=
  SCAN.NUMBER 1 + 1 DO
   CURVE.XSECT[ I , ! ] S-N.VALUE + S-N.VALUE :=
  LOOP
  S-N.VALUE SCAN.NUMBER / S-N.VALUE :=
;

/Plot the curves and the average

: PLOT.CURVES
  VIDEO.SET
  DOTTED
  RAMP.DELAY SUB[ 1 , N.OF.P ]
  S-N.VALUE SUB[ 1 , N.OF.P ]
  XY.AUTO.PLOT
  SOLID
  SCAN.NUMBER 1 + 1 DO
   CURVE XSECT[ I , ! ] TAMPON :=
   RAMP.DELAY SUB[ 1 , N.OF.P ]
   TAMPON SUB[ 1 , N.OF.P ]
   XY.DATA.PLOT
  LOOP
;

/Rejection of a curve

: CURVE.REJECTION
  CR ." Enter the number of the curve to reject"
     ." ( 0 to quit ) = "
  #INPUT
  REJ.NO :=
  REJ.NO 0 = NOT IF
   CURVE XSECT[ REJ.NO , ! ] TAMPON :=
   CURVE XSECT[ SCAN.NUMBER , ! ]
   CURVE XSECT[ REJ.NO , ! ] :=
   TAMPON CURVE XSECT[ SCAN.NUMBER , ! ] :=
   SCAN.NUMBER 1 - SCAN.NUMBER :=
  THEN
;

/Analysis of the curves
```

```
: CURVE.ANALYSIS
  0 ICOUNT :=
  SCAN.NUMBER 1 + 1 DO
   ICOUNT 1 + ICOUNT :=
   CURVE XSECT[ ICOUNT , ! ] NOISE -
   CURVE XSECT[ ICOUNT , ! ] :=
  LOOP
  BEGIN
   MEAN.CURVE
   PLOT.CURVES
   CURVE.REJECTION
   0 REJ.NO =
  UNTIL
;

/Plot value of photodiode

: SET.PHOTO
  VIDEO.SET
  HORIZONTAL NO.LABELS
  VERTICAL 0 2 LABEL.POINTS
  HORIZONTAL 0 100 WORLD.SET
  VERTICAL 2000 4000 WORLD.SET
  XY.AXIS.PLOT
  DOTTED
;

: PLOT.PHOTO
  ICOUNT ICOUNT.ARRAY [ 1 ] :=
  PHOTO.READ MEAN.V [ 1 ] :=
  ICOUNT.ARRAY MEAN.V XY.DATA.PLOT
;

/Set the motors to zero

: SET.ZERO
  OUT.CHNL.1
  D/A.INIT
  2048 D/A.OUT
;

/Auto-adjustment of the photodiode

: AUTO.ADJUST
  0 MOTOR :=
  3 1 DO
   0 ICOUNT :=
   MOTOR 1 + MOTOR :=
   SET.PHOTO
   1 MOTOR = IF
    CR ." Set the switch to motor 1 "
   ELSE
```

```
 CR ." Set the switch to motor 2 "
THEN
CR ." and press any key when ready."
PCKEY ?DROP DROP
850 SPEED :=
0 TEMP :=
0 PHOTO.READ :=
OUT.CHNL.1
D/A.INIT
IN.CHNL.3
A/D.INIT
BEGIN
 ICOUNT 1 + ICOUNT :=
 TEMP PHOTO.READ > IF
  2050 SPEED - 2050 + SPEED :=
  SPEED 2050 > IF
   SPEED 150 - SPEED :=
  THEN
 THEN
 PHOTO.READ TEMP :=
 0 PHOTO.IN :=
 SPEED D/A.OUT
 1 MOTOR = IF
  2000 MSEC.DELAY
 ELSE
  500 MSEC.DELAY
 THEN
 SET.ZERO
 100 MSEC.DELAY
 21 1 DO
  A/D.IN
  PHOTO.IN [ I ] :=
 LOOP
 PHOTO.IN MEAN
 PHOTO.READ :=
 PLOT.PHOTO
 2050 SPEED =
UNTIL
SET.ZERO
LOOP
;

/Acquisition set-up and parameters

: DT2801.ACQUIRE
 DT2800
 SET.ZERO
 SCREEN.CLEAR
 CR ." Enter 0 for auto adjustment or"
    ." 1 for acquisition = "
 #INPUT
 CHOICE :=
```

```
0 CHOICE = IF
 AUTO.ADJUST
THEN
SCREEN.CLEAR
0 I.SCAN :=
CR ." Enter 1 for NOISE or 2 for SIGNAL = "
#INPUT
IRUN :=
CR ." Enter 0 to change or 1 to keep"
   ." the same conditions = "
#INPUT
CHOICE :=
0 CHOICE = IF
 CR ." Enter the amplifier gain = "
 #INPUT AMP.GAIN :=
 CR ." Enter the laser frequency = "
 #INPUT LASER.FREQ :=
 CR ." Enter the starting delay = "
 #INPUT
 .1 * START.DELAY :=
 CR ." Enter the stopping delay = "
 #INPUT
 .1 * STOP.DELAY :=
 CR ." Enter the delay interval = "
 #INPUT
 .1 * INTERVAL.DELAY :=
 STOP.DELAY START.DELAY - INTERVAL.DELAY / N.OF.P :=
 RAMP.DELAY []RAMP
 RAMP.DELAY SUB[ 1 , N.OF.P ] INTERVAL.DELAY *
 RAMP.DELAY SUB[ 1 , N.OF.P ] :=
THEN
SCREEN.CLEAR
SET.PLOT.POINTS
CR ." How many scans do you want = "
#INPUT
SCAN.NUMBER :=
BELL
CR ." Press any key to start data acquisition"
BEGIN
 ?KEY
UNTIL
KEY DROP
SCREEN.CLEAR
CR ." *DATA ACQUISITION IN PROGRESS*"
SCAN.NUMBER 1 + 1 DO
 I.SCAN 1 + I.SCAN :=
 0 ICOUNT :=
 N.OF.P 1 + 1 DO
  1 ICOUNT + ICOUNT :=
  RAMP.DELAY [ ICOUNT ]  OUTPUT.DELAY.1 :=
  ACQUIRE.DATA
  FIND.MEAN
```

```
    PLOT.POINTS
   LOOP
  LOOP
  SCREEN.CLEAR
  BELL
  ." *ACQUISITION TERMINATED*"
  CR ." Press any key to continue"
  BEGIN
   ?KEY
  UNTIL
  KEY DROP
  IRUN 2 = IF
   CURVE.ANALYSIS
   GET.S-N.VALUE
  THEN
  IRUN 1 = IF
   0 ICOUNT :=
   0 NOISE :=
   SCAN.NUMBER 1 + 1 DO
    ICOUNT 1 + ICOUNT :=
    CURVE XSECT[ ICOUNT , ! ] NOISE + NOISE :=
   LOOP
   NOISE SCAN.NUMBER / NOISE :=
  THEN
  INSTRUCTIONS
;

/Exit Asyst

: EXIT.SYS
  BYE
;

/Screen plot of acoustic wave

: VIDEO.PLOT
  VIDEO.SET
  AXIS.DEFAULTS
  SOLID
  RAMP.DELAY SUB[ 1 , N.OF.P ]
  S-N.VALUE SUB[ 1 , N.OF.P ]
  XY.AUTO.PLOT
;

/Plot of acoustic wave on the H.-P.

: HP.PLOT
  HP7470
  PLOTTER.DEFAULTS
  VERTICAL GRID.OFF
  HORIZONTAL GRID.OFF
  PLOT.ROTATE
```

```
  1 COLOR
  RAMP.DELAY SUB[ 1 , N.OF.P ]
  S-N.VALUE SUB[ 1 , N.OF.P ]
  XY.DATA.FIT
  XY.AXIS.PLOT
  NORMAL.COORDS
  .4 .975 POSITION
  CR ." Enter the title = "
  "INPUT LABEL
  .5 .05 POSITION
  CR ." Enter the X-AXIS name = "
  "INPUT LABEL
  270 LABEL.DIR
  .025 .6 POSITION
  CR ." Enter the Y-AXIS name"
     ." ( " S-N.VALUE []MAX . ."  ) = "
  "INPUT LABEL
  WORLD.COORDS
  2 COLOR
  RAMP.DELAY SUB[ 1 , N.OF.P ]
  S-N.VALUE SUB[ 1 , N.OF.P ]
  XY.DATA.PLOT
  0 LABEL.DIR
  PLOT.ROTATE
;

/Save data on file

: SAVE.DATA
  DEF.FILE.TEMPLATE
  N.OF.P N.OF.P.ARRAY :=
  SCREEN.CLEAR
  CR ." Enter the filename = "
  "INPUT
  FILENAME ":=
  FILENAME DEFER> FILE.CREATE
  FILENAME DEFER> FILE.OPEN
   1 SUBFILE N.OF.P.ARRAY ARRAY>FILE
   2 SUBFILE ABSORBANCE ARRAY>FILE
   3 SUBFILE S-N.VALUE ARRAY>FILE
   4 SUBFILE RAMP.DELAY ARRAY>FILE
  FILE.CLOSE
  INSTRUCTIONS
;

/Plot data on screen or on the plotter

: PLOT.DATA
  SCREEN.CLEAR
  CR ." Enter 1 for VIDEO or 2 for HP = "
  #INPUT
  CHOICE :=
```

```
  1 CHOICE = IF
   VIDEO.PLOT
  ELSE
   HP.PLOT
  THEN
  INSTRUCTIONS
;

/Load a data file

: LOAD.DATA
  DEF.FILE.TEMPLATE
  SCREEN.CLEAR
  CR ." Do you want to load 1 or 2 files = "
  #INPUT
  CHOICE :=
  CR ." Enter the filename"
  CR ." FILE 1 = "
  "INPUT
  FILENAME ":=
  FILENAME DEFER> FILE.OPEN
   1 SUBFILE N.OF.P.ARRAY FILE>ARRAY
   2 SUBFILE ABSORBANCE FILE>ARRAY
   3 SUBFILE S-N.VALUE FILE>ARRAY
   4 SUBFILE RAMP.DELAY FILE>ARRAY
  FILE.CLOSE
  CHOICE 2 = IF
   CR ." FILE 2 = "
   "INPUT
   FILENAME ":=
   FILENAME DEFER> FILE.OPEN
    1 SUBFILE N.OF.P.ARRAY.2 FILE>ARRAY
    2 SUBFILE ABSORBANCE.2 FILE>ARRAY
    3 SUBFILE S-N.VALUE.2 FILE>ARRAY
    4 SUBFILE RAMP.DELAY.2 FILE>ARRAY
   FILE.CLOSE
  THEN
  N.OF.P.ARRAY [ 1 ] N.OF.P :=
  N.OF.P.ARRAY.2 [ 1 ] N.OF.P.2 :=
  INSTRUCTIONS
;

/Correct for a difference in absorbance

: ABSORBANCE.CORRECTION
  ABSORBANCE [ 1 ] NEG 10 ** ABS.CORR :=
  ABSORBANCE.2 [ 1 ] NEG 10 ** ABS.2.CORR :=
  S-N.VALUE.2 ABS.2.CORR / ABS.CORR *
  S-N.VALUE.2 :=
;

: ABS.CORR.QUESTION
```

```
   SCREEN.CLEAR
   CR ." Do you want a correction for the absorbance"
   CR ." Enter 0 for no correction or 1 for correction"
   CR ." CHOICE = "
   #INPUT
   CHOICE :=
   CHOICE 1 = IF
    ABSORBANCE.CORRECTION
   THEN
;

/Plot two curves on the same graph

: PLOT.2.CURVES
   ABS.CORR.QUESTION
   PLOT.DATA
   CHOICE 2 = IF
    PLOT.ROTATE
   THEN
   RAMP.DELAY.2 SUB[ 1 , N.OF.P.2 ]
   S-N.VALUE.2 SUB[ 1 , N.OF.P.2 ]
   XY.DATA.PLOT
   CHOICE 2 = IF
    PLOT.ROTATE
   THEN
   INSTRUCTIONS
;

/Substraction of two sets of data

: CURVES.SUBSTRACTION
   SCREEN.CLEAR
   CR ." *This program substract File 1 - File 2*"
   CR ." Press any key to continue"
   BEGIN
    ?KEY
   UNTIL
   KEY DROP
   ABS.CORR.QUESTION
   S-N.VALUE TAMPON :=
   TAMPON S-N.VALUE.2 - S-N.VALUE :=
   PLOT.DATA
   CR ." Enter 1 if you want to save the data = "
   #INPUT
   CHOICE :=
   1 CHOICE = IF
    SAVE.DATA
   THEN
   TAMPON S-N.VALUE :=
   INSTRUCTIONS
;
```

```
/File template for the results

: FILE.TEMPLATE.1
  FILE.TEMPLATE
   REAL DIM[ 5 , 10 ] SUBFILE
   REAL DIM[ 10 ] SUBFILE
   REAL DIM[ 1 ] SUBFILE
   INTEGER DIM[ 1 ] SUBFILE
  END
;

/Save results on file

: SAVE.RESULTS.FILE
  FILE.TEMPLATE.1
  SCREEN.CLEAR
  SAMPLE.NUMBERS SAMPLE.NUMBER [ 1 ] :=
  DELAY.COUNT DELAY.COUNT.ARRAY [ 1 ] :=
  CR ." Enter the filename = "
  "INPUT
  FILENAME ":=
  FILENAME DEFER> FILE.CREATE
  FILENAME DEFER> FILE.OPEN
   1 SUBFILE RESULTS ARRAY>FILE
   2 SUBFILE CONCENTRATION ARRAY>FILE
   3 SUBFILE SAMPLE.NUMBER ARRAY>FILE
   4 SUBFILE DELAY.COUNT.ARRAY ARRAY>FILE
  FILE.CLOSE
;

/Plot the results on the H.-P.

: H.P.PLOT.RESULTS
  HP7470
  1 COLOR
  PLOTTER.DEFAULTS
  PLOT.ROTATE
  NORMAL.COORDS
  .4 .975 POSITION
  CR ." Enter the title = "
  "INPUT LABEL
  .5 .05 POSITION
  CR ." Enter the X-AXIS name = "
  "INPUT LABEL
  270 LABEL.DIR
  .025 .6 POSITION
  CR ." Enter the Y-AXIS name ( "
     RESULTS.1 []MAX .  ." ) = "
  "INPUT LABEL
  0 LABEL.DIR
  WORLD.COORDS
;
```

```
/Plot results on screen

: VIDEO.PLOT.RESULTS
  VIDEO.SET
  AXIS.DEFAULTS
;

/Regression coefficient of the results

: REG.COEFF
  0 SOMXY :=
  0 SOMY2 :=
  SAMPLE.NUMBERS N :=
  CONCENTRATION  ^SUM TOTAL.N :=
  TOTAL.N [ N ] SOMX :=
  RESULTS.1 ^SUM TOTAL.N :=
  TOTAL.N [ N ] SOMY :=
  N 1 + 1 DO
   CONCENTRATION [ I ] RESULTS.1 [ I ] * SOMXY + SOMXY :=
  LOOP
  N 1 + 1 DO
   RESULTS.1 [ I ] 2 ** SOMY2 + SOMY2 :=
  LOOP
  SOMX SOMY * N / NEG SOMXY + PARA [ 1 ] * NUMERATOR :=
  SOMY2 SOMY 2 ** N / - DENOMINATOR :=
  NUMERATOR DENOMINATOR / SQRT R2 :=
  SCREEN.CLEAR
  CR ." The slope = " PARA [ 1 ] .
  CR ." The intercept = " PARA [ 2 ] .
  CR ." The regession coefficient = " R2 .
  CR ." Press any key to continue "
;

/Plot results on screen or on the H.-P.

: PLOT.RESULTS
  SCREEN.CLEAR
  CR ." Enter the number of the delay ( 0 to quit) = "
  #INPUT
  DELAY.NUMBER :=
  DELAY.NUMBER 0 = NOT IF
   CR ." Enter 0 for video or 1 for H.P. = "
   #INPUT
   CHOICE :=
   CHOICE 1 = IF
    H.P.PLOT.RESULTS
   ELSE
    VIDEO.PLOT.RESULTS
   THEN
   " *" SYMBOL
   RESULTS XSECT[ DELAY.NUMBER , ! ]
```

```
 RESULTS.1 :=
 CONCENTRATION SUB[ 1 , SAMPLE.NUMBERS ]
 RESULTS.1 SUB[ 1 , SAMPLE.NUMBERS ]
 XY.AUTO.PLOT
 CONCENTRATION SUB[ 1 , SAMPLE.NUMBERS ]
 RESULTS.1 SUB[ 1 , SAMPLE.NUMBERS ]
 1 LEASTSQ.POLY.FIT
 PARA :=
 REG.COEFF
 CONCENTRATION SUB[ 1 , SAMPLE.NUMBERS ] SORT DUP
 CONCENTRATION SUB[ 1 , N ] :=
 PARA [ 1 ] *
 PARA [ 2 ] + RESULTS.1 SUB[ 1 , SAMPLE.NUMBERS ] :=
 SOLID
 2 COLOR
 CONCENTRATION SUB[ 1 , SAMPLE.NUMBERS ]
 RESULTS.1 SUB[ 1 , SAMPLE.NUMBERS ]
 XY.DATA.PLOT
 1 CHOICE = IF
  PLOT.ROTATE
 THEN
THEN
BEGIN
 ?KEY
UNTIL
KEY DROP
;

/Save results on file

: SAVE.RESULTS
 DELAY.COUNT 1 = IF
  CR ." Enter the sample number = "
  #INPUT
  SAMPLE.NUMBERS :=
  CR ." Enter the concentration = "
  #INPUT
  CONCENTRATION [ SAMPLE.NUMBERS ] :=
 THEN
 MAX.VALUE MIN.VALUE - RESULTS
 [ DELAY.COUNT , SAMPLE.NUMBERS ] :=
 CR ." Enter 1 to save the results on file = "
 #INPUT
 CHOICE :=
 CHOICE 1 = IF
  SAVE.RESULTS.FILE
 THEN
 CR ." Enter 1 to plot the results = "
 #INPUT
 CHOICE :=
 CHOICE 1 = IF
  PLOT.RESULTS
```

```
  THEN
;

/Find min and max of the curve

: FIND.MIN/MAX
  SCREEN.CLEAR
  CR ." Enter 1 for File 1 or 2 for File 2 = "
  #INPUT
  CHOICE :=
  CHOICE 1 = IF
   S-N.VALUE TAMPON :=
  ELSE
   S-N.VALUE.2 TAMPON :=
  THEN
  TAMPON SORT&INDEX
  SORT.INDEX.ARRAY :=
  SORT.ARRAY :=
  0 DELAY.COUNT :=
  BEGIN
   SORT.ARRAY [ 1 DELAY.COUNT + ]  MIN.VALUE :=
   SORT.ARRAY [ 100 DELAY.COUNT - ]  MAX.VALUE :=
   SORT.INDEX.ARRAY [ 1 DELAY.COUNT + ] MIN.DELAY.INDEX :=
   SORT.INDEX.ARRAY [ 100 DELAY.COUNT - ]
   MAX.DELAY.INDEX :=
   RAMP.DELAY [ MIN.DELAY.INDEX ] 10 * MIN.DELAY :=
   RAMP.DELAY [ MAX.DELAY.INDEX ] 10 * MAX.DELAY :=
   DELAY.COUNT 1 + DELAY.COUNT :=
   SCREEN.CLEAR
   CR ." The minimum value = " MIN.VALUE .
      ." at " MIN.DELAY . ." % of the aperture. "
   CR ." The maximum value = " MAX.VALUE .
      ." at " MAX.DELAY . ." % of the aperture. "
   CR CR ." Enter 1 to save the results = "
   #INPUT
   CHOICE :=
   CHOICE 1 = IF
    SAVE.RESULTS
   THEN
   CR CR ." Enter 0 to quit or 1"
         ." to have other MIN/MAX values "
   #INPUT
   CHOICE :=
   0 CHOICE =
  UNTIL
  INSTRUCTIONS
;

/Load results from file

: LOAD.RESULTS
  SCREEN.CLEAR
```

```
 FILE.TEMPLATE.1
 CR ." Enter the filename = "
 "INPUT
 FILENAME ":=
 FILENAME DEFER> FILE.OPEN
  1 SUBFILE RESULTS FILE>ARRAY
  2 SUBFILE CONCENTRATION FILE>ARRAY
  3 SUBFILE SAMPLE.NUMBER FILE>ARRAY
  4 SUBFILE DELAY.COUNT.ARRAY FILE>ARRAY
 FILE.CLOSE
 SAMPLE.NUMBER [ 1 ] SAMPLE.NUMBERS :=
 DELAY.COUNT.ARRAY [ 1 ] DELAY.COUNT :=
 CR ." Enter 1 to plot the results = "
 #INPUT
 CHOICE :=
 CHOICE 1 = IF
  PLOT.RESULTS
 THEN
 INSTRUCTIONS
;

/Start the program

: RUN
 VIDEO.SET
 INSTRUCTIONS
 F1 FUNCTION.KEY.DOES DT2801.ACQUIRE
 F2 FUNCTION.KEY.DOES PLOT.DATA
 F3 FUNCTION.KEY.DOES SAVE.DATA
 F4 FUNCTION.KEY.DOES LOAD.DATA
 F5 FUNCTION.KEY.DOES PLOT.2.CURVES
 F6 FUNCTION.KEY.DOES CURVES.SUBSTRACTION
 F7 FUNCTION.KEY.DOES FIND.MIN/MAX
 F8 FUNCTION.KEY.DOES FFT.OF.DATA
 F9 FUNCTION.KEY.DOES LOAD.RESULTS
 F10 FUNCTION.KEY.DOES EXIT.SYS
 INTERPRET.KEYS
;

CR ." Enter RUN please"
```

APPENDIX D

CALCULATION OF THE NUMBER OF EXCITED MOLECULES

Experimental conditions and constants:

- Energy of the pulse: $I_0 = 2,5$ mJ
- Plank's constant: $h = 6,63 \times 10^{-34}$ J.s
- Wavelength of the exciting beam: $\lambda = 335$ nm
- Speed of light: $c = 3 \times 10^8$ m s^{-1}
- Absorbance of TiO_2: $a_T = 0,2$
- Concentration of the dye: $[D] = 2,0 \times 10^{-5}$ M
- Light pathlength: $l = 0,2$ cm
- Size of the exciting beam: $r = 0,1$ cm
- Avogodro's number: $N_a = 6,023 \times 10^{23}$ molec.$^{-1}$
- Absorbance of the dye: $a_D = 0,03$

Calculations

- Energy of one photon at 355 nm: $E_{ph} = \frac{hc}{\lambda} = 5,60 \times 10^{-19}$ J
- Number of photons in the exciting pulse: $N_{ph} = \frac{I_0}{E_{ph}} = 4,46 \times 10^{15}$ ph
- Number of photons absorbed by the TiO_2: $N_T = (1 - e^{-a}) N_{ph} = 1,65 \times 10^{15}$ ph
- Residual number of photons: $N_r = N_{ph} - N_T = 2,81 \times 10^{15}$ ph
- Volume of the exciting pulse: $V = \pi r^2 l = 6,28 \times 10^{-6}$ l
- Number of dye molecules in V: $D = [D] V N_a = 7,56 \times 10^{12}$ molec.

- Number of photons absorbed by the dye: $N_D = (1 - e^{-a}) N_r = 8,31x10^{13}ph$